TECHNISCHE UNIVERSITÄT WIEN

DIPLOMARBEIT

Constraining Low Fine Tuned Supersymmetric Models With Simplified Models Spectra Results Based On CMS and ATLAS Searches

ausgeführt am Institut für Hochenergiephysik (HEPHY)
der Österreichischen Akademie der Wissenschaften (ÖAW)
und am Atominstitut (E141)
eingereicht an der Technischen Universität Wien, Fakultät für Physik

unter der Anleitung von
Dr. rer. nat. Suchita Kulkarni
DI Dr. rer. nat. Wolfgang Waltenberger
Doz. DI Dr. techn. Claudia-Elisabeth Wulz

durch

Veronika Magerl

June 3, 2015

Abstract

The ATLAS and CMS collaborations at the Large Hadron Collider (LHC) have performed a wide range of searches for physics beyond the standard model (BSM), during their run 1 at 8 TeV. Many of these searches target supersymmetric signatures. In order to ease the interpretation of these results, simplified models have been introduced recently. They provide a context in which the experimental results are interpreted as upper limits on production cross sections, introducing only a limited set of new BSM particles. Given a full theoretical model, it is nevertheless still a non-trivial task to decide, whether any of these simplified models results exclude the theory or not.

A software framework called SModelS has been developed recently. It decomposes a given $\mathbb{Z}_2$-symmetric BSM model into its simplified models spectra (SMS) topologies and matches them with a database of the experimental simplified models results. The database that contains the experimental upper limits was maintained and improved within the scope of this thesis. A software tool to access the database as conveniently as possible was developed and constantly enhanced. This tool was used to validate the framework and restructure the database.

The latest official version of the software tool, SModelS v1.0.3 was applied to a scan over a parameter space determined by a low fine tuned (LFT) scenario. This scenario is a subset of the 19-parameter phenomenological minimal supersymmetric model (pMSSM). The motivation behind this region of parameter space is the question of "naturalness" within the pMSSM, i.e. how the mass of the newly found Higgs boson is stabilized at the electroweak scale. Another instance is to understand, if the concept of naturalness is compatible with the fact, that no experimental evidence for the existence of supersymmetry has been found so far.

The scan is analysed and interpreted in this thesis. The mass spectrum in this LFT scenario is found to have very light top and bottom squarks often accompanied by light electro weak sparticles, allowing rather complex decay patterns. Amongst others this results in several interesting SMS topologies, for which no applicable simplified model results are available by now. Those topologies are understood in terms of supersymmetric decay chains. Regions of parameter space, which still remain unchallenged by current SUSY searches at the LHC are provided. Interesting new topologies for future SMS interpretation of data collected by the ATLAS and the CMS collaborations are proposed.

Kurzfassung

Im Laufe der ersten Betriebsphase des Large Hadron Collider (LHC) wurden von den Kollaborationen ATLAS und CMS zahlreiche Suchen nach neuer Physik, also Physik jenseits des Standard Modells (BSM) durchgeführt und veröffentlicht. Viele dieser Untersuchungen hatten supersymmetrische Signaturen zum Ziel. Um die Interpretation der Ergebnisse derartiger Suchen zu erleichtern, wurde in jüngster Zeit vermehrt auf vereinfachte Modelle zurück gegriffen. Diese erlauben die Interpretation experimenteller Ergebnisse in Form von oberen Grenzwerten für die Wirkungsquerschnitte der Teilchenproduktion, wobei jeweils nur ein sehr beschränkter Satz an neuen BSM Teilchen eingeführt wird. Betrachtet man nun ein vollständiges theoretisches Modell, so ist es dennoch keine leichte Aufgabe zu entscheiden, ob dieses Modell durch eines dieser vereinfachten Modelle ausgeschlossen werden kann.

Aus diesem Grund wurde kürzlich ein Programm namens SModelS entwickelt. Mit diesem Programm kann jedes beliebige $\mathbb{Z}_2$ symmetrische BSM Modell in seine jeweiligen Spektren vereinfachter Modelle (SMS Topologien) zerlegt werden, welche dann mit einer Datenbank für derartige Ergebnisse verglichen werden. Diese Datenbank wurde im Rahmen der Diplomarbeit gewartet und verbessert. Ein Software Werkzeug, das einen zweckmäßigen Zugriff auf die Datenbank ermöglicht wurde entwickelt und laufend erweitert. Dieses Werkzeug wurde verwendet, um das SModelS Programm zu validieren und die Datenbank neu zu strukturieren.

Die neueste Version des Programms, SModelS v1.0.3 , wurde für die Sondierung eines Parameterraums verwendet, welcher durch ein gering abgestimmtes Szenario bestimmt ist. Dieses Szenario entspricht einem Teilbereich des 19-Parameter phenomenolgischen minimalen supersymmetrischen Modells (pMSSM). Die Wahl dieser Region wird durch die Frage nach der "Natürlichkeit" innerhalb des pMSSM motiviert, also wie die Masse des kürzlich gefundenen Higgs Boson auf der elektroschwachen Energieskala stabilisiert wird. Darüber hinaus gilt es zu verstehen, ob das Konzept der Natürlichkeit mit der Tatsache vereinbar ist, dass bisher noch keine experimentellen Hinweise auf Supersymmetrie gefunden wurden.

Die Resultate dieser Sondierung werden in dieser Arbeit analysiert und interpretiert. Es zeigt sich, dass das Massenspektrum in diesem Szenario sehr leichte top und bottom squarks enthält, die häufig gemeinsam mit leichten elektroschwachen supersymmetrischen Teilchen auftreten, wodurch sehr komplexe Zerfallsschemata ermöglicht werden. Daraus ergeben sich unter anderem einige interessante SMS Topologien, für die bis jetzt noch keine anwendbaren Ergebnisse vereinfachter Modelle zur Verfügung stehen. Diese Topologien werden in Form von supersymmetrischen Zerfallsketten erklärt. Es wird auf Bereiche des Parameterraums hingewiesen, die bis jetzt noch nicht durch die gegenwärtigen Suchen nach Supersymmetrie am

LHC geprüft wurden. Es werden interessante neue Topologien vorgeschlagen, die herangezogen werden können, um die Daten, welche in Zukunft von ATLAS und CMS gesammelt werden, im Rahmen vereinfachter Modelle zu interpretieren.

Acknowledgement

First, I would like to thank Claudia-Elisabeth Wulz for all her support in organisational issues not only for the final exam but also for the visit at CERN. I would like to express the deepest appreciation to my supervisor Wolfgang Waltenberger for introducing me to this exciting field of physics already during my project work at HEPHY and for everything he taught me.

Especially I want to thank Suchita Kulkarni for all her support, for her patience in proof-reading this thesis, for the endless discussions about supersymmetry and naturalness, for encouraging me, ... I would not have made it without your help.

Furthermore I would like to thank the whole SModelS team for the enjoyable company during the SModelS-Fest in Grenoble. Special thanks are directed to Ursula Laa for supporting me in my first few weeks and to Andre Lessa for all the exhilarating discussions about physics and beyond during his stay in Vienna. I would like to express my gratitude to Wolfgang Adam for the inspiring tour at CERN and his experienced advice.

In addition I want to thank Wolfgang Magerl for his professional advice regarding programming and for solving all my problems with LaTeX. Furthermore, I am grateful for the financial support by the FEMtech initiative of the BMVIT of Austria.

Finally, my sincere thanks belong to Michael Traub for sharing our lives and every thing else, to my parents for emotional and financial support over all the years of my studies and to my brother and sister who always supported and encouraged me unconditionally.

Contents

Chapter 1

Introduction

With the discovery of a new particle, which is most likely the long-desired Higgs boson, at the Large Hadron Collider (LHC) [1, 2] it seems that the last remaining piece in the puzzle of the standard model (SM) was brought in its place. Nevertheless the SM itself is just one part of the big picture. One of the problems, that can not be solved by the SM is the so called hierarchy problem, i.e. what stabilises the mass of the Higgs boson at the weak scale. Also the question of dark matter, which was introduced to explain various cosmological phenomena like the discrepancies between observations and expectations of rotational curves of galaxies, remains completely unanswered.

This thesis focuses on one of the most promising extensions of the SM to solve some of these problems, namely supersymmetry (SUSY). More precisely it concentrates on a specific SUSY model, the R-parity conserving phenomenological minimal supersymmetric model, short RPC pMSSM. The lack of experimental evidence makes it clear that SUSY is not an exact symmetry. Hence, its introduction comes at the cost of more than 100 new parameters, occurring in the theory due to electro weak symmetry breaking. Fortunately this vast amount of parameters can be reduced to no more than 19 within the pMSSM. In contrary to other SUSY models (e.g. cMSSM) it makes no assumptions about the underlying parameters of the theory, like for example the gaugino mass parameters M_1, M_2 and M_3. Within the cMSSM these parameters are assumed to be unified at very high energy scales leading to specific relations among them at the weak scale. Whereas the pMSSM is driven by experimentally motivated constraints, thus offering increased parameter freedom. At collider experiments like the LHC, such an R-parity conserving scenario will result in typical detector signatures, i.e. final states of SM particles and missing energy (MET) carried away by the lightest supersymmetric particle (LSP) which escapes detection. If SUSY is the choice of nature an excess above the SM will be found in such events.

However, probing 19 parameters at once is very complicated and computationally expensive. Hence, results of searches for events with SM final states and MET cannot be easily interpreted within the pMSSM. An alternative approach to interpret such event counts in terms of specific supersymmetric decays was developed by experimentalists in the ATLAS and CMS collaborations. That is the Simplified Models Spectra approach, or SMS for short, an

effective Lagrangian description that involves only a reduced number of BSM particles. Such a model is purely phenomenological. Moreover, the branching ratio for a specific decay mode is usually assumed to be 100%. A wide range of SUSY searches concentrates on such SMS interpretations. Numerous of these analyses have been published by the two big collaborations (ATLAS and CMS) making the most out of the data collected during the first run of the LHC with $\sqrt{s} = 7$ and 8 TeV [3, 4].

Nevertheless it is not straightforward to apply results interpreted in terms of SMS to a given pMSSM point. That is because a general pMSSM point may incorporate a great number of available decay modes and many SMS results may be applicable depending on these modes. On the other hand, it is also possible that none of these results is useful, given the fact that SMS interpretations are always based on specific assumptions, e.g. on the underlying event kinematics. At this point SModelS comes into play. SModelS is a software tool to bridge the gap between a theoretical model and the SMS results, as they are published by the collaborations. It allows not only to apply the relevant experimental constraints to a given model, but additionally provides some suggestions on new SMS topologies that could also constrain it.

While this thesis is written the LHC and its detectors prepare for the second run with even higher energy and luminosity. One aim of the SModelS group is to suggest simplified models, that may be worth to be studied with the data collected in this second run.

To demonstrate the virtue of SModelS and the usefulness of its functionalities, the framework was applied to a set of pMSSM points characterised by a low fine tuning (LFT). Within this scenario the 19 pMSSM parameters are chosen such that they predict a SM like Higgs boson mass in accordance with the experimental value, without the need of severe cancellations between the individual mass terms. Broad regions of the LFT parameter space were found to be unchallenged by current experimental results. Among others, SMS topologies have been encountered for which no interpretations are available so far. In particular, these involve gluinos undergoing cascade decays, as well as all-hadronic final states of SM vector boson decays. Furthermore, several asymmetric topologies were found to be useful in order to probe this scenario with regard to the stop and gluino masses. Last but not least an associated production of right handed squarks and the LSP was found to result in a final state characterised by a single hadronic jet. A detailed interpretation of these findings is given in chapter 6.

The rest of the thesis is structured as follows. A brief discussion of the experimental side (cf. chapter 2) - the LHC and its detectors - is followed by an overview of the underlying theoretical considerations (cf. chapter 3). After a description of the SMS approach and the current status of SUSY searches at the LHC (cf. chapter 4), an explanation of the SModelS framework and its basic functionalities is given (cf. chapter 5). Finally, the LFT parameter space and the investigation of the model set is described in detail in chapter 6.

Chapter 2

Experimental Side - The LHC

CERN (Conseil Européenne pour la Recherche Nucléaire) is one of the most prestigious centres for fundamental physics research in the world. It was founded in 1954 and ever since it has pushed forward the frontiers of our understanding of the origin of the universe. It has achieved remarkable scientific discoveries and technological developments that not only enlarged our knowledge about physics. Moreover, thanks to technologies like the world wide web, that was invented at CERN in 1989, it has even fundamentally changed our daily life. This organisation brings together scientists and engineers from all over the world. At present it has 21 member states and a large number of non-member states have cooperation agreements with CERN.

2.1 The Large Hadron Collider and its Detectors

After 24 years of planing, developing and constructing, on the 10^{th} of September in 2008 the first bunch of protons made it across the entire ring of the LHC, bringing about one of the most exciting periods in the history of physics. This section will give an overview of this great machine and the two big general purpose experiments ATLAS and CMS. Both experiments pursue the same physics programs, but have different experimental realisations, thus results obtained with one of these two can be reviewed by the other.

The detector layouts and main functionalities of ATLAS (cf. subsection 2.1.2) and CMS (cf. subsection 2.1.3) are described briefly, whereby the focus lies on the latter since the author is a member of the CMS collaboration.

2.1.1 LHC

The LHC (Large Hadron Collider) is the world's largest particle collider and often referred to as the "biggest machine ever built by mankind". It is located in a 27 km tunnel 100 m beneath the ground, crossing the Franco-Swiss border near Geneva. The tunnel originally constructed for the Large Electron Positron Collider (LEP) was adapted after LEP was dismantled in 2001. The LHC consists of a ring of superconducting magnets, which focus, accelerate and keep the particle beam on track. Unlike a particle antiparticle accelerator like LEP, the LHC is a

particle particle collider. This means that two beam pipes with counter-rotating beams are needed, each one encapsulated in a separate tube.

The magnetic system is cooled down with superfluid helium to 1.9 K, thus allowing the magnets to work in a superconducting state providing a magnetic field of 8.33 T. It is noteworthy that this makes the LHC the coldest region in the known universe (empty space has a temperature of approximately 2.73 K according to measurements of the cosmic microwave back ground).

Inside the two beam pipes bunches of protons are travelling in opposite directions close to the speed of light. To avoid unintended collisions with gas molecules the pipes have to provide a high vacuum, that is often said to be "emptier than interplanetary space". All these superlative characteristics of the LHC would be worth nothing without the rest of CERN's accelerator complex (cf. Figure 2.1). The protons that are simply hydrogen atoms stripped of their electrons, undergo a long chain of different accelerators, that push their energies to higher and higher levels (cf. Table 2.1). The first step in this chain is called LINAC2. The protons acquire energies of roughly 50 MeV by traversing this linear accelerator. After this the beam energy is raised to the GeV-level by the Proton Synchrotron Booster and even further by the subsequent Proton Synchrotron. The last pre acceleration stage is the Super Proton Synchrotron that accelerates the protons up to 450 GeV. Finally the particles are injected into LHC's two beam pipes, where after circulating for a while they gain their maximal energy of 4 TeV in the first and 7 TeV in the second run.

Accelerator	*Energy of the Proton*
LINAC 2	50 MeV
Proton Synchrotron Booster (PSB)	1.4 GeV
Proton Synchrotron (PS)	25 GeV
Super Proton Synchrotron (SPS)	450 GeV

Table 2.1: Pre-acceleration steps for the LHC and the respective proton energy

The LHC ring is then filled with 2808 bunches of protons, each consisting of 1.1×10^{11} protons travelling at 0.999999991 times the speed of light (at the designed maximal beam energy of 7 TeV). These bunches are brought to collision at four points along the ring, where the main experiments ALICE, ATLAS, CMS, and LHCb are located.

Luminosity

To conveniently characterise the performance of the LHC a parameter called luminosity $\mathcal{L}$ is introduced. The luminosity only depends on parameters of the beam. Therefore it allows to derive the rate of events $dN_{process}/dt$ one has to expect for a certain process with a cross section $\sigma_{process}$ (2.1).

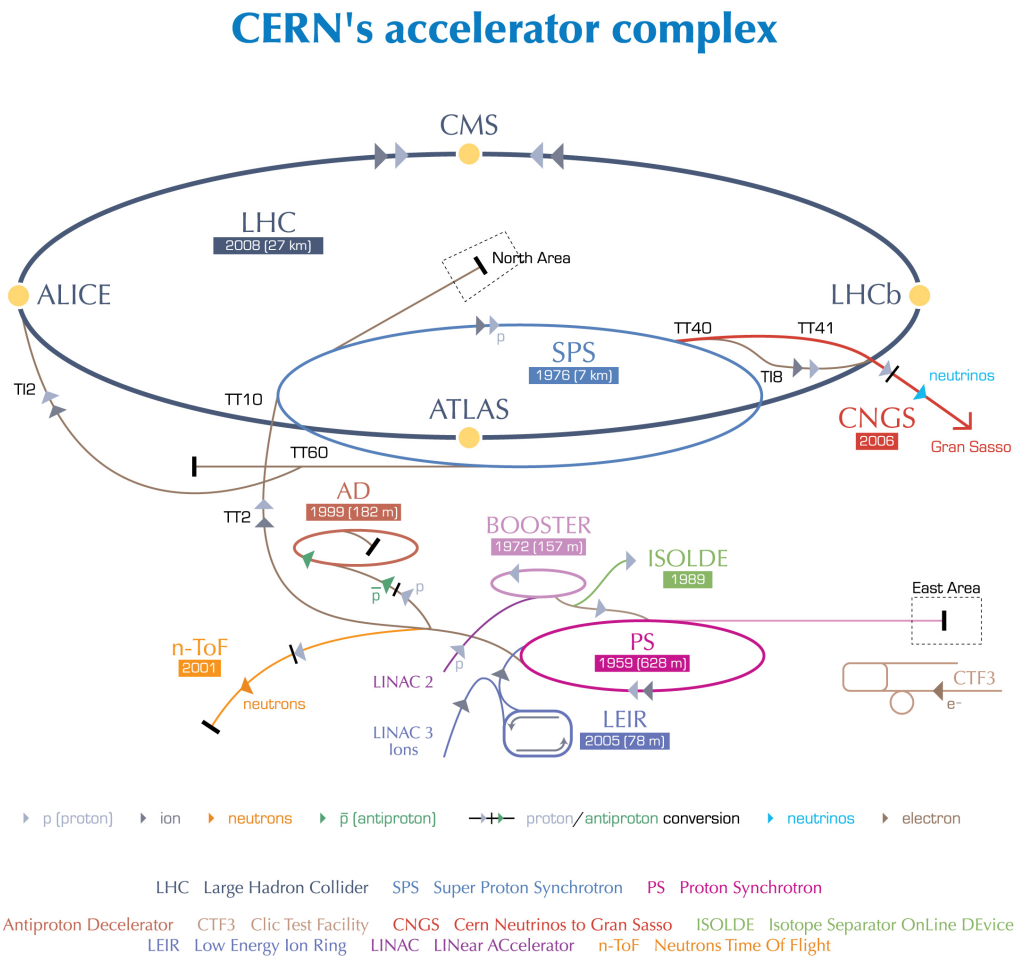

Figure 2.1: Schematic illustration of the whole accelerator complex at CERN. The protons (p) undergo the four pre-accelerating structures of the LHC.[5].

$$\frac{dN_{process}}{dt} = \mathcal{L}\,\sigma_{process} \tag{2.1}$$

The designed maximal luminosity $\mathcal{L}$ of the LHC is 10^{34} cm^{-2}s^{-1}, which will hopefully be reached in the second run. To obtain the number of events the integrated luminosity $L = \int \mathcal{L} dt$ is multiplied with the cross section.

2.1.2 ATLAS Detector

ATLAS (A Toroidal LHC ApparatuS) was designed to investigate a wide range of SM physics and beyond. It has six subsystems, positioned as layers around the interaction point, to measure trajectory, momentum and energy of every single particle that is produced in a collision. ATLAS is by far the biggest of the LHC experiments. It has a diameter of 25 m, is 44 m long and weighs 7000 tonnes.

Its detector layout is shown in Figure 2.2. The innermost subsystem consists of several layers of semiconducting pixel and strip detectors, which have to face high requirements of speed and radiation hardness. This subset is surrounded by a thin superconducting solenoid to provide the high magnetic field that is needed to curve the tracks of high energetic charged particles. This configuration allows for high resolution measurements of their momenta.

The solenoid is accompanied by three large superconducting toroidal magnets, one barrel and two end-caps. It is surrounded by a liquid argon high granularity electromagnetic calorimeter, followed by a scintillator-tile calorimeter for measuring the energy of electrons or photons and hadrons, respectively.

On the outer side of the barrel the muon detectors are located, as well as in the two end-caps, determining ATLAS' outer dimensions.

The main physics requirements for the ATLAS and CMS detector are very similar, but the experimental realisation differs in various details. Not only the design and arrangement of the sub-detectors but also the active detector materials vary significantly. ATLAS' main advantages are a continued tracking of particles even for large radii due to the transition radiation tracker (TRT) and an independent muon spectrometer that allows for stand-alone measurements. One of the disadvantages in comparison to CMS is the inferior momentum resolution of the tracking system.

A very detailed and extended description of the ATLAS detector and its supporting systems can be found elsewhere [7].

Since the beginning of LHC activities ATLAS published the imposing number of 380 papers [8], covering a wide range of different physics fields like detailed measurements of SM predictions, characteristics of the top quark, searches on τ-decays, etc. Amongst these numerous different subjects there are 80 publications on SUSY searches. These experimental results were partially used in this work (see section 5.3).

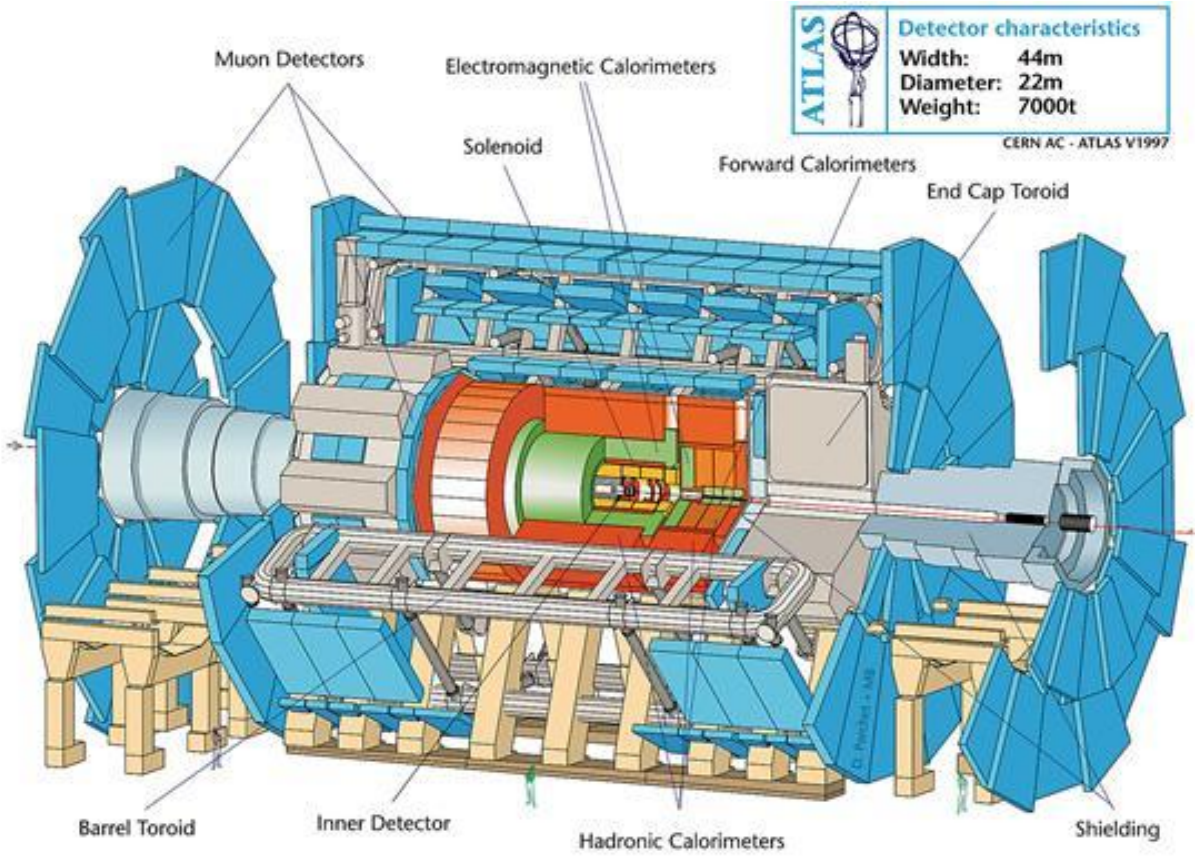

Figure 2.2: Scheme of the ATLAS detector [6].

2.1.3 CMS Detector

CMS stands for Compact Muon Solenoid. Unlike the somewhat vacuous naming of ATLAS, this is a very telling name in the sense that it explains its main features very concisely. *Compact* refers to the relatively small dimensions compared with the weight of the detector. *Muon* indicates that one of the advantages of this experiment is the detection of muons with a very high resolution. *Solenoid* indicates that CMS operates using a strong magnetic field. Overall the detector is 21 m long, 15 m in width and hight and its weight is 14,000 tonnes.

Motivation

The physics motivation and main purposes for this apparatus are:

- Search for Higgs Boson(s) - this effort lead to the discovery of a SM like Higgs boson in 2012 - and further studies of its decay modes and its properties.
- Searches for BSM physics, like SUSY and extra spatial dimensions.
- Studying the behaviour of QCD matter under extreme conditions, achieved by collisions of heavy ions.

Design and Experimental Requirements

The design of the detector is driven by the multiple requirements it has to face, as there are:

- A high resolution of missing-transverse-energy $\not{E}_T$ and dijet-masses, provided by the hadron calorimeters.
- Measurement of photon- and electron-energies with high resolution and wide geometric coverage.
- The detection of muons over a wide range of momenta with high mass resolution of dimuon events and precise measurement of their charge.
- An exact reconstruction of the tracks of charged particles, requiring a silicon based tracking system.

Figure 2.3 shows the schematic detector layout of CMS. Its central feature is a super conducting solenoid with an internal diameter of 6 m, which generates a magnetic field of 4 T. This strong field bends the trajectories of highly energetic charged particles and thus allows to measure their momentum.

In the very centre of this solenoid lies the interaction point, where the particles are brought to collision. The innermost layer of the detector surrounding this interaction point is the full silicon-based inner tracking system. It has a diameter of 2.6 m and is about 5.8 m long. This tracking system has to meet extreme requirements, such as radiation hardness, speed and high

resolution. It consist of three layers of pixel detectors (100×150 μm^2) followed by ten layers of strip detectors (10 cm$\times80$ μm). This design allows to concisely track charged particles produced in the primary vertex.

Besides the trajectories of the particles there is another characteristic variable that has to be measured in order to pin down the properties of particles, namely their energy. To measure this variable is the task of the two calorimeters, also located inside the solenoid. First comes the electromagnetic calorimeter (ECAL) that is made of lead tungstate crystals ($PbWO_4$) with attached avalanche photodiodes to detect the energy of electrons and photons. The ECAL is surrounded by the hadron calorimeter (HCAL), a brass/scintillator calorimeter, constructed of plastic scintillator tiles. Brass serves as absorber material and wavelength-shifting fibres are embedded in the active material to read out the scintillating light, that is detected by photodiodes.

The outermost sub-detector of CMS is the muon-system. Muons in comparison to electrons have the advantage that they are less effected by radiative loss in the inner tracking materials and hence escape to the outer regions of the detector. They are of particular interest for the detection of Higgs decays and BSM physics. For example the H $\rightarrow$ ZZ decay is often referred to as "golden plate" in the case all four leptons, the Z-Boson further decays to, are muons. CMS's muon systems consists of three parts, one cylindrical barrel and two end-caps, all of them gas detectors. Whereas the barrel is constructed of several layers of drift tube chambers and resistive plate chambers, the end-caps have cathode strip chambers.

A more detailed description of the CMS detector, together with a definition of the coordinate system used and the relevant kinematic variables, can be found in Ref. [10].

A large list of various searches and results published by the collaboration, sorted according to the field of physics and nicely arranged on a time line, can be found on CMS's public web-page [11]. From January 2010 until March 2015 a total of 385 papers has been published that are concerned with as different topics as B physics, heavy ions and Higgs searches, to name but a few. Out of this impressive number 49 papers on SUSY searches where published that investigate the typical $\not{E}_T$ signatures as they are expected from an R-parity conserving scenario as it is considered in this thesis.

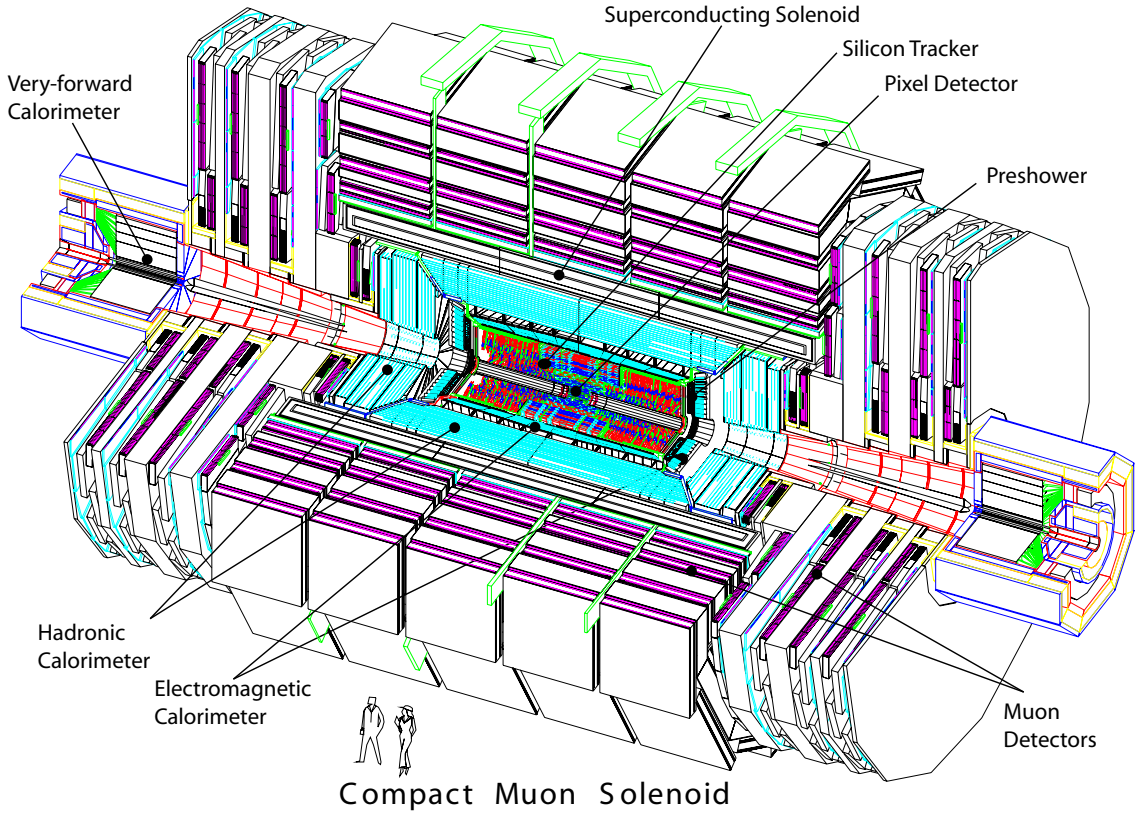

Figure 2.3: Scheme of the CMS detector layout [9].

Chapter 3

Theoretical Side - The pMSSM

3.1 The Standard Model and its Deficiencies

The Standard Model (SM) of particle physics is a mathematical formulation that incorporates the classification and interactions of matter, based on quantum field theory (QFT). In QFT the Lagrangian, that describes simply the difference between the kinetic and the potential energy in classical mechanics, is given as a density and represents the propagation of a field and its interactions with other fields and itself. Each of these QFTs is based on certain symmetries which can act either locally, i.e. independently at each point in spacetime, or globally. If the Lagrangian is invariant under local gauge transformations, represented by symmetry groups, such a QFT is considered a gauge theory. The gauge particles emerge through quantisation of the corresponding gauge fields.

Developed throughout the mid and late 20^{th} century, today the SM is known to be one of the most successful physics theories. Its predictions are tested experimentally with very high precision, e.g. the measurements of the fine-structure constant $\alpha_F = 7.2973525698 \times 10^{-3} \pm 2.4 \times 10^{-12}$ [12] attained an accuracy of 10^{-8} %.

A big part of the SM was formed in the 1970s by Sheldon Glashow [13], Abdus Salam [14] and Steven Weinberg [15], who shared the Nobel Prize in Physics in 1979 for the unification of the electromagnetic and the weak force. The incorporation of the strong interaction, to which a lot of different groups contributed, was brought into its present form in the early 1970s. Eventually the comprehension of the mechanism that gives mass to all the SM particles, the so called Higgs-machanism [16, 17], made the SM final and absolute. Its main assertions are:

- All matter is built from a set of spin $\frac{1}{2}$ particles - the fermions.
- All forces that describe the interactions between these matter particles are mediated by particles with integral spin, called bosons.
- The masses of all fundamental particles are generated by the Higgs mechanism.
- All particles are seen as quantisations of the quantum fields in a spontaneously broken gauge theory.

3.1.1 The Particle Content of the SM

Figure 3.1 gives an overview of the particles of the SM. As indicated by the arrangement into three nested rings, the SM consists of three components, each having distinct characteristics and certain tasks within the SM. This section gives a short explanation of these three ingredients.

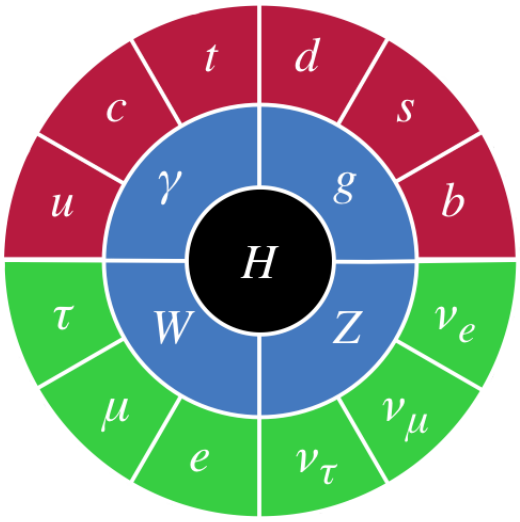

Figure 3.1: Scheme of the particle content of the SM [18]. Quarks are depicted in red, leptons in green, bosons in blue and the Higgs boson in black.

From the outer to the innermost ring:

- Fermions (f): fundamental constituents of matter, grouped into three families, or generations, of leptons (l) and quarks (q) that build the matter sector (cf. page 12)
- Bosons: carriers of fundamental forces as described in the force sector of the SM (cf. page 13)
- Higgs Boson: a consequence of the mechanism that generates the particle masses (cf. page 15)

Matter sector

In the SM, the matter sector consists of spin $\frac{1}{2}$ particles, the fermions which are divided into two different groups, the leptons and the quarks. Leptons have an electrical charge $Q = \pm 1$ and couple to the electromagnetic interaction. Whereas the quarks with $Q = \pm\frac{1}{3}$ and $\pm\frac{2}{3}$ also interact via the strong force and carry an additional charge, the colour. Both groups of particles couple to the weak force characterised by the weak isospin. In terms of QFT these particles are represented by fermionic fields that form left-handed (LH) isospin doublets and right-handed (RH) isospin singlets, for each of the three generations (cf. Table 3.1). All members of different families interact equally but have distinct flavour quantum numbers. The flavour eigenstates of the LH down-type quarks are mixtures of the mass eigenstates, as described by the Cabibbo-Kobayashi-Maskawa matrix (CKM) [19], thus allowing for CP violating processes. Here the neutrinos form an exception since in the SM they are considered to be massless and, as is known from experiments, are only realized as LH chiral states. In the SM the fermions acquire mass through Yukawa couplings to the Higgs field.

	first generation	*second generation*	*third generation*
leptons	$\begin{pmatrix}\nu^e\\ e^-\end{pmatrix}_L$ e^-_R	$\begin{pmatrix}\nu^\mu\\ \mu^-\end{pmatrix}_L$ μ^-_R	$\begin{pmatrix}\nu^\tau\\ \tau^-\end{pmatrix}_L$ τ^-_R
quarks	$\begin{pmatrix}u\\ d\end{pmatrix}_L$ u_R, d_R	$\begin{pmatrix}c\\ s\end{pmatrix}_L$ c_R, s_R	$\begin{pmatrix}t\\ b\end{pmatrix}_L$ t_R, b_R

Table 3.1: SM fermion fields grouped into three generations of leptons and quarks, respectively.

Force sector

The four elementary forces known in physics are summarised in Table 3.2. Except gravity, all of them are jointly described within the force sector of the SM as interchange of spin 1 particles, the so called force carrier bosons. The strength of each force is defined by the respective gauge coupling. Although these parameters are called "constants", their values depend on the energy scale where a certain interaction takes place.

Interaction	*Range*	*Mediator*	*Source*	*Coupling Constant*
strong	$\leq 10^{-15}$ m	gluon G	colour charge	α_s
weak	10^{-18} m	W- and Z-Boson $W^\pm$, Z^0	weak charge	α_W
electromagnetic	∞	photon γ	electric charge	α_F
gravitational	∞	graviton g	mass	α_G

Table 3.2: Overview of the three fundamental interactions in the SM.

QFT description of interactions:

Mathematically the interaction between the force carriers and the matter constituents listed above is described in terms of a Lagrangian formulation. Hereby bosons and fermions occur as quantisations of the fundamental fields involved in a spontaneously broken gauge theory with the gauge group structure $SU(3)_C \otimes SU(2)_L \otimes U(1)_Y$. The index refers to the charge that is the generator of the respective group. Table 3.3 summarises these three gauge groups corresponding to the three local symmetries of the SM and lists the respective fields and generators. As will be explained below, the $SU(3)_C$ describes the strong interaction and $SU(2)_L \otimes U(1)_Y$ represent the unbroken symmetry of the unified electroweak interaction. In particular, the symmetry of $SU(2)_L$ is the invariance under local rotations of the weak isospin. The index L indicates that this transformations act on the LH fermions. $U(1)_Y$, the electromagnetic part of this unified gauge group, is the local symmetry with respect to the hypercharge Y.

Gauge Group	*Charge*	*Gauge Fields*	*Coupling Strength*
$SU(3)_C$	color	G^a_μ (gluon color octet $a \in [1, 8]$)	g_s
$SU(2)_L$	weak isospin	W^i_μ (iso triplet $i = 1, 2, 3$)	g
$U(1)_Y$	hypercharge	B_μ	g'

Table 3.3: Overview of SM gauge groups and their corresponding fields.

Electromagnetic interaction: The QFT that describes the electromagnetic interaction is the quantum electrodynamics (QED), a gauge theory with the Lagrangian (3.1) being invariant under transformations of the symmetry group $U(1)_{EM}$ generated by the electric charge Q.

$$\mathcal{L}_{QED} = -\frac{1}{4}F_{\mu\nu}F^{\mu\nu} + i\bar{\Psi}\gamma^\mu\Psi - m\bar{\Psi}\Psi + e\bar{\Psi}\gamma^\mu A_\mu\Psi \tag{3.1}$$

Where $F_{\mu\nu} = \partial_\mu A_\nu - \partial_\nu A_\mu$ is the electromagnetic field strength tensor and Ψ denotes the field spinor of the Dirac fermions, e.g. the spinor of the electron positron field. From left to right the terms represent the kinetic energy of the free field, the kinetic energy of the free fermion, the rest mass of the free fermion and the interaction with the electromagnetic field A_μ. The Lagrangian contains no mass term of the form $mA_\mu A^\mu$ which would violate the gauge invariance, hence the corresponding particle, the photon is massless.

Strong interaction: In a very similar way the strong interaction can be described within the quantum chromodynamics (QCD) that is invariant under $SU(3)_C$ symmetry group generated by the colour charge C (3.2).

$$\mathcal{L}_{QCD} = -\frac{1}{4}G^a_{\mu\nu}G^{\mu\nu}_a + \bar{q}(i\gamma^\mu\partial_\mu - m)q - g_s(\bar{q}\gamma^\mu T_a q)G^a_\mu \tag{3.2}$$

$G^a_{\mu\nu} = \partial_\mu G^a_\nu - \partial_\nu G^a_\mu - g_s f_{abc} G^b_\mu G^c_\nu$ is the field strength tensor of the gluonic field, with the structure constants f_{abc} and the coupling strength g_s. Furthermore q denotes the quark field in a vector representation in colour space. The terms of the QCD Lagrangian are similar to the one describing QED. But there is a difference in the definition of the field strength tensor, namely its third term. In fact this third term, which contains the non-derivative field, results in interactions among the gluons themselves. The last term in Equation 3.2 which describes the interaction between the gluons and the quarks involves the eight matrices T_a which form the algebra of the $SU(3)$.

The quantisation of the gluonic field $G^a_{\mu\nu}$ leads to eight massless gluons that mediate the interaction between the quarks. Again, the construction of a mass term would violate the local gauge symmetry and is therefore forbidden.

Electroweak interaction: The same approach of constructing a gauge invariant Lagrangian is used with the symmetry group $SU(2)_L$ generated by the weak isospin I_3. As proposed by

Gell-Man and Nishijima this charge is related to the electrical charge via $Y = 2(Q - I_3)$ where Y denotes the so called hypercharge that generates the $U(1)_Y$. As already mentioned above (cf. Table 3.1) the LH fermionic fields, transform as $SU(2)_L$ doublets and the RH ones as $SU(2)_L$ singlets, whereas the $U(1)_Y$ applies to all fermions in the same way. This gauge theory of electroweak interaction, which unifies electromagnetic and weak interactions, based on the $SU(2)_L \otimes U(1)_Y$ symmetry, is known as the Glashow-Salam-Weinberg theory. This model contains three massless gauge fields for the $SU(2)_L$ with coupling strength g and one for the $U(1)_Y$ with coupling strength g' (see Table 3.3). Since the third W field and the B field carry the same quantum numbers, they can be linearly combined. This mixing forms the neutral field Z_μ and the photon field A_μ, whereas the first and second W fields form the charged electroweak boson fields $W_\mu^\pm$ (3.3 - 3.5).

$$Z_\mu = \cos\Theta_W W_\mu^3 - \sin\Theta_W B_\mu \tag{3.3}$$

$$A_\mu = \sin\Theta_W W_\mu^3 + \cos\Theta_W B_\mu \tag{3.4}$$

$$W_\mu^\pm = \frac{1}{\sqrt{2}}(W_\mu^1 \mp W_\mu^2) \tag{3.5}$$

Where Θ_W is the Weinberg angle and all particles are still massless. In contradiction it is known from the relatively short range of the weak force, that the mediating bosons must be heavy, whereas the carrier of the electromagnetic force with infinite range is massless. The electroweak symmetry must be broken, which is achieved by spontaneous break down of $SU(2)_L \otimes U(1)_Y$ to $U(1)_{EM}$ under the virtue of the Higgs mechanism.

Higgs sector

In order to introduce the mass terms to the Lagrangian of the SM without destroying the gauge invariance of the theory, the electroweak symmetry has to be broken spontaneously. This is achieved by means of a scalar field, that interacts with itself providing a non vanishing ground state energy. Figure 3.2 depicts the so called "sombrero potential", which describes this kind of symmetry breaking. By interacting with the Higgs field, which is essentially a new degree of freedom, leptons, bosons and quarks gain their masses.

The Lagrangian of such a scalar field is given by (3.6). For simplification the scalar field is chosen to be real thus exemplifying the Higgs mechanism.

$$\mathcal{L}_{scalar} = \frac{1}{2}(\partial\phi)^2 - (\frac{1}{2}\mu^2\phi^2 + \frac{1}{4}\lambda\phi^4) \tag{3.6}$$

Hereby μ denotes the mass parameter and λ is called quartic coupling, the strength of the Higgs self interaction. If $\mu^2 < 0$ and $\lambda > 0$ the minimal value of this potential is non vanishing with a value of $\phi_0 = \sqrt{\frac{-\mu^2}{\lambda}} = v$, thus breaking the electroweak symmetry. Here the ground state of this self-interaction potential is of $v \approx 246$ GeV, which is called the vacuum expectation value (VEV). This ground state value is related to the Fermi coupling constant G_F via the relation

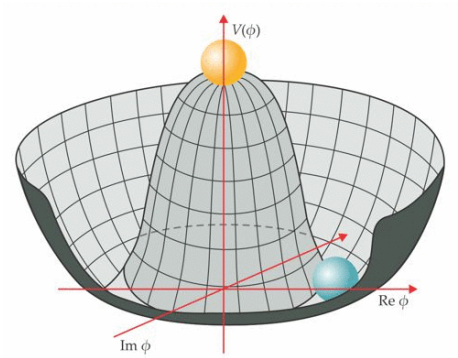

Figure 3.2: Illustration of the Higgs potential [20]. The blue pellet indicates the stable, real and non vanishing ground state, whereas the yellow pellet marks the unstable vanishing VEV.

$v = 1/(\sqrt{2}G_F)$. Thus the ground state of the Higgs field is related to the electroweak scale, defined by the masses of the W- and the Z-boson.

With regard to the quantum fluctuations around the ground state, one adds a small perturbative term to the scalar field: $\phi(x) = v + h(x)$. Therefore the Lagrangian in (3.6) changes to

$$\mathcal{L}_{scalar} = \frac{1}{2}(\partial_\mu h)^2 - \lambda v^2 h^2 - \lambda v h^3 - \frac{1}{4}\lambda h^4 \tag{3.7}$$

This mechanism gives rise to the existence of a massive spin 0 particle, namely the Higgs boson, which can be seen as an excitation of the scalar field. This boson acquires a mass of $m_h^2 = 2\lambda v^2$ through the second term in (3.7).

The actual Higgs field in the SM is given as a complex scalar field which is used to generate the W and Z boson masses. It can be written as

$$\Phi = \begin{pmatrix} \phi^+ \\ \phi^0 \end{pmatrix} \tag{3.8}$$

with a potential of the form

$$V = \mu^2|\Phi^\dagger\Phi| + \lambda(|\Phi^\dagger\Phi|)^2 \tag{3.9}$$

that has its minimum in

$$\langle\Phi\rangle = \frac{1}{\sqrt{2}}\begin{pmatrix} 0 \\ v \end{pmatrix} \tag{3.10}$$

This complex field is again treated within the terms of perturbation theory with small fluctuations around the VEV

$$\langle\Phi\rangle = \frac{1}{\sqrt{2}}\begin{pmatrix} 0 \\ v + H(x) \end{pmatrix} \tag{3.11}$$

This results in mass terms in the basic Higgs Lagrangian, thus the weak gauge bosons acquire masses via gauge coupling (cf. Table 3.4). Where the vanishing mass eigenvalue of the photon is related to the fact that the $U(1)_{EM}$ is a preserved symmetry.

Interaction	*Boson Field*	*Boson*	*Mass*
charged weak	$W^{\pm} = \frac{1}{\sqrt{2}}(W^1_\mu \mp W^2_\mu)$	W^+, W^-	$M^2_W = \frac{1}{4}g^2\,v^2$
neutral weak	$Z^0 = \frac{-g'B_\mu + gW^3_\mu}{\sqrt{g'^2+g^2}}$	Z^0	$M^2_Z = \frac{1}{4}(g^2+g'^2)\,v^2$
electromagnetic	$A_\mu = \frac{g'B_\mu + gW^3_\mu}{\sqrt{g'^2+g^2}}$	photon	$M^2_\gamma = 0$

Table 3.4: Fields and masses of the electroweak bosons in the SM.

On the contrary the fermions interact with the Higgs-field via Yukawa coupling (3.12).

$$\mathcal{L}_Y = Y_f \bar{f} f \Phi \quad \Rightarrow \quad m_f = \frac{Y_f v}{\sqrt{2}} \tag{3.12}$$

There are two different ways of interpreting the Higgs mechanism. On the one hand, from a rather technical or mathematical point of view, this mechanism leads to non vanishing fermion and boson mass-terms, while guaranteeing the gauge invariance and the renormalisability of the Lagrangian theory of the SM. On the other hand, the SM particles gain their masses from constantly interacting with the homogeneous and isotropic Higgs field. These interactions change the mass values in the propagator terms of the scatter amplitudes from zero to non-zero and thus limit the range of the interactions.

Nowadays all the particles predicted by the SM have been experimentally substantiated, whereby the last one was the Higgs boson[1], that was found at the LHC to have a mass of roughly 125 GeV [1, 2]. Hence the SM is one of the most successful theories in the history of physics. It is confirmed by experiments to a high level of precision, at least up to the electroweak energy scale. Nevertheless, it cannot explain all phenomena that exist from the lowest to the highest scales, or better to say it is not valid up to arbitrary high energies. Some of the deficiencies that give rise to the question of what lies beyond the SM are:

Gravity: The fourth of the fundamental forces is not included in the SM at all.

Running of gauge couplings: Gauge couplings depend on the energy scale a certain interaction takes place and are not constants. This behaviour leads to the interesting fact, that the coupling constants of the different forces tend to converge at higher energies. This gives rise to the idea of force unification. If all fundamental forces could be unified at high energies (Grand Unified Theory or GUT), the gauge couplings should coincide at

[1] It is often said that "the Higgs boson" was found, in fact it is more correct to say that a spin 0 particle was found, whose properties are consistent with the SM Higgs predictions.

a certain point, referred to as $m_{GUT} \approx 10^{15}$ GeV. This is not the case if the SM is extended up to higher scales.

Introduction of the Higgs mechanism: The Higgs term is inserted into the Lagrangian in order to break the electroweak symmetry. Thus the choice of $\mu^2 < 0$ and $\lambda > 0$ is driven by this task and cannot be predicted by the theory itself.

The asymmetry between matter and antimatter: According to the well-established Big Bang theory equal amounts of matter and antimatter were produced in the early universe. In contrary the observations today imply a preponderance of matter over antimatter of the order of 10^9 that can not be explained within the SM.

Furthermore there are two major problems, described in detail below, namely the hierarchy problem (cf. subsection 3.1.2) and the problem of dark matter (DM) (cf. subsection 3.1.3).

3.1.2 The Hierarchy Problem

The so called hierarchy problem is the question, why the electroweak scale, defined by the mass of the Z-Boson is so far below the Planck scale (3.13). It is highly intertwined with the problem of naturalness and the sensitivity of SM boson masses to BSM physics, as described below.

$$M_{Planck} = \sqrt{\frac{\hbar c}{8\pi G_N}} \approx 2.4 \times 10^{18} \text{ GeV} \tag{3.13}$$

The SM is an effective QFT. The parameters of this theory can be calculated with the framework of perturbation theory. Whereby one has to take into account higher orders of perturbation corrections, if their contributions are not small enough or if the problem in question is very sensitive to their values. These higher order corrections occur either as vertex corrections or as self energy terms. In the respective Feynman graphs the self energy is represented by virtual particles circling in closed loops, hence the name "loop corrections".

Virtual particles do not have to obey the conservation of energy and momentum, as it holds for real particles. Therefore this procedure offers the problem of divergences that results in unphysical infinities. The concept of renormalisation is the standard technique to get rid of such infinities. Hereby a physical quantity is thought of as the "bare" quantity "dressed" by the virtual processes. This "bare" parameter, i.e. the value of a parameter obtained in the absence of self-interactions, is unmeasurable. The renormalised value is the physical quantity that can be obtained from the experiment.

The SM is renormalisable in principle up to infinite energies, that means that the cut-off scale Λ in the loop integrals (3.14) is not restricted.

$$\int^{\Lambda} d^4k \, f(k, external\, momenta) \tag{3.14}$$

An example within the SM that is often referred to, is the self-energy of the electron. In classical electrodynamics the electron receives a term in the expression for its self-energy, that is linearly divergent with respect to the inverse of the radius. In QED this term is cured by the existence of the positron up to a logarithmically divergent term (3.15), that can be shuffled into the bare mass.

$$\delta m \sim \alpha_F m \ln \Lambda \tag{3.15}$$

This implies that $m \sim \delta m$ even for cut-off scales in the region of the Planck mass (3.13).[2]

If one tries to apply the same deliberations to the self energy corrections of the Higgs boson mass, it turns out that there arises a problem. Considering the "sombrero potential" (cf. Figure 3.2) as it is defined in (3.6) with the minimum of this potential (at tree level) interpreted as the VEV

$$\langle \phi_0 \rangle = \frac{1}{\sqrt{2}} v = \sqrt{\frac{-\mu^2}{2\lambda}} \tag{3.16}$$

where the Higgs mass $m_h^2 = 2v^2\lambda$ is defined by the VEV and the strength of the Higgs self-interaction λ. At one loop-level the four boson interaction contributes to the mass term with a correction proportional to

$$\delta {m_h}^2 \sim \lambda \Lambda^2 \tag{3.17}$$

thus showing a quadratic divergence with respect to the cut-off scale Λ. From the experiment it is known that $m_h \sim 125$ GeV and hence ${m_h}^2 \sim 10^4$. But if the cut-off scale Λ goes up to energies as high as the Planck scale, the one-loop corrections would be of the order 10^{38}. In order to get the right Higgs boson mass after inclusion of the first loop, one has to set the "bare" ${m_h}^2$ to a value comparable to these corrections. This "finely tuned" cancellation seems to be very unnatural. In other words there is no symmetry within the SM that protects the smallness of the Higgs boson mass.

This problem can be solved in a very elegant way if one considers the fermionic loop corrections as well.
Instead of a virtual boson circling the loop a pair of fermion and antifermion can be produce from a scalar boson ϕ and annihilated again. Thus resulting in another quadratic divergent contribution to the mass squared correction

$$\delta {m_h}^2 \sim -Y_f^2 \Lambda^2 \tag{3.18}$$

where Y_f denotes the Yukawa coupling of the respective fermion f. Combining both quadratic divergent terms, the fermionic and the bosonic loop contributions, leads to a correction of the form

$$\delta {m_h}^2 \sim (\lambda - Y_f^2)\Lambda^2 \tag{3.19}$$

Thus, the loop corrections proportional to Λ^2 would vanish, if $\lambda = Y_f^2$ and one would be left with the logarithmic divergent terms of both contributions.

[2] The higher order corrections in QFT are expanded as a power series in the respective coupling constant. In Equation 3.15 this is $\alpha_F \approx \frac{1}{137}$, the *fine structure constant* or coupling constant of electromagnetic interactions.

From these considerations it can be seen, that a symmetry between bosons and fermions could avoid the problem of fine tuning in the sense that it would protect the mass of the Higgs boson (and with it the masses of the W and Z) from growing indecently via quadratically divergent loops in the same way, the chiral symmetry protects the masses of the fermions. This fermion-boson-symmetry, or supersymmetry (SUSY) stabilizes the hierarchy of the scales in a natural way, if the masses of the SUSY partners of the SM particles are not too far away from the weak scale.

What looks like a striking solution to the hierarchy problem causes a new inconvenience. This symmetry is obviously broken, otherwise the SUSY particles would have been discovered already. The mechanism of SUSY breaking is achieved at the cost of numerous new parameters. This vast amount of degrees of freedom can be reasonably reduced in various different SUSY models as described below by the example of the pMSSM (cf. section 3.2).

3.1.3 Dark Matter

From cosmological observations it is known that "visible" matter, i.e. matter as described in the SM, represents only roughly 5% of the universe.[3] The rest is dark matter (DM) and dark energy (cf. Figure 3.3a). All experimental evidences for the existence of DM are based on gravitational interaction.

Observed Evidences for DM

observations by Fritz Zwicky: The first evidence for the existence of DM was discovered as early as 1933 by Fritz Zwicky. He related the velocity of galaxies in a galaxy cluster with its gravitational potential and thus could derive the mass of the cluster. From observations the ratio between the mass and the luminosity of e.g. a star is known. Zwicky however recognized that there was a huge discrepancy between this "mass-to-light ratio" of a star and the value he obtained for the galaxy cluster. Hence he predicted the existence of non luminous matter which contributes to the mass but not to the luminosity of the cluster.

rotational curve of galaxies: Stars in the outer regions of galaxies rotate much faster, compared to the velocity expected from the gravitational force produced by the visible matter only. Figure 3.3b shows an illustration of the observed and expected rotational velocity as a function of the radius. The observed curve can only be explained if the disk of luminous matter forming the galaxy is overlaid by a halo of dark matter.

gravitational lensing: Within the framework of general relativity the attractive force of gravity causes light rays to bend, i.e. gravity acts on the photons. This results in a characteristic distortion of the images of light sources, if there is a high concentration of mass between

[3] A special position is assigned to the neutrinos, which are taken to be massless in the SM. Although observations indicate that neutrinos do have at least small masses, they are still relativistic particles and hence disfavoured as DM candidates.

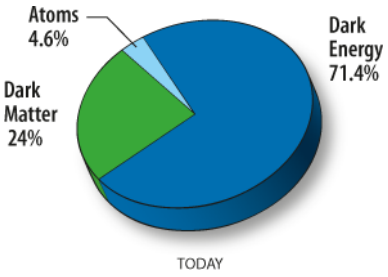

(a) The Segmentation of Matter and energy in the universe at present [21].

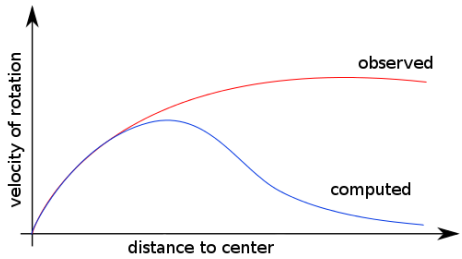

(b) Observed rotational velocity in galaxies as function of the distance to their center[22].

Figure 3.3: Illustration of the balance of matter and energy in the universe (a) and of the rotational velocity of galaxies (b).

the source and the observer. Applying this phenomenon to estimate the mass of galaxies or galaxy clusters, again shows a discrepancy between visible matter and gravitational force.

All these observations point to the existence of an additional source of gravity. Down to the present day the phenomenon of DM is an object of intense studies and its origin is still unclear. The theoretical treatment of DM requires a deep understanding of cosmology that goes beyond the scope of this thesis. Nevertheless the fundamental deliberations for the characterisation of the energy and matter content of the universe shall be outlined in the following section.

Balance of Energy and Matter in the Universe

The fundamental equations to describe space and time in cosmology are Einstein's equations of general relativity. They describe the idea that mass curves the spacetime and follows this curvature. For simplification one can change the underlying metric to describe a homogeneous, isotropic and expanding universe. Using this kind of metric to solve the field equations in general relativity leads to the so called Friedman-equation (3.20).

$$H^2(t) = \left(\frac{\dot{R(t)}}{R(t)}\right)^2 = -\frac{kc^2}{R^2} + \frac{8\pi G}{3}\rho + \frac{\Lambda}{3} \tag{3.20}$$

Where R denotes the scale parameter that increases with the expansion of the universe and H is the Hubble constant that measures the velocity of expansion. The first term in (3.20) describes the curvature of space whereby k can be $-1, 0$ or 1 ("closed", "flat" or "open" universe). The second term represents the density of matter and energy and Λ is the cosmological constant. Further simplification is achieved by dividing (3.20) by H^2 and normalising all densities with a critical value ρ_c to dimensionless parameters $\Omega = \frac{\rho}{\rho_c}$ This leads to (3.21) which describes the balance of matter and energy in the universe.

$$\Omega_0 = \Omega_M + \Omega_\Lambda \tag{3.21}$$

Hereby Ω_0 holds the one $(^{H^2}/_{H^2})$ as well as the curvature term and Ω_M denotes the content of luminous and baryonic matter, DM, neutrinos and radiative energy $\Omega_M = \Omega_B + \Omega_{DM} + \Omega_\nu + \Omega_\gamma$. Conveniently the Hubble constant at present is given by $H_0 = H(t = t_0) = 100h$ km/(sec Mpc) using the dimensionless parameter h, which allows to give all results in units of h and therefore independently of the value of H itself.

Assertions can be made on all these normalised densities by different experimental observations like the cosmic microwave background (measured by e.g. WMAP [23] and the Planck-satellite [24]), the primordial nucleosynthesis, observations on super novea etc. From these and other observations it is known, that about 70% of the total energy density are given by the yet completely unknown dark energy, roughly 25% consist of DM and only 5% can be ascribed to luminous and baryonic matter, i.e. SM matter (see Figure 3.3a).

Characteristics of DM

Regarding all the observations mentioned one could summarise the characteristics of DM as follows:

- non luminous, hence electrically neutral
- cold, i.e. non relativistic
- stable with respect to the lifetime of the universe and therefore non-baryonic, otherwise it would have decayed already
- only weakly interacting because it remains undetected
- massive enough to cause the observed amount of gravitational attraction

It may well be that DM is a single particle species in beyond the SM physics. Surprisingly there is an appropriate candidate for such a particle, namely the lightest supersymmetric particle (LSP) as it would be provided by certain R-parity (cf. Equation 3.24) conserving SUSY theories.

A particle which fulfils all the requirements stated above is called WIMP (weakly interacting massive particle). Its origin can be explained as follows. WIMPs could have been produced in the Big Bang and, because they are assumed to be stable (or at least very long-lived), still be present in the form of a thermal relic. Since the very early universe was in thermal equilibrium and then it cooled down and expanded, the rate of interactions between the particles dropped and the equilibrium was disturbed. This process is referred to as "freeze-out" of the particles. According to this the number density of DM particles has evolved asymptotically to a constant value which is observable today and called the "thermal relic density".

If the LSP is indeed the WIMP and this is the only source of DM, a given SUSY theory should be able to predict the right value for the thermal relic density.

3.2 A Possible Solution - The pMSSM

As indicated above, SUSY could provide a natural way of cancellation of the divergent amplitudes in the loop-corrections of SM particles. Furthermore it could provide a fitting candidate for DM. The basic idea behind all SUSY models is a symmetry between bosons and fermions, hence there is a symmetry transformation that changes the spin of a given particle by $\frac{1}{2}$. These deliberations lead to the prediction of a doubled set of particles (cf. Figure 3.4), where each SM particle gets its SUSY partner. The somewhat unhappy naming convention adds a prefixed "s" to the superpartners of the fermions, e.g. "squark" as partner of the SM quark. Whereas for partners of SM gauge bosons the suffix "ino" is added, thus calling the supersymmetric Higgs boson "higgsino", for example. Except for the spin these have the same quantum numbers as their SM partners. The fact that so far none of these SUSY particles has been found makes it obvious, that SUSY is not an exact symmetry but must be broken.

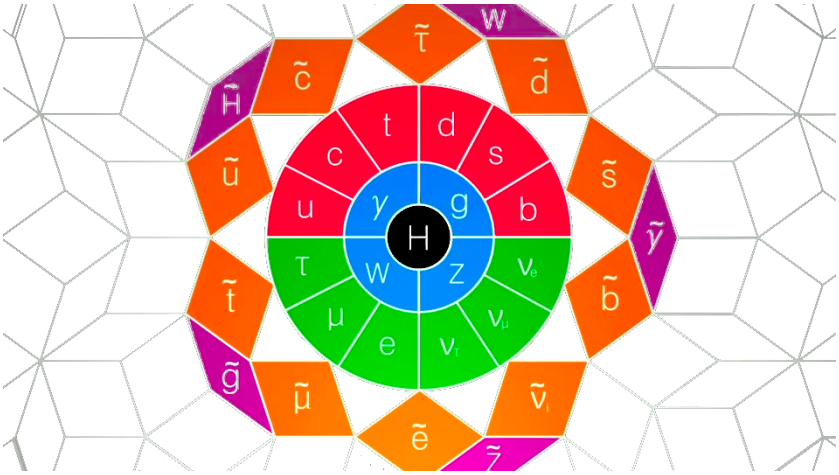

Figure 3.4: Illustration of the SM particles and their SUSY partners embedded in some superior symmetry as shown in the film "Particle Fever" [18].

After a brief discussion of some of the common features of SUSY theories a specific model, the pMSSM, will be described in detail.

General Considerations in SUSY models

The SUSY transformation relates particles that follow different quantum statistics. Fermionic and bosonic fields, that are linked in such a way, form supermultiplets. In general there are two different types, chiral and vector multiplets.

chiral supermultiplet ϕ: Three fields are comprised in this kind of multiplet, a complex scalar field, one Weyl fermion field [4] and a complex field that is non dynamical, i.e. not a propagating field, and hence can be eliminated from the respective Lagrangian. This

[4] Weyl spinors fulfil the relation: $\frac{1-\gamma_5}{2}\psi = \psi$

Lagrangian has one term with a potential that corresponds to the kinetic energy. The second term holds the superpotential of the chiral supermultiplet that describes the Yukawa couplings of the fermionic and the bosonic components of ϕ.

vector supermultiplet: This multiplet corresponds to the SUSY generalization of the SM gauge fields. It also consists of three different fields, one Weyl fermion, the so called "gaugino", one vector gauge field and again a non dynamical real scalar field, that can be eliminated from the Lagrangian.

The important fact that arises from this Lagrangian is that all supermultiplets are mass degenerated if SUSY is unbroken, hence one has to think about ways of breaking the symmetry. In fact there are various mechanisms of spontaneous symmetry breaking but within a low-energy effective QFT this can be achieved by adding explicitly symmetry breaking terms to the Lagrangian.

$$\mathcal{L} = \mathcal{L}_{SUSY} + \mathcal{L}_{soft} \tag{3.22}$$

Hereby $\mathcal{L}_{SUSY}$ holds the unbroken part, i.e. everything that is invariant under supersymmetric transformations. In particular these are the gauge and Yukawa interactions among the supermultiplets. This part of the Lagrangian introduces 19 new parameters according to the 19 parameters of the SM. On the other hand $\mathcal{L}_{soft}$ includes all the terms that are needed to break the symmetry explicitly. These are called "soft terms" which means that they should not spoil the protection of the Higgs mass, or to say the one-loop radiative corrections to the Higgs mass must be of the form

$$\delta m^2 \sim m_{soft}^2 \ln\left(\frac{\Lambda}{m_{soft}}\right) \tag{3.23}$$

with m_{soft} being the typical scale of the SUSY breaking parameters. $\mathcal{L}_{soft}$ comprises a total of 105 new parameters, like the mass terms for the scalar fermions and their trilinear couplings to the Higgs boson, to name but a few. Fortunately in the pMSSM this vast amount of new parameters can be reduced under certain assumptions as described below (cf. subsection 3.2.1).

Supermultiplets in the MSSM

The MSSM is the minimal extension of the SM with respect to the particle content. Like the SM it is a gauge theory with the group structure $SU(3)_C \otimes SU(2)_L \otimes U(1)_Y$. In a first step towards constructing such a model, all the SM fields are extended to supermultiplets. As mentioned above, these are the chiral supermultiplets (cf. Table 3.6) and the gauge supermultiplets (cf. Table 3.5). Left handed and right handed SM fermionic fields form LH Weyl spinors by charge conjugating the RH fields. The SUSY equivalent of the SM Higgs doublet $\begin{pmatrix}\phi_+\\ \phi_0\end{pmatrix}$ is embedded into the H_U with hypercharge $Y = 1$ that couples to the up-type quarks, whereas H_D with $Y = -1$ couples to the down-type quarks. Both complex $SU(2)$ Higgs doublets are necessary in order to avoid gauge anomalies due to their spinor components.

Names	*spin* 1	*spin* $\frac{1}{2}$
gluons, gluinos	g	$\widetilde{\mathsf{g}}$
W bosons, winos	$\mathsf{W}^{\pm}$, W^{0}	$\widetilde{\mathsf{W}}^{\pm}$, $\widetilde{\mathsf{W}}^{0}$
B boson, bino	B	$\widetilde{\mathsf{B}}$

Table 3.5: The gauge multiplets in the MSSM with the SM gauge bosons and their respective SUSY partners, the gauginos.

Names	*Supermultiplet*	*spin* $\frac{1}{2}$	*spin 0*
three families	Q	$\begin{pmatrix}\mathsf{u}_L\\ \mathsf{d}_L\end{pmatrix}$	$\begin{pmatrix}\widetilde{\mathsf{u}}_L\\ \widetilde{\mathsf{d}}_L\end{pmatrix}$
of (s)quarks	$\overline{\mathsf{u}}$	$\overline{\mathsf{u}}_L \sim (\mathsf{u}_R)^c$	$\overline{\widetilde{\mathsf{u}}}_L$, $\widetilde{\mathsf{u}}_R$
	$\overline{\mathsf{d}}$	$\overline{\mathsf{d}}_L \sim (\mathsf{d}_R)^c$	$\overline{\widetilde{\mathsf{d}}}_L$, $\widetilde{\mathsf{d}}_R$
three families	L	$\begin{pmatrix}\nu_L\\ \mathsf{e}_L\end{pmatrix}$	$\begin{pmatrix}\widetilde{\nu}_L\\ \widetilde{\mathsf{e}}_L\end{pmatrix}$
of (s)leptons	ℓ	$\bar{\ell}_L \sim (\ell_R)^c$	$\bar{\widetilde{\ell}}_L$, $\widetilde{\ell}_R$
higgs(inos)	H_U	$\begin{pmatrix}\widetilde{\mathsf{H}}^{+}{}_U\\ \widetilde{\mathsf{H}}^{0}{}_U\end{pmatrix}$	$\begin{pmatrix}\mathsf{H}_U{}^{+}\\ \mathsf{H}_U{}^{0}\end{pmatrix}$
	H_D	$\begin{pmatrix}\widetilde{\mathsf{H}}^{0}{}_D\\ \widetilde{\mathsf{H}}^{-}{}_D\end{pmatrix}$	$\begin{pmatrix}\mathsf{H}_D^{0}\\ \mathsf{H}_D^{-}\end{pmatrix}$

Table 3.6: The MSSM chiral multiplets with their fermionic (spin $\frac{1}{2}$) and bosonic (spin 0) components.

R-Parity

Despite the necessity of two Higgs doublets, the strategy of forming supermultiplets gives rise to another problem that needs to be solved. The gauge invariance of the Lagrangian allows for terms that break the conservation of baryon number B and lepton number L. These terms indicate a possible decay of the proton that is known to be stable with respect to the lifetime of the universe, hence a suitable theory should conserve B and L. To solve this problem a discrete symmetry is introduced, namely the R-parity (3.24).

$$P_R = (-1)^{3(B-L)+2s} \tag{3.24}$$

Due to the spin s in the exponent, all SM particles have even and all SUSY particles odd R-parity. Conservation of this new symmetry has some important consequences. First of all

sparticles can only be produced and annihilated pairwise. This leads directly to the fact, that the lightest supersymmetric particle (LSP) has to be stable. If one considers the LSP to be electrically neutral and only weakly interacting, it is the perfect candidate for being the particle source of DM. In addition this means, that there is a very typical signature for collider experiments, events with missing energy that is carried away by the LSP escaping detection (cf. chapter 4).

3.2.1 pMSSM

As indicated by the prefix *p* for phenomenological, the pMSSM is an approach to reduce the number of parameters via experimentally motivated constraints. The pMSSM mainly relies on certain assumptions:

- There are no new sources for CP violation. Experimental investigations of the electric moment of electrons and neutrons, as well as measurements on the K system, yield constraints on such CP violating sources. Therefore all CP violating phases in the potential of $\mathcal{L}_{soft}$ are set to zero.
- Flavour changing neutral currents (FCNC) are forbidden. In fact most of the new parameters allow for FCNC, e.g. non-diagonal terms in the scalar fermion mass matrices and the trilinear couplings. This is taken into account by assuming these matrices to be diagonal.

Applying these assumptions on the soft terms leaves a total of 19 weak scale parameters as summarised below:

M_1, M_2 *and* M_3 ... gaugino mass parameters

μ *and* m_A ... higgsino mass parameter and pseudo scalar higgs mass

$\tan\beta = \frac{v_U}{v_D}$ ... ratio of the higgs VEVs

A_t, A_b *and* A_τ ... three trilinear couplings for the third generation

$m_{\tilde{f}}$ ... ten scalar fermion mass parameters

Particle content of the pMSSM

Table 3.7 summarises all SM particles and their respective SUSY partners within the pMSSM.

sfermions: The scalar fermions form the largest group of new particles, since there is a SUSY partner for every chirality state of the massive SM fermions. Hereby the index L and R indicate the chirality of the SM fermion a certain sparticle is partnered with. It has to be emphasised again, that the name sfermion is misleading in the sense, that these sparticles are actually bosons. From phenomenological observations it is known that

Names	*mass eigenstates* $(P_R = +1)$	*spin*	*mass eigenstates* $(P_R = -1)$	*spin*
quarks, squarks	$\mathsf{u}_{L,R}$, $\mathsf{d}_{L,R}$, $\mathsf{c}_{L,R}$, $\mathsf{s}_{L,R}$, $\mathsf{t}_{L,R}$, $\mathsf{b}_{L,R}$	$\frac{1}{2}$	$\widetilde{\mathsf{u}}_{L,R}$, $\widetilde{\mathsf{d}}_{L,R}$, $\widetilde{\mathsf{c}}_{L,R}$, $\widetilde{\mathsf{s}}_{L,R}$, $\widetilde{\mathsf{t}}_{1,2}$, $\widetilde{\mathsf{b}}_{1,2}$	0
leptons, sleptons	$\mathsf{e}_{L,R}$, ν_{e_L}, $\mu_{L,R}$, ν_{μ_L}, $\tau_{L,R}$, ν_{τ_L}	$\frac{1}{2}$	$\widetilde{\mathsf{e}}_{L,R}$, $\widetilde{\nu}_{\mathsf{e}_L}$, $\widetilde{\mu}_{L,R}$, $\widetilde{\nu}_{\mu_L}$, $\widetilde{\tau}_{1,2}$, $\widetilde{\nu}_{\tau_L}$	0
gluons, gluinos	g^A	1	$\widetilde{\mathsf{g}}^A$	$\frac{1}{2}$
bosons, eweakinos	h^0, H^0, A^0, $\mathsf{H}^\pm$, $\mathsf{W}^\pm$, Z^0	$0, 1$	$\tilde{\chi}_1^0$, $\tilde{\chi}_2^0$, $\tilde{\chi}_3^0$, $\tilde{\chi}_4^0$, $\tilde{\chi}_1^\pm$, $\tilde{\chi}_2^\pm$	$\frac{1}{2}$

Table 3.7: The particle spectrum in the pMSSM consists of R-parity positive mass eigenstates (the SM particles) and their SUSY partners which have negative R-parity.

interfamily mixings are very small, hence such mixings are not allowed in the pMSSM. Generally speaking all scalar fermions that carry the same quantum numbers (electrical charge, R-parity, colour) can mix via matrices defined by the respective mixing angle θ to form mass eigenstates $\widetilde{f}_1 < \widetilde{f}_2$.

$$\begin{pmatrix} \widetilde{f}_1 \\ \widetilde{f}_2 \end{pmatrix} = \begin{pmatrix} \cos\theta_{\tilde{f}} & -\sin^*\theta_{\tilde{f}} \\ \sin\theta_{\tilde{f}} & \cos\theta_{\tilde{f}} \end{pmatrix} \begin{pmatrix} \widetilde{f}_L \\ \widetilde{f}_R \end{pmatrix} \tag{3.25}$$

With this orthogonal mixing the matrix $\mathbf{M}_{\tilde{\mathbf{f}}}{}^2$ (3.27) in the mass term of the soft Lagrangian (3.26) can be diagonalised.

$$\mathcal{L}_{m(\tilde{f})} = -\begin{pmatrix} \widetilde{f}_L^* & \widetilde{f}_R^* \end{pmatrix} \mathbf{M}_{\tilde{\mathbf{f}}}{}^2 \begin{pmatrix} \widetilde{f}_L \\ \widetilde{f}_R \end{pmatrix} \tag{3.26}$$

$$\mathbf{M}_{\tilde{\mathbf{f}}}{}^2 \approx \begin{pmatrix} M_{(\tilde{f}_L^* \tilde{f}_L)}{}^2 & \propto Y_f \\ \propto Y_f & M_{(\tilde{f}_R^* \tilde{f}_R)}{}^2 \end{pmatrix} \tag{3.27}$$

Because the Yukawa couplings of the first two generations of fermions are neglected, the off-diagonal elements in $\mathbf{M}_{\tilde{\mathbf{f}}}{}^2$ vanish. Hence the LH and RH components of the light flavoured squarks do not mix. In contrary the third generation squarks and sleptons could show substantial mixing due to their large Yukawa couplings. Equation 3.28 explicitly states the mixing matrix of the sbottoms.

$$\begin{pmatrix} m_{Q_3}{}^2 + \Delta_{\tilde{\mathsf{d}}_L} & Y_b v \cos\beta(A_b - \mu\tan\beta) \\ Y_b v \cos\beta(A_b - \mu\tan\beta) & m_{\bar{d}_3}{}^2 + \Delta_{\tilde{\mathsf{d}}_R} \end{pmatrix} \tag{3.28}$$

Whereby the soft masses receive a contribution from electroweak symmetry breaking defined by:

$$\Delta_{\tilde{f}} = (T_{3\tilde{f}} - Q_{\tilde{f}} \sin\theta_W{}^2)\cos(2\beta) m_Z{}^2 \tag{3.29}$$

with $T_{3\tilde{f}}$ and $Q_{\tilde{f}}$ being the third component of the weak isospin and hypercharge, respectively.
In contrary the mixing matrix for the stops involves an additional term equal to ${m_t}^2$. Furthermore the correction $\Delta_{\tilde{\mathrm{d}}_R}$ for the down-type squarks is replaced by the one for the up-type squarks $\Delta_{\tilde{\mathrm{u}}_R}$. Finally in the off-diagonal elements $\sin\beta$ and $\cos\beta$ are interchanged.

$$\begin{pmatrix} {m_{Q_3}}^2 + {m_t}^2 + \Delta_{\tilde{\mathrm{u}}_L} & Y_t v \sin\beta(A_t - \mu\cot\beta) \\ Y_t v \sin\beta(A_t - \mu\cot\beta) & {m_{\tilde{u_3}}}^2 + {m_t}^2 + \Delta_{\tilde{\mathrm{u}}_R} \end{pmatrix} \tag{3.30}$$

.

gluinos: The gluinos occur as colour octet fermion and, since this is a unique behaviour within the pMSSM, they cannot mix with any other multiplet.

Higgs particles: As already mentioned, within the pMSSM there are two Higgs doublets, denoted by H_U and H_D. Each of these doublets comprises four real scalar fields and thus leads to eight degrees of freedom before symmetry braking. Three of these eight are swallowed up by the three SM bosons $\mathrm{W}^{\pm}$ and Z, leaving five degrees of freedom to form five physical scalar particles:

- CP-even scalars h^0, H^0
- CP-odd scalar A^0
- charged scalars H^+, H^-

These are the mass eigenstates which arise through mixing of the gauge eigenstates in the Higgs sector.

neutralinos and charginos: The four neutral gauge eigenstates $\widetilde{H}_U^0$, $\widetilde{H}_D^0$, $\widetilde{\mathrm{B}}^0$ and $\widetilde{\mathrm{W}}^0$ mix to form four neutralinos $\widetilde{\chi}_1^0$, $\widetilde{\chi}_2^0$, $\widetilde{\chi}_3^0$ and $\widetilde{\chi}_4^0$. The index running from one to four indicates the ascending masses of these neutral spin $\frac{1}{2}$ particles. In the 19 parameter pMSSM the $\widetilde{\chi}_1^0$ is considered the LSP.

In the gauge eigenstate basis $\begin{pmatrix} \widetilde{\mathrm{B}} \\ \widetilde{\mathrm{W}}_3 \\ \widetilde{H}_D^0 \\ \widetilde{H}_U^0 \end{pmatrix}$ the mass matrix for the neutralinos can be written as

$$\mathbf{M}_{\widetilde{\chi}^0} = \begin{pmatrix} M_1 & 0 & -m_Z s_W c_\beta & m_Z s_W s_\beta \\ 0 & M_2 & m_Z c_W c_\beta & m_Z c_W s_\beta \\ -m_Z s_W c_\beta & m_Z c_W c_\beta & 0 & -\mu \\ m_Z s_W s_\beta & -m_Z c_W s_\beta & -\mu & 0 \end{pmatrix} \tag{3.31}$$

Whereby the abbreviations $s_W = \sin\theta_W$, $c_W = \cos\theta_W$, $c_\beta = \cos\beta$ and $s_\beta = \sin\beta$ are used. To obtain the actual mass eigenstates $\mathbf{M}_{\widetilde{\chi}^0}$ has to be diagonalized via a unitary matrix $\mathbf{N}$. Hence the ith neutralino mass eigenstate can be described as

$$\widetilde{\chi}_i^0 = N_{i1}\widetilde{\mathsf{B}} + N_{i2}\widetilde{\mathsf{W}}_3 + N_{i3}\widetilde{H}_D^0 + N_{i4}\widetilde{H}_U^0 \tag{3.32}$$

whereby the fractions of the gauge eigenstate are

$$f(\widetilde{\mathsf{B}}) = |N_{i1}|^2, \quad f(\widetilde{\mathsf{W}}_3) = |N_{i2}|^2, \quad f(\widetilde{\mathsf{H}}^0) = |N_{i3}|^2 + |N_{i4}|^2 \tag{3.33}$$

In a similar way, the charged gauge eigenstates $\widetilde{H}_U^+$, $\widetilde{H}_D^-$, $\widetilde{\mathsf{W}}^+$ and $\widetilde{\mathsf{W}}^-$ are mixed into the so called charginos $\widetilde{\chi}_1^\pm$ and $\widetilde{\chi}_2^\pm$. Again the index 1 and 2 sorts the particles according to their masses.

The chargino mass matrix as it occurs in the mass term of the Lagrangian defined in the gauge eigenbasis $\begin{pmatrix} \widetilde{\mathsf{W}}^+ \\ \widetilde{\mathsf{H}}^+{}_U \\ \widetilde{\mathsf{W}}^- \\ \widetilde{\mathsf{H}}^-{}_D \end{pmatrix}$ can be written in block form with the diagonal elements $\mathbf{0}_{2\times 2}$ and the off-diagonal elements (from left to right) $\mathbf{X}$ and $\mathbf{X}^T$, where

$$\mathbf{X} = \begin{pmatrix} M_2 & \sqrt{2}m_W s_\beta \\ \sqrt{2}m_W c_\beta & -\mu \end{pmatrix} \tag{3.34}$$

Hence the mass eigenstates can be obtained via the unitary 2×2 matrices $\mathbf{U}$ and $\mathbf{V}$ according to

$$\begin{pmatrix} \widetilde{\chi}_1^+ \\ \widetilde{\chi}_2^+ \end{pmatrix} = \mathbf{V} \begin{pmatrix} \widetilde{\mathsf{W}}^+ \\ \widetilde{H}_U^0 \end{pmatrix} \qquad \begin{pmatrix} \widetilde{\chi}_1^- \\ \widetilde{\chi}_2^- \end{pmatrix} = \mathbf{U} \begin{pmatrix} \widetilde{\mathsf{W}}^- \\ \widetilde{H}_D^0 \end{pmatrix} \tag{3.35}$$

A more detailed and extended description of the general theory of SUSY and the pMSSM as a particular SUSY model can be found elsewhere [25].

Chapter 4

Searching for SUSY at LHC

Down to the present day none of the sparticles predicted by the pMSSM (cf. subsection 3.2.1) has been found. Nevertheless, if the MSSM is the choice of nature and a "natural" solution to the hierarchy problem exists (cf. subsection 3.1.2), it is believed that there will be experimental evidence in the second run of LHC with $\sqrt{s} = 13$ TeV.

This chapter is dedicated to the experimental search strategies and the current way of interpreting the data, performed by the experimentalists groups at LHC.

4.1 Production and Decay Modes of Sparticles

Within the pMSSM the conservation of R-parity determines the rules of sparticle production and decay in every vertex. Consequently SUSY particles can be produced in pairs only and must decay pairwise. The resultant detector signatures are therefore events with large missing energy, or $\not{E}_T$ (cf. section 4.1.2).

4.1.1 Sparticle Productions

As explained in chapter 2 the LHC is a hadron collider. In such a machine SUSY particles could be produced as pairs in partonic interactions. This results in an inclusive signal of various such interactions that can be divided into two groups:

strong interactions: On the level of partons the LHC can be seen as a gluon gluon, gluon quark or quark quark collider. Figure 4.1a shows the most important Feynman diagramms for the s- and the t-channel for squark and gluino production via gluon-gluon and gluon-quark fusion. This group of production modes is the dominant one at the LHC and its

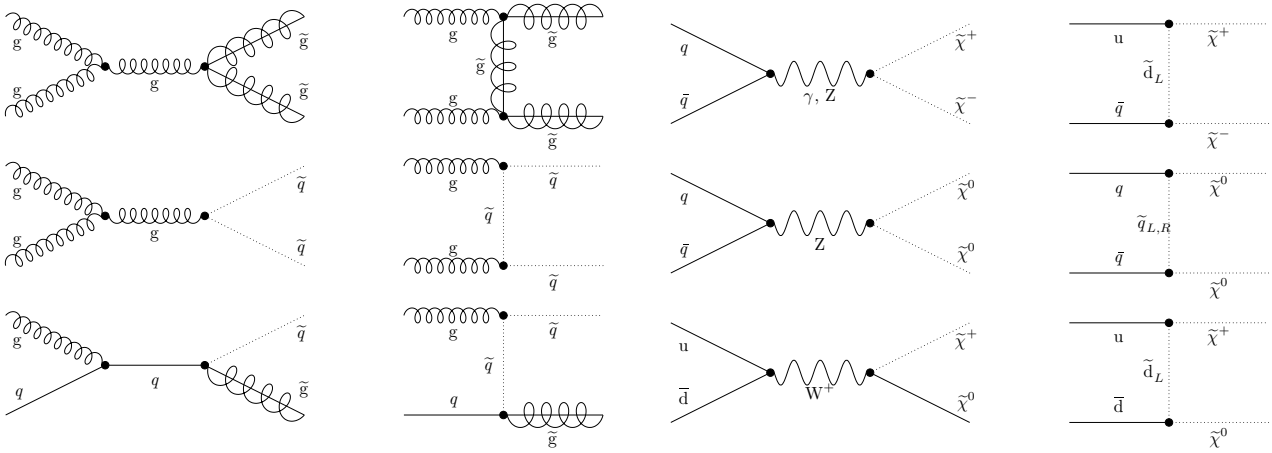

(a) production of gluinos and squarks via gluon gluon and gluon quark fusion.

(b) production of charginos and neutralinos via quark-antiquark annihilation.

Figure 4.1: s- and t-channel Feynman graphs for various strong (a) and electroweak (b) production mechanisms of SUSY particles at the LHC

main processes can be summarised as follows:

$$\begin{aligned} gg &\to \tilde{g}\tilde{g}, \tilde{q}\bar{\tilde{q}} \\ gq &\to \tilde{g}\tilde{q} \\ q\bar{q} &\to \tilde{g}\tilde{g}, \tilde{q}\bar{\tilde{q}} \\ qq &\to \tilde{q}\tilde{q} \end{aligned} \tag{4.1}$$

electroweak interactions: Chargino and neutralino production from quark-antiquark annihilation is an additional possibility (cf. Figure 4.1b). Which specific channel has the highest production cross section is determined by the nature of the involved chargino and neutralino[1] (as this effects the couplings to various bosons) and by the respective kinematics. Collisions with electroweak interactions could also result in the production of charged and neutral sleptons:

$$\begin{aligned} q\bar{q} &\to \tilde{\chi}^{\pm}\tilde{\chi}^{\mp},\ \tilde{\chi}_2^0\tilde{\chi}_2^0,\ \tilde{\ell}^{\pm}\tilde{\ell}^{\mp},\ \tilde{\nu}_L\tilde{\nu}_L \\ u\bar{d} &\to \tilde{\chi}^{+}\tilde{\chi}_2^0,\ \tilde{\ell}_L^{+}\tilde{\nu}_L \\ d\bar{u} &\to \tilde{\chi}^{-}\tilde{\chi}_2^0,\ \tilde{\ell}_L^{-}\tilde{\nu}_L \end{aligned} \tag{4.2}$$

[1] i.e. the fraction of the gaugino content in the respective eweakino

Furthermore, there may be as well an associated production of a chargino or neutralino with a squark or gluino. This channel can be quite relevant in certain regions of the pMSSM parameter space, as will be discussed in chapter 6.

4.1.2 Sparticle Decays

To understand the event signatures expected for a R-parity conserving (RPC) pMSSM with a neutralino LSP, it is necessary to also look at the possible decay modes of the sparticles. Which decay channels are open and favoured fundamentally depends on the kinematics of the involved SUSY and SM particles and the nature of the SUSY particles.

Eweakinos: The admixture of the electroweak gaugino eigenstates ($\widetilde{\mathrm{W}}^{\pm}$, $\widetilde{\mathrm{W}}^{0}$ and $\widetilde{\mathrm{B}}$) results in pursuant couplings to weak interactions, thus controlling the branching ratios for the decays depicted in Figure 4.2. Depending on the underlying kinematic relations, the intermediate bosons, that can be scalar fermions or SM vector bosons, are either on-shell or off-shell.

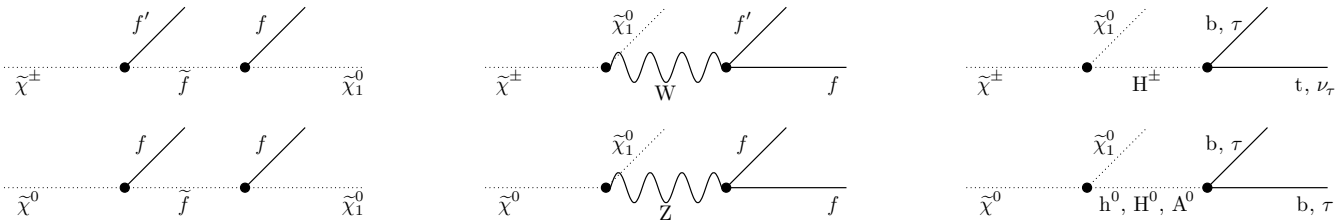

Figure 4.2: Possible decays for neutralinos and charginos with the lightest neutralino as LSP, depicted as Feynman diagrams. The eweakinos decay either as two body decays if the intermediate bosons are on-shell or via three body decays for off-shell scalar and vector bosons, respectively. f and f' denote fermions which belong to the same $SU(2)$ multiplet and f incorporates l plus q.

For eweakinos with considerable large higgsino admixtures, the possibility of decays into third generation quark-squark pairs can be heavily augmented by the Yukawa coupling of the top to the neutral higgsino gauge eigenstate. This, of course, is only possible if the respective decay is an open channel, i.e. allowed by kinematics. If the chargino and neutralino in question are light in comparison to the rest of the sparticles, it may well be that not a single two body decay is allowed, hence the only remaining modes are three body decays.

Gluinos: The only possibility for gluinos to decay within the pMSSM is via real and virtual squarks (cf. Figure 4.3). If the masses of the gluino and the squark are not decoupled and therefore the squark is on-shell, the decay $\widetilde{\mathrm{g}} \to \widetilde{q}q$ is dominant, due to the fact that the coupling of squark, gluino and quark has QCD strength. Here $\widetilde{q}$ denotes all three families of squarks but in fact, in the pMSSM the stop ($\widetilde{\mathrm{t}}$) and sbottom ($\widetilde{\mathrm{b}}$) are usually

considered to be the lightest squarks. This consideration is driven by the fact that the reach of the LHC is still low for stops and sbottoms. Hence, the two body decay channel for gluinos will most likely proceed via an on-shell third generation squark ($\widetilde{\mathrm{g}} \to \widetilde{\mathrm{t}}\mathrm{t}$ and $\widetilde{\mathrm{g}} \to \widetilde{\mathrm{b}}\mathrm{b}$). Certainly the intermediate squarks will decay further. This can lead to long and complicated cascade decays.

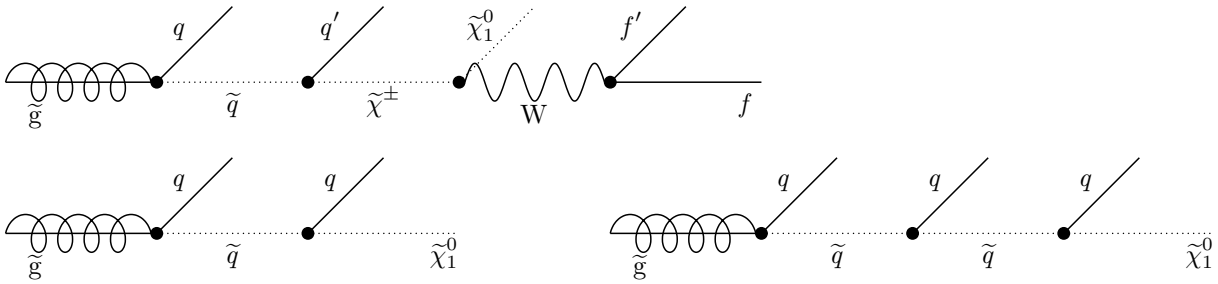

Figure 4.3: Small selection of accessible gluino decays with the lightest neutralino as LSP, depicted as Feynman diagrams. The cascades can be arbitrarily long. Depending on the respective kinematical relations, the intermediate particles can be on- or off-shell.

Squarks: Similar to the gluinos, the squarks will decay dominantly via $\widetilde{q} \to \widetilde{\mathrm{g}}q$ if kinematically allowed. Again this behaviour is accounted for by QCD strength of the $\widetilde{q}$-$\widetilde{\mathrm{g}}$-q coupling. In the decoupling limit ($m_{\widetilde{\mathrm{g}}} \gg m_{\widetilde{q}}$), however, the main decays are of the form $\widetilde{q} \to \widetilde{\chi}^0 q$ and $\widetilde{q} \to \widetilde{\chi}^{\pm} q'$.

Sleptons: Since SM leptons are typically very light and due to the slepton couplings to the gauginos, the two body decays $\widetilde{\ell} \to \ell\widetilde{\chi}_1^0$ and $\widetilde{\ell} \to \nu\widetilde{\chi}_1^{\pm}$ are almost always kinematically allowed and favoured. Hereby, the LH sleptons couple to $\widetilde{\mathrm{W}}$ and $\widetilde{\mathrm{B}}$, whereas the RH couple only to $\widetilde{\mathrm{B}}$. Hence, the left handed sleptons may prefer to decay via chargino instead direct decay to the LSP. This can be understood from the fact, that the coupling to $\widetilde{\mathrm{W}}$ is proportional to the $SU(2)$-coupling strength which is higher than the $\widetilde{\mathrm{B}}$-related $U(1)$-coupling.

Transverse Missing Energy:

Due to RPC all decays which can be interpreted as pMSSM processes result in final states with two LSPs, e.g. two neutralinos, that escape undetected. In principle these two sparticles carry two times the mass of the lightest neutralino ($\widetilde{\chi}_1^0$), that would be missing in the energy balance of such a process. However, at a hadron collider like the LHC experimentalists measure a component called transverse missing energy ($\not{E}_T$ or MET). This is the part of the total missing energy which represents the momenta transverse to the beam. Considering the possible decays described above, the signals involving supersymmetric particles can be generally characterised as n leptons, m hadronic jets and MET. Unfortunately there are prominent SM processes that result in similar final states and hence represent a large background for these signals.

In particular decays of W and Z bosons, that often involve undetectable neutrinos, are such background contributions. These have to be suppressed by choosing smart search strategies and cuts on the signal region. Several of these search strategies, developed by the ATLAS- and CMS-collaboration are summarised in the following section.

4.1.3 Search Strategies at the LHC

The search strategies described in this section are explained in greater detail in [26] and in the corresponding analysis notes given in Table 5.1. The ATLAS- and the CMS-collaboration have developed very similar search strategies and have published akin interpretations for the data collected in LHC run 1. This and all sections below will follow the CMS naming convention for analysis classification and SMS topologies, explained in subsection 4.2.2, whereby no claim to completeness is raised. As mentioned above, the common target of all these experimental analyses is the detection of signals involving the production of new particles, which decay into final states with $\not{E}_T$ and SM particles.

Hadronic Analysis: Selected events have two or more jets with a very high transverse momentum (p_T) and reasonably large MET. For reduction of the background contributions from top-antitop, W and Z production there is a veto on isolated leptons. Several different variables can be used to perform hadronic analyses, e.g. α_T [27], $\not{H}_T$ [28] or M_{T2} [29]. This type of analyses is especially suitable for squark and gluino searches.

Single Lepton Searches: The event selection concentrates on isolated high p_T leptons accompanied by jets plus $\not{E}_T$ and can be further classified by the number of jets and b-tagging [2]. Single lepton searches are most sensitive to processes which involve the production of W bosons, e.g. chargino decays.

Opposite and Same Sign Dileptons: These analyses require explicitly events with two leptons, that are either equally charged (same sign SS), or have different charges (opposite sign OS). Background contributions are suppressed in various ways, e.g. by using special kinematic variables or an artificial neural network (ANN) for signal background separation. This class of analyses is applicable to e.g. neutralino decays involving Z bosons (OS) or direct slepton production.

Multilepton Searches: Events are selected that have three or more leptons plus jets. One possibility to reduce the top-antitop background is to reject b-tagged jets. Multilepton searches are sensitive to e.g. decays of eweakinos via sleptons which produce leptons in the final state.

Inclusive Searches: Inclusive analyses incorporate various event selections. One example is the "razor analysis" [30] which exploits a variable that measures the ratio of the mass of the jets to the transverse mass. Generally an inclusive search strategy is not specialised

[2] a jet which is identified as originating from a bottom quark

in a certain channel. Roughly speaking it rather searches for any kind of excess above the SM background.

4.2 The Simplified Models Approach

All the different search strategies, described above, are used to discriminate a possible SUSY signal from the SM background. The data collected this way is given in terms of event counts and can be seen as "raw material" that has to be interpreted further. A standard technique for interpreting these event counts is the framework of simplified models spectra (SMS).

4.2.1 Basic Concepts of SMS

The outcome of any search at LHC is the number of observed events N_{obs}, which includes the SM background. Hence the number of events which stem from the BSM process can be written as $N_{signal} = N_{obs} - N_{SM}$. The resultant event counts N_{signal} can be described dependent on several physical quantities according to Equation 4.3.

$$N_{signal} = L \times (\mathcal{A} \times \epsilon) \times (\sigma \times BR) \tag{4.3}$$

Whereby:

$\boldsymbol{L}$: the integrated luminosity as described in section 2.1.1

$\boldsymbol{\mathcal{A}}$: the acceptance is a geometrical quantity that depends on the architecture of the detector describing the fraction of events which actually reach the detector

$\boldsymbol{\epsilon}$: the efficiency represents the ratio of the number of events that pass a certain analysis' criteria to the total number of events impinging on the detector

$\boldsymbol{\sigma}$: the production cross sections of the involved BSM mother particles assumed to be produced in the primary vertex

$\boldsymbol{BR}$: the branching ratios for the decays of the mother particles that have to be considered in the chosen BSM scenario

$(\sigma \times BR)$ is a function of the masses of the involved BSM states and hence a model dependent quantity. It links the measured event counts to the BSM scenario regarded by the analysis.

A general BSM model usually predicts numerous observables e.g. a full mass spectrum of SUSY particles and their decay patterns. In principle the experimental data can be applied to exclude particular regions of the parameter space of such a model. However this procedure is highly sophisticated and demands much CPU time. Fortunately the phenomenologies predicted by a wide range of different models that may be based on SUSY or other BSM scenarios are very similar. This gives rise to the simplified models interpretation of the data obtained at LHC's experiments.

In principle different decay modes can contribute to N_{obs} for a given analysis. In order to interpret N_{obs} in terms of physical parameters, the simplest decay chain can be chosen.[3] Consequently, a reduced set of BSM particles is assumed to be light, whereas all other BSM states are decoupled, i.e. their masses are set to very high values. Furthermore all branching ratios are set to zero except the one representing this simplest decay which is then 100%. Such a configuration - production of very few mother particles plus their assumed decays - is called a simplified model.

Within the SMS formulation the event counts can be interpreted in terms of one specific simplified model. Hence $(\sigma \times BR)$ in Equation 4.3 can be replaced by $(\sigma \times BR)_{SMS}$. In the simplest case this is a function of the mother and the daughter particle.

$$N_{signal} \simeq L \times (\mathcal{A} \times \epsilon) \times (\sigma \times BR)_{SMS} \tag{4.4}$$

This expression can be used to derive $(\sigma \times BR)_{SMS}$ of the notional mother particle. Therefore it is transformed into

$$(\sigma \times BR)_{SMS} \simeq \frac{N_{signal}}{(\mathcal{A} \times \epsilon) \times L} \tag{4.5}$$

The integrated luminosity is known from the experiment, whereas the experimental quantity $(\mathcal{A} \times \epsilon)$ has to be determined. Therefore this value is calculated for several masses of the mother and the daughter particle using Monte Carlo (MC) simulations, thus yielding a so called efficiency map (cf. Figure 4.4a). Hence in every point of this efficiency map the $(\sigma \times BR)_{SMS}$ is known (cf. Equation 4.5). From this in each point an upper limit on the production cross section σ_{UL} can be derived on the base of statistical 95% confidence level (C.L.) following prescriptions such as [31]. These σ_{UL} are presented as upper limit (UL) maps (cf. Figure 4.4b).

Each entry in such an UL map can be compared with the theoretical prediction for its value. A certain point in the mass plane is excluded by the simplified model, if the derived σ_{UL} is below its theoretical prediction. Thus the excluded region in the respective mass plane is obtained. These exclusions are often indicated by so called "exclusion lines" or "exclusion contours" that are plotted on top of the related UL map (cf. Figure 4.4b).

A listing of the most common so called simplified model topologies, as used in current ATLAS and CMS analyses, is given below.

[3] arbitrary complications of these simplest decay chains are now under consideration for the next run of LHC with $\sqrt{s} = 13$ TeV

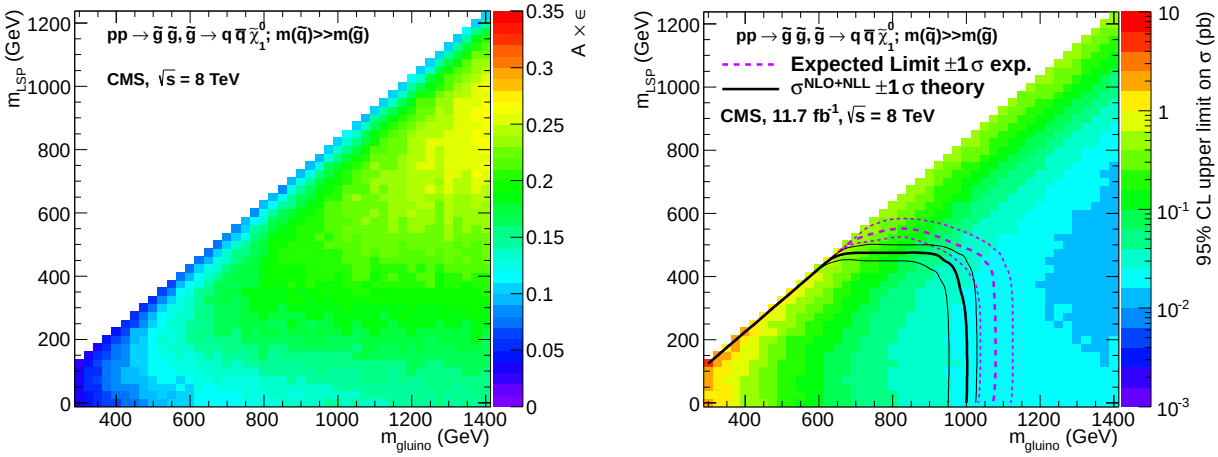

(a) Efficiency Map

(b) Upper limit map

Figure 4.4: Example for efficiency map (a) and upper limit map (b) for a simplified model with $\tilde{g} \rightarrow q\bar{q}\tilde{\chi}_1^0$ in the $m_{\tilde{g}} - m_{\tilde{\chi}_1^0}$ mass plane. [27]

4.2.2 SMS Topologies

Since the development of the SMS framework at LHC, the topologies used by the two collaborations were constantly enhanced to best meet the requirements of the experimentalists' and the theorists' community. This section lists a small sample of the most common simplified models, following the CMS naming convention. In general a simplified model, or topology, is named "TNx". Where *T* states that it is an SMS topology, *N* usually is an odd (gluino-production) or even (squark-production) number that indicates the length of the decay chain, but if necessary it refers directly to the produced particle (e.g. *Chi* for neutralino production). The suffixed *x* may be left out and is used to denote eventual SM final states to prevent ambiguity.

Gluino Topologies: Every topology with an odd number in its name, refers to a pair production of gluinos decaying via off-shell squarks, as summarised in Table 4.1. All squarks are assumed to be decoupled and the two light flavoured quark families are not distinguished.

TNx	*Decay*
T1	$\tilde{g} \rightarrow q\bar{q}\tilde{\chi}_1^0$
T1tttt	$\tilde{g} \rightarrow t\bar{t}\tilde{\chi}_1^0$
T1bbbb	$\tilde{g} \rightarrow b\bar{b}\tilde{\chi}_1^0$
T5ZZ	$\tilde{g} \rightarrow t\bar{t}\tilde{\chi}_2^0 \rightarrow Z\tilde{\chi}_1^0$

Table 4.1: Examples for gluino topologies.

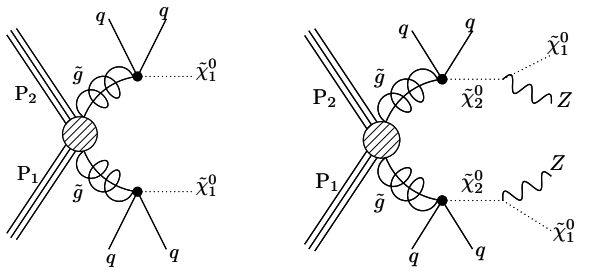

Figure 4.5: Feynman diagrams for T1 and T5ZZ.

Squark Topologies: Topologies with even numbers assume pair production of squarks, that decay further. Table 4.2 shows possible appearances of such decay chains. Again the two light flavoured quark families are taken as mass degenerate and the gluino is in the decoupling regime ($m_{\tilde{g}} \gg m_{\tilde{q}}$).

TNx	*Decay*
T2	$\tilde{q} \to q\tilde{\chi}_1^0$
T2tt	$\tilde{t} \to t\tilde{\chi}_1^0$
T2bb	$\tilde{b} \to b\tilde{\chi}_1^0$
T6bbWW	$\tilde{t} \to b\tilde{\chi}^\pm \to W\tilde{\chi}_1^0$
T6ttWW	$\tilde{b} \to t\tilde{\chi}^\pm \to W\tilde{\chi}_1^0$

Table 4.2: Various squark topologies. The intermediate W boson can be on- or off-shell.

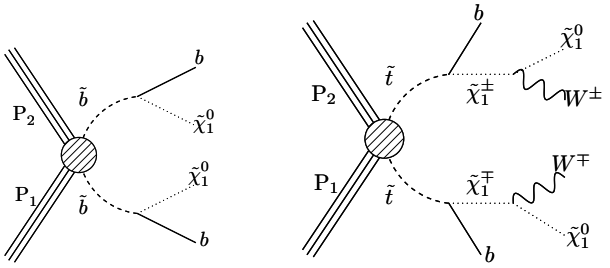

Figure 4.6: Feynman diagrams for T2bb and T6bbWW.

Eweakino Topologies: If the topology name contains no numbers but "Chi" instead, it considers direct production of neutralinos and/or charginos, whereby in the case of charginos the sign of the charges is stated explicitly if necessary (cf. Table 4.3). The produced eweakinos undergo diverse decay chains having mostly leptonic final states or such with on- or off-shell SM bosons. Hereby the capital "L" in the name of the topology, e.g. in "TChiChipmSlepL", stands for all three generations of leptons, whereas "l" indicates the first two families only.

TNx	*Decay*
TChiWW	$\tilde{\chi}^\pm \to W\tilde{\chi}_1^0$
TChiWZ	$\tilde{\chi}^\pm \to W\tilde{\chi}_1^0$
	$\tilde{\chi}_2^0 \to Z\tilde{\chi}_1^0$
TChiChipmSlepL	$\tilde{\chi}^\pm \to L\tilde{L} \to L\tilde{\chi}_1^0$
	$\tilde{\chi}_2^0 \to L\tilde{L} \to L\tilde{\chi}_1^0$

Table 4.3: Example eweakino topologies with decays either directly to W and Z, or via intermediate slepton ($\tilde{L}$).

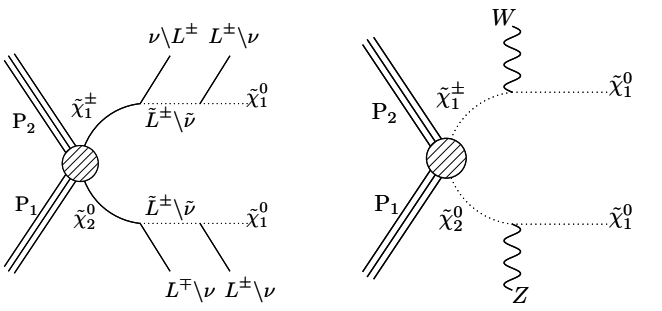

Figure 4.7: Feynman diagrams for TChiChipmSlepL and TChiWZ.

4.2.3 CMS summary plots

One big advantage of the interpretation of experimental data in terms of simplified models is the possibility to present comparisons of different results in an eye-catching fashion. Such a presentation allows to get an impression of the big picture in the sense of which search strategies provide the best constraints on sparticle masses. Various of these so called summary plots [32] were produced for the CMS collaboration. These official summary plots were presented at several international SUSY conferences last of which was ICHEP 2014 [33].

Figure 4.8 presents two examples of these kind of plots, one for a gluino topology and one for a squark topology. The exclusion contours for several analyses are plotted on top of each other. Figure 4.8a shows that the single lepton analysis which requires six or more jets plus MET in addition to a single lepton in the final state (SUS-13-007 [34]) excludes the largest region in the gluino-LSP mass plane for the T1tttt topology. Whereas the summary plot for T2 in Figure 4.8b indicates that the all-hadronic search strategy exploiting the M_{T2} variable (SUS-13-019 [29]) provides the best exclusions for this squark topology. Furthermore the exclusion lines labelled with "one light $\tilde{q}$" depict how the excluded region shrinks, if the light flavoured squarks are not assumed to be degenerated in mass.

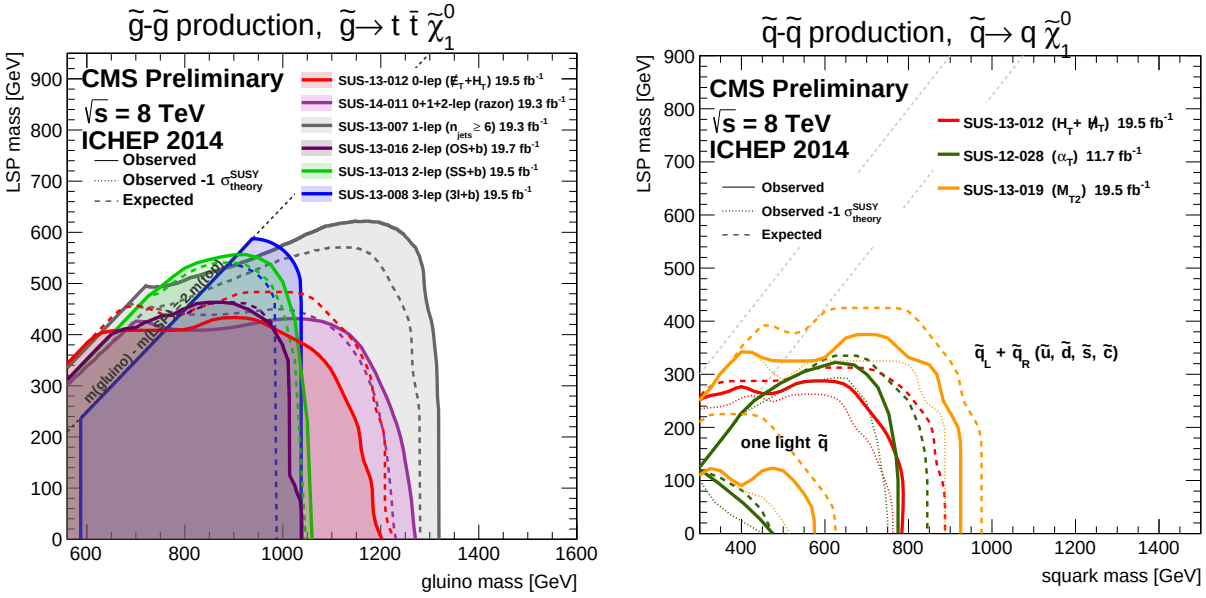

(a) T1tttt (b) T2

Figure 4.8: CMS summary plot for the T1tttt (a) and T2 (b) topologies presented at ICHEP 2014 [32].

In order to facilitate the creation of such plots and to keep them as updated as possible, one needs access to various experimental results. Such a well-resourced compilation of results

is provided by the SModelS-database as described in detail in section 5.3.

These summary plots provide an intuitive insight in the current status of experimental results for SUSY searches. Nevertheless, one has to be careful when using these results. Figure 4.8a indicates that the mass of the gluino cannot be smaller than 1.3 TeV for LSP masses of roughly 0.6 TeV. But at this point it should be emphasized, that this is only applicable if the branching ratio is 100%, as will be shown eventually in chapter 6.

Chapter 5

Connecting Theory and Experiment - SModelS

To date a common way of interpreting LHC limits on the masses of SUSY particles as published by the ATLAS- and CMS-collaboration is based on the concept of simplified models spectra (cf. section 4.2). These effective Lagrangian descriptions consider only a reduced set of sparticles and are based on a definite set of assumptions. Hence such an interpretation is only applicable for a specific topology. On the contrary, a full BSM model defines a set of underlying parameters, e.g. the 19 parameters of the pMSSM, which span the according parameter space within their given ranges. A general model point in this parameter space may incorporate several decay channels, and is therefore sensitive to various SMS topologies. Hence, it is not straight forward to compare such a model point to all applicable SMS interpretations given by the experimentalists. In order to perform this comparison in a quick and convenient way a software package named SModelS was developed and introduced in the original SModelS-paper [35].

Within the scope of this thesis the code of the framework as well as the accompanying results database were restructured, in order to reduce computing time and to fit the needs for publication. After an intense validation procedure the tool was published as SModelS v1.0 [36] at the end of 2014 and has received several updates to date. Further information about the SModelS group, a dictionary for all SMS topologies used within the framework and an extended html-manual can be found on the official SModelS web-page [37].

This chapter gives an overview of the main concepts and functionalities of the software tool. The database which is shipped together with the code is explained in detail, as well as the maintenance work that was necessary to bring it into a publishable format. Finally the validation procedure and the tools developed during this process are introduced.

5.1 Basic Concepts and Motivation

The central assumption within the SModelS framework is, that acceptance times efficiency $(\mathcal{A} \times \epsilon)$ and the kinematics of a process are mainly a function of the BSM masses involved

and do not depend on characteristics such as e.g. spin (cf. section 4.2). Under this SMS assumption it is possible to map the signal of a full BSM model point onto its signal topologies, each of which describes a specific decay, or rather a specific final state. Indeed most of the published interpretations of search results aim at providing model independent constraints.

In principle SModelS can deal with any $\mathbb{Z}_2$-symmetric BSM model. In order to probe such a theoretical model, e.g. an RPC pMSSM model, usually a great number of model points are generated by varying the values of the individual parameters. Such a point in the parameter space can be seen as defined by three basic ingredients:

1. its mass spectrum
2. the production cross sections σ_{prod} of the involved BSM particles
3. the branching ratios BR for all possible decays

If these three ingredients are provided, e.g. in SLHA file format, it is possible to decompose the spectrum of the model point into a set of individual topologies and derive the respective $\sigma_{prod} \times BR$, or "weight" in the SModelS jargon. Thus the theoretical weights predicted by the model can be systematically compared with the UL maps provided by the experimentalists. This basic working scheme is illustrated in Figure 5.1 and will be explained more detailed below by the example of a full pMSSM model point.

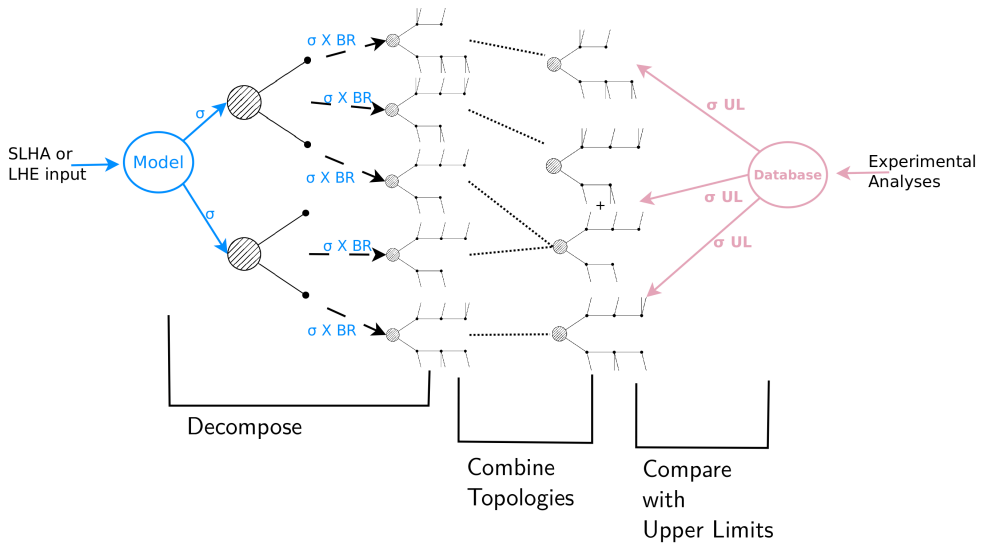

Figure 5.1: Illustration of SModelS' method of operating. The input on the left represents the full theoretical model. Its model points are decomposed into their signal topologies, which are combined and checked against the experimental database, shown on the right [35].

SModelS allows to attain an overview of the status of the current SUSY searches and also helps to identify blind spots in the parameter space, as described eventually in subsection 5.2.5.

5.2 SModelS Functionalities

Following the work flow to probe a given point in the pMSSM parameter space, in this section SModelS' main functionalities will be described step by step.

5.2.1 Input of a Full pMSSM Model Point

In principle SModelS supports two possible input formats for BSM model points, Monte Carlo (MC) based event simulation using the LHE file format and direct usage of decay tables defined in SLHA files. The former needs a MC generation of parton level events which are mapped onto SMS topologies. Unless one simulates a large number of events this method has the disadvantage that the decomposition results are afflicted with high MC uncertainties on $\sigma_{prod} \times BR$. Whereas its big advantage is the suitability for any kind of $\mathbb{Z}_2$-symmetric BSM model. The SLHA based method in contrary is specialised on SUSY models and since this thesis focuses on the pMSSM, shall be described in greater detail.

The desire to have a standard to define a specific SUSY model point and interface between various event generators and spectrum calculators lead to the development of the SLHA file format [38, 39]. SLHA files are structured in blocks, where each block comprises a different type of information. Listing 5.1 shows the block defining the stop mixing matrix.

Listing 5.1: An example SLHA file block containing the mixing matrix for the stops.

```
BLOCK STOPMIX  # Stop Mixing Matrix
  1  1     9.95787700E-01   # cos(theta_t)
  1  2    -9.16889117E-02   # sin(theta_t)
  2  1     9.16889117E-02   # -sin(theta_t)
  2  2     9.95787700E-01   # cos(theta_t)
```

To compute the mass spectrum and the decay patterns for a SUSY model point defined by an SLHA file, a wide range of public codes are available, e.g SOFTSUSY [40], SUSYHIT [41] and SPheno [42] to name but a few. Finally, the production cross sections have to be computed which can be done at leading order (LO) using a MC generator e.g. Pythia [43]. For QCD production modes precision can be (in case of the MSSM must be) increased by computing cross sections at next-to-leading order (NLO) with e.g. PROSPINO [44] and for squarks and gluinos at next-to-leading logarithm (NLL) using for example NLL-fast [45].
An interface to conveniently compute the production cross sections using Pythia 6.4.27 [46] as well as NLL-fast versions 1.2 and 2.1 [45] (see also [47–53]) is incorporated in SModelS v1.0 and all following versions. In addition SModelS uses a modified version of PySLHA [54] to process the input SLHA files. The computed production cross sections can be added to the SLHA file in accordance with the SLHA standard [55], as exemplified in Listing 5.2.

Following this procedure the given model point is defined by its mass spectrum, the branching ratios of the decays and the production cross sections of the SUSY particles. Thus the SLHA file holds all the information necessary to perform the decomposition as described below.

Listing 5.2: Example XSEC block format in an SLHA file for LO and NLL production cross sections.

```
XSECTION  8.00E+03  2212 2212 2 -1000024 1000023 # Nevts: 50000 xsec unit: fb
0  0  0  0  0  0    8.66814281E+01 SModelS 1.0

XSECTION  8.00E+03  2212 2212 2 1000002 1000021 # Nevts: 50000 xsec unit: fb
0  2  0  0  0  0    3.11934668E+02 SModelS 1.0
```

At this point the cross sections and the respective branching ratios are combined to derive the weight ($\sigma_{prod} \times BR$) for all the signal topologies comprised in the BSM model point. Out of this plethora of topologies only those are kept which have weights exceeding a given limit. This limit is denoted $sigmacut$, per default it is 0.03 fb and can be set by the user.

5.2.2 Decomposition

Continuing with the example of a pMSSM model point, once all the detailed characteristics of such a point are incorporated in the SLHA file in form of production cross sections, decay tables and the mass block, it can be decomposed into its signal topologies.

Since SModelS was designed to deal with $\mathbb{Z}_2$-symmetric models, every topology can be described as pair production of BSM particles. Each of these BSM particles decays directly or via a cascade into a final state which consists of SM particles plus a stable BSM state, the LSP. In the case of an RPC pMSSM model point an arbitrary topology may for example look like Figure 5.2a.

To describe such topologies a labelling system was invented which is not only model independent but also terse and clearly structured. This labelling scheme, "constraints" in SModelS language, is general enough to describe all kinds of topologies. Figure 5.2 shows the procedure to obtain a SModelS description - a "constraint" - of a given signal topology. The Feynman graph on the left (cf. Figure 5.2a) depicts the associated production of a sbottom and a gluino. The sbottom decays via top plus chargino which decays further into an on-shell W boson plus the LSP. Whereas the gluino undergoes a three body decay to two bottoms and the LSP.
The constraint for such a topology is constructed employing a system of nested brackets. The overall structure is determined by the two branches demanded by R-parity conservation and written as outer brackets $[[branch\,I], [branch\,II]]$. In the next step an empty bracket is inserted for every vertex in a branch. The topology in Figure 5.2b has two vertices in the first branch and only one in the second, thus resulting in $branch\,I = [\,], [\,]$ and $branch\,II = [\,]$ or inserted $[[[\,], [\,]], [[\,]]]$. In such a way the structure of a given topology is mapped. It is likely that there are several signal topologies of this structure, hence the description has to be specified further by means of the outgoing SM particles in every vertex, like in the case of Figure 5.2b $[[[t], [W]], [[b, b]]]$.

The second information that has to be kept in order to link the topology to the BSM states involved, is the mass vector for each branch. The same overall structure as the nested bracket

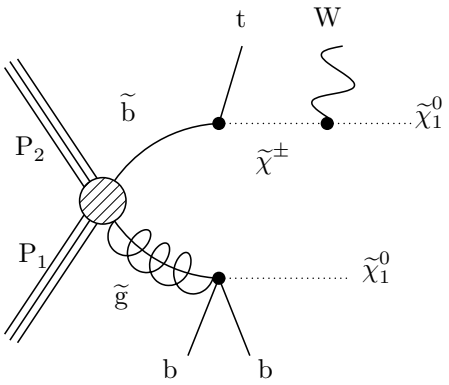

(a) SMS topology for gluino sbottom production with the sbottom undergoing a cascade decay via chargino and on-shell W and the gluino decaying into two bottoms.

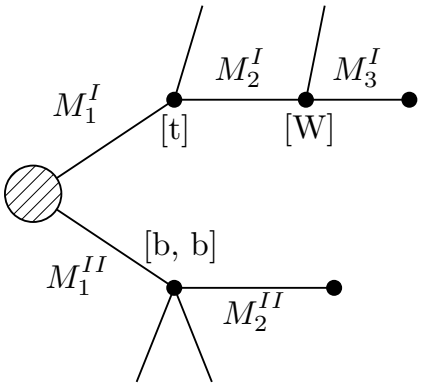

(b) The SModelS equivalent of the SMS topology shown in (a) which is described via the constraint $[[[t],[W]],[b,b]]]$.

Figure 5.2: An arbitrary SMS topology to exemplify the SModelS labelling system.

notation is used, thus the masses are ordered according to the number of the vertices linked by this BSM particle. For the example pMSSM topology in Figure 5.2b the mass vectors would be $[[M_1^I,\ M_2^I,\ M_3^I],[M_1^{II},\ M_2^{II}]]$.

The constraint, the mass vector and the $(\sigma_{prod} \times BR)$ together provide a full characterisation of a topology. In very simple cases, e.g. a stop decay into top plus MET (T2tt), a topology described in such a way can be directly compared with the UL maps stored in the results database.

However, the decay chains can be more complicated, thus more aspects have to be taken into account. First of all, topologies considered by the experimental analyses may encapsulate contributions from several signal topologies which therefore have to be combined (cf. subsection 5.2.3). Additionally, it is possible that the final state contains either very soft or invisible particles. Such a topology is modified by discarding these particles. The process of discarding particles is called "compression":

invisible decays: One example for a topology compressed due to an invisible decay, might well be the one depicted in Figure 5.2a. This is understandable if one assumes, that the final BSM state in the upper branch is not the neutralino one ($\tilde{\chi}_1^0$) but instead a more complex structure. The chargino ($\tilde{\chi}^{\pm}$) for example might decay into a W boson and the second lightest neutralino ($\tilde{\chi}_2^0$), which decays further into the $\tilde{\chi}_1^0$ and a neutrino anti-neutrino pair (cf. Figure 5.3a). This invisible decay will not be taken into account rather the mass of the $\tilde{\chi}_1^0$ will be replaced by the mass of the $\tilde{\chi}_2^0$. In terms of constraints this means that $[[[t],[W],[\nu,\bar{\nu}]],[[b,b]]]$ will be replaced by $[[[t],[W]],[[b,b]]]$. Invisible decays can only be treated this way if they occur at the end of a decay chain, i.e. there is no visible particle after the invisible one.

soft final states: The second situation a compression will take place is that of very soft SM

final states. This is the case if the mass splitting between two BSM states is so small that they can be seen as quasi degenerated. If the energy of the SM particles produced in such a decay is negligibly small from the experimental point of view, the decay will be completely ignored and the respective topology will be replaced by a simpler one. This can be understood if one considers the lower branch of Figure 5.2a. The gluino may decay into the two bottoms and a $\widetilde{\chi}_2^0$ instead of the $\widetilde{\chi}_1^0$ (cf. Figure 5.3b). This $\widetilde{\chi}_2^0$ could decay into an off-shell Z boson and the LSP. Assuming the mass splitting between both neutralinos is below a defined value, the decay products of the Z boson, e.g. an electron positron pair, would be soft enough to not be detected by the experiment and therefore will not appear in the constraint for this topology. The threshold value for the difference between two BSM masses is represented by the parameter $minmassgap$ and can be set by the user explicitly. The default value for this parameter is 5 GeV.

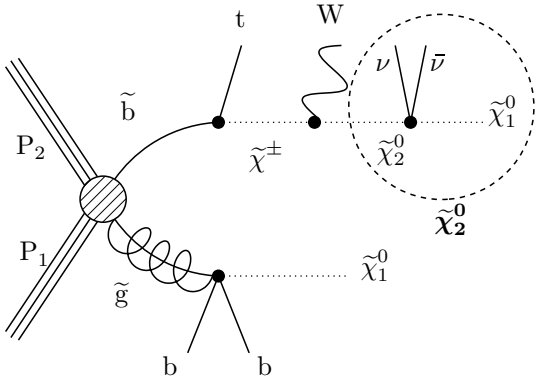

(a) Example for an invisible decay $\widetilde{\chi}_2^0 \to \nu\bar{\nu}\widetilde{\chi}_1^0$ at the end of the decay chain in the upper branch, indicated by the dashed circle.

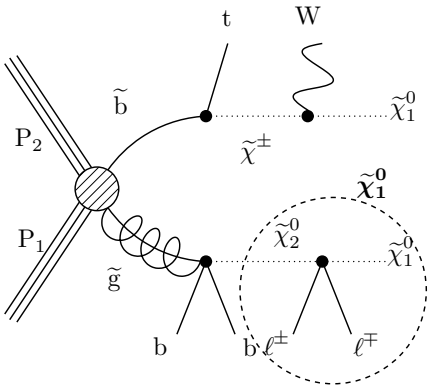

(b) Mass compression exemplified by the decay $\widetilde{\chi}_2^0 \to Z^*_{(lep)}\widetilde{\chi}_1^0$. The very soft decay products of the off-shell Z boson are discarded and the decay in the dashed circle is taken as the LSP.

Figure 5.3: Same signal topology as in Figure 5.2a but with an invisible decay shown in (a) and compressed soft final states illustrated in (b).

The information on the signal topologies in terms of constraints, masses and weights of a given model point can now be used to decide which experimental results can constrain it. To do so, obviously the experimental data has to be described in a similar manner as will be explained in the next section.

5.2.3 Experimental Results Characteristics

As already mentioned, it has become a standard to present experimental results in terms of upper limits on $(\sigma \times BR)$ (cf. section 4.2). Therefore most analyses, which follow specific search strategies and procedures to discriminate signal and background, have results for more than one topology, or "TNx". Consequently in the SModelS' language an analysis denotes

a definite publication, conference note (ATLAS-CONF) or physics analysis summary (CMS-PAS) presenting results interpreted in terms of SMS. In this context a result denotes exactly one UL map. In case a given topology represents a simple one step decay such a result can be used directly by SModelS. It is then defined by a specific combination of an analysis and a topology. On the other hand, in case of topologies which represent decay chains with intermediate masses, a single UL map can not be used. Instead a set of at least two results, or UL maps, is needed in order to interpolate between them. The results comprised in such a set are identified by an analysis-topology pair plus additional information to discriminate between them, as will be explained later.

Figure 5.4 shows two examples for such results, one from ATLAS (cf. Figure 5.4b) and one from CMS (cf. Figure 5.4a). Both plots depict the 95% C.L. UL maps with the observed and expected exclusion contours plotted on top of it. This information is collected in the SModelS-database, as will be described eventually in section 5.3. However, to make use of such results it has to be taken into account that some of them are based on specific assumptions, as shall be exemplified by the two results depicted in Figure 5.4.

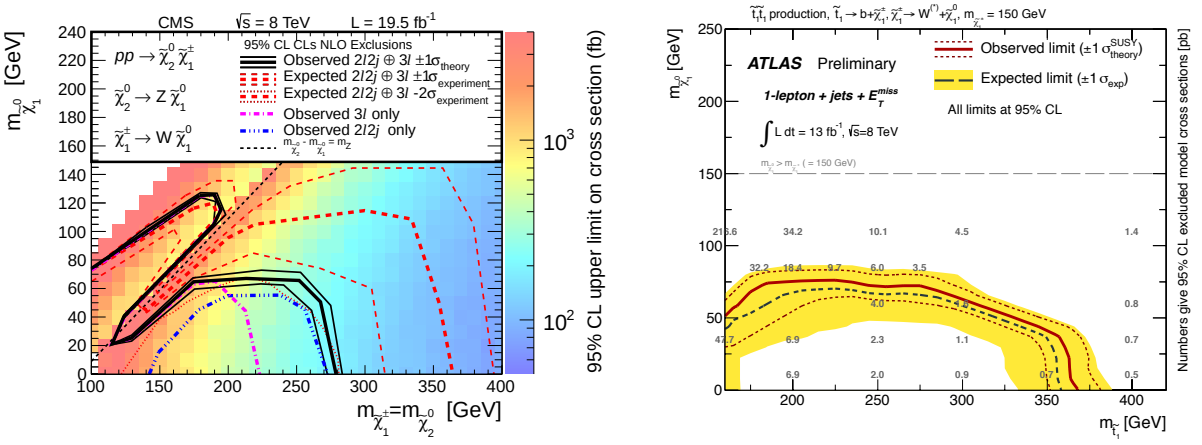

(a) Result plot for the TChiWZ result of CMS-SUS-13-006 [56].

(b) Result plot for the T6bbWW result of ATLAS-CONF-2012-166 [57].

Figure 5.4: Example results from two different experimental analyses. The upper limits on production cross section as function of the BSM masses are depicted by the temperature (a) and the numbers (b), respectively. The excluded regions and the 1σ uncertainty are indicated by the overlaid lines.

Initially the "TNx" considered by a given analysis have to be described in terms of constraints as explained above. For the CMS result depicted in Figure 5.4a the "TChiWZ"-topology in question represents an associated chargino neutralino production, whereby the neutralino decays via an on- or off-shell Z boson into the LSP. The chargino decays in the same way via an on- or off-shell W boson. It is assumed that the masses of the initial chargino and neutralino are degenerated, hence the mass vectors have to represent this fact:

$[[M_1^I,\ M_2^I],[M_1^{II},\ M_2^{II}]] = [[m_{\tilde{\chi}_1^\pm}/m_{\tilde{\chi}_2^0}, m_{\tilde{\chi}_1^0}],[m_{\tilde{\chi}_1^\pm}/m_{\tilde{\chi}_2^0}, m_{\tilde{\chi}_1^0}]]$.

Furthermore, many results incorporate on- and off-shell regions for the involved SM particles, since the detector signal does not change when a particle goes off-shell[1]. Within SModelS , in contrary, the distinction between on- and off-shell regions is stated explicitly in terms of constraints.

Listing 5.3: SModelS' description of the TChiWZ result of CMS-SUS-13-006.

```
constraint: TChiWZ -> [[['W']],[['Z']]]
constraint: TChiWZoff -> 71.*([[['mu+','mu-']],[['l','nu']]] + [[['e+','e-'
    ]],[['l','nu']]])
condition: TChiWZ -> None
condition: TChiWZoff -> [[['mu+','mu-']],[['l','nu']]] > [[['e+','e-']],[['l'
    ,'nu']]]
fuzzycondition: TChiWZ -> None
fuzzycondition: TChiWZoff -> Cgtr([[['mu+','mu-']],[['l','nu']]],[[['e+','e-'
    ]],[['l','nu']]])
axes: TChiWZ: M1 M0, TChiWZoff: M1 M0
```

Listing 5.3 illustrates this by the example of the result depicted in Figure 5.4a. The constraint for the off-shell region, TChiWZoff, describes actually a sum of signal topologies, that can be constrained by this result. The lower case l in $[l, nu]$ denotes the electron and the muon but not the tau which in many analyses is not treated as l lepton since it results in a very different detector signal. For the leptons which stem from the Z decay, the charge is considered to be opposite (OS lepton search). This fact has to be taken into account by stating the lepton charge explicitly. The TChiWZoff example shows that the constraint description of the SMS topology for a given result, is not exclusively defined by its decay. Instead, additional it is driven by specific features of the respective analysis.

The lines initialized with "condition" and "fuzzycondition" in Listing 5.3 take into account another special characteristic of this result. Both light lepton flavours are assumed to contribute equally to the $(\sigma \times BR)$ for TChiWZoff but the detector efficiency for the muons exceeds the one for the electrons. Hence, in order to be more conservative the contribution of the muonic signal topology is assumed to be equal or greater than the electronic one, as indicated by the condition. However this characteristic of the result does not have to be fully satisfied in order to use the result. This conjuncture is taken into account by the fuzzycondition which is a function $Cgtr(signal\ topology\ I, signal\ topology\ II)$ that maps the derived $(\sigma_{prod} \times BR)$ for each signal topology onto the interval $[0, 1]$. Thus $Cgtr()$ is actually a number that gives a quantitative impression of how severely violated the condition assumed by the result is: 0 means full satisfaction and 1 means full violation. It can be decided by the

[1] For example SM bosons are identified by their decay products, the SM fermions. Hence, whether they are on- or off-shell is controlled solely by the kinematics of the respective process. In Figure 5.4a the on- and off-shell regions are obviously differentiated by the form of the exclusion line but for most results this is not the case.

user which level of violation he or she will tolerate by setting the parameter $maxcondition$, which has a default value of 0.2.

As mentioned above, a result denotes the UL map of a given analysis topology combination. These UL maps hold the σ_{UL} as a function of the masses of the BSM states. Hence a result can be addressed unambiguously by the name of the analysis and the "TNx", if the SMS topology involves only two non-degenerate BSM states, i.e. σ_{UL} is a two dimensional function. Such experimental results can be described unambiguously by means of constraints and conditions. Nevertheless the SModelS database contains various analyses which consider topologies involving more than two non-degenerate BSM states. In these cases a set of results is needed that comprises two or more such results. Each of these σ_{UL} is at least a three dimensional function of the BSM state masses. In order to present the individual result as an UL map in a specific two-dimensional mass plane, an additional relation between the three masses is assumed by the experimentalists. Hence, it is necessary to declare this mass parametrisation explicitly. How this is done within SModelS shall be exemplified by the T6bbWW result set from the ATLAS analysis ATLAS-CONF-2012-166. A member of this result set is shown in Figure 5.4b. T6bbWW denotes a stop pair production with symmetric branches. The stop decays into a bottom and a chargino, which decays further into an on- or off-shell W boson and the LSP. It is clear that the mass vectors for both branches are equal and involve three sparticle masses $[m_{\tilde{t}_1}, m_{\tilde{\chi}_1^\pm}, m_{\tilde{\chi}_1^0}]$. The UL map can be given in form of any slice in the mass space spanned by the mass vector.

In Figure 5.4b the UL map is given in the $m_{\tilde{t}_1} - m_{\tilde{\chi}_1^0}$ plane and the value of the intermediate mass is fixed ($m_{\tilde{\chi}_1^\pm} = 150$ GeV). This information is stored in the database under the heading "axes". The axes entry for the ATLAS-T6bbWW result set discussed here is shown in Listing 5.4, together with its constraint and condition.
The token `C150` denotes the fixed value of the intermediate mass, `M1` is the mass of the mother particle on the x-axis and `M0` represents the mass of the LSP, here on the y-axis (cf. Figure 5.4b). The second entry in this axes field, `M1 M0 x200`, refers to a second member of this set which is again given in the $m_{\tilde{t}_1} - m_{\tilde{\chi}_1^0}$ plane. For this result the intermediate mass is assumed to be two times the LSP mass.

Listing 5.4: SModelS' description of T6bbWW result of ATLAS-CONF-2012-166

```
constraint: T6bbWW -> [[['b'],['W']],[['b'],['W']]]
condition: T6bbWW -> None
fuzzycondition: T6bbWW -> None
axes: T6bbWW: M1 M0 C150 - M1 M0 x200
```

The information about the slices of the mass space is necessary to interpolate between the values given by the experimental results. It has to be emphasized again that analyses considering topologies with intermediate BSM states have to provide at least two different slices for each result set to be useful for SModelS.

Generally, there is no common way of slicing in order to obtain the mass planes the UL

maps are given in. Instead the slicing methods used by various analyses show significant differences, as will be described in section 5.3.

5.2.4 Matching Between Signal Topologies and the Experimental Results

At this point the exemplifying pMSSM model point is defined in an SLHA file (cf. subsection 5.2.1) and it is decomposed into its SMS topologies (cf. subsection 5.2.2) which are described in the SModelS language. On the other hand the relevant experimental results are recorded in a similar fashion (cf. subsection 5.2.3). The last remaining step is to confront the model point with the experimental results. As explained above, one result can constrain a sum over signal topologies, rather than a single topology. Therefore it may be necessary to combine these signal topologies of the pMSSM model point, which means to sum up their weights in order to fit the respective result.

In addition it has to be assured that the conditions described above are satisfied, i.e. every combination of topologies for which the fuzzycondition (cf. page 48) exceeds the given $maxcondition$ is discarded. Finally the theoretical predictions for $(\sigma \times BR)_{theory}$ obtained from combining the relevant topologies can be compared to the corresponding upper limit on the theory prediction given by the experimentalists, $(\sigma \times BR)_{experiment}$.

An arbitrary BSM model point for which the predicted weight of at least one topology is greater than the experimental upper limit is considered to be excluded. In other words, if the given model point was sufficiently valid, an excess above the SM background would have been discovered in the data covering this particular point of the underlying parameter space.

However, in most cases a given model point is constrained by more than one result (or result set in case of cascade decays). These results are summarised in a table and sorted according to their relevance, i.e. the level at which the theoretical prediction exceeds the experimental UL. Conveniently this table which incorporates the information on the topologies and analyses used for constraining the model, is written into a summary file as shown in Listing 5.5.

The first seven lines give some general information about the input:

- the status of the decomposition (potential errors that may occur)
- the most important parameters set by the user
- the version of the results database that was used

These lines are followed by the results table which closes with the highest value of the ratio of $(\sigma \times BR)_{theory}$ to $(\sigma \times BR)_{experiment}$, or *r value* for short. The summary file in Listing 5.5 was obtained by applying SModelS to an examplifying pMSSM model point. It shows two r values greater than one, thus the point is excluded by the first two results listed in the table.

Listing 5.5: A snippet of the results table as given in the SModelS output summary.

```
Input status: 1
Decomposition output status: 1 #decomposition was successful
#Input File: /scratch/magerl/LowFTScan/slha/24.txt
#maxcond = 0.2
#minmassgap = 5.
#sigmacut = 0.01
#Database version: v1.0.2
================================================================================
#Analysis Tx_Name Sqrts Cond.Violation Theory_Value(fb) Exp_limit(fb) r

CMS-PAS-SUS-13-019     T2 8.00E+00  0.0  1.762E+01  6.976E+00  2.526E+00
#[[['jet']],[['jet']]]
--------------------------------------------------------------------------------
ATLAS-SUSY-2013-02     T2 8.00E+00  0.0  1.762E+01  1.350E+01  1.305E+00
#[[['jet']],[['jet']]]
--------------------------------------------------------------------------------
CMS-SUS-13-012         T2 8.00E+00  0.0  1.762E+01  1.823E+01  9.664E-01
#[[['jet']],[['jet']]]

================================================================================
The highest r value is = 2.53E+00
```

5.2.5 Missing Topologies

At the bottom of a summary file there is another table entitled "missing topologies" as can be seen in Listing 5.6. This is an additional functionality of SModelS, which can be used to identify regions of parameter space that have not been experimentally challenged so far.

Listing 5.6: The missing topologies table in the SModelS output summary.

```
================================================================================
Missing topologies with the highest cross-sections (up to 10):
Sqrts (TeV)   Weight (fb)        Element description
8.00E+00   6.312E+00    #                                    [[],[[jet]]]
8.00E+00   2.675E+00    #                                 [[[W]],[[W]]]
8.00E+00   1.052E+00    #                              [[[Z]],[[higgs]]]
8.00E+00   5.146E-01    #                                 [[[Z]],[[Z]]]
8.00E+00   3.741E-01    #                           [[[higgs]],[[higgs]]]
8.00E+00   3.556E-01    #                           [[[b],[W]],[[t],[Z]]]
```

SModelS' missing topology tool finds all the signal topologies for which no experimental constraints were found in the database and marks them as missing. In contrary to the topologies that were found to have an experimental equivalent, a missing topology is always a sum over all signal topologies described by the same constraints but independently of the according mass vector. Hence one has to be extremely careful when interpreting these missing topologies

as will eventually be explained in chapter 6.

In the missing topologies table up to ten such topologies are recorded sorted according to their $(\sigma \times BR)$.

5.3 Collecting Experimental Results - The Database

A tool for phenomenological interpretation such as SModelS can only be as good as the results database it is based on. Therefore keeping the database as up to date and accurate as possible is a vital point for the success of SModelS. This section describes the evolution of the SModelS-database, the "databaseBrowser" a tool that had to be developed in order to maintain it and finally the validation of the database and the framework.

SModelS' results database evolved from predecessor versions which served several needs. In the first place the database was built in order to produce the CMS summary plots as described in subsection 4.2.3. Hence, it contained CMS results only and all the analyses gathered within this database followed the CMS naming convention. Later on it had to fulfil another purpose that was to provide necessary information for the "pMSSM-walkding", an online tool to explore a given theory point, its decay spectrum and limits on the involved sparticle masses. Eventually the "walkding" became a part of SModelS [58]. Finally, with the development of the SModelS framework it became necessary to include further information e.g. the description via constraints and conditions, as well as a multitude of ATLAS analyses. Due to this confluence of multiple purposes the database had an organically grown structure not only concerning the naming conventions and the arrangement system but also the quality of information it was comprised of.

Within the scope of this thesis the database underwent several iterations of restructuring. First of all the folders which hold the respective analyses were renamed to represent the analysis identification number instead of the internal CMS naming. To give an example, the folder formally named *alphaT* was then renamed to *SUS12028* and finally to *CMS-SUS-12-028*. Furthermore several new analyses were included into the database, some of which were already fully approved and published and hence could be used for the SModelS framework. Yet others were included for summary plot purposes only and therefore not fully implemented.

In the context of publication of SModelS v1.0 all the analyses used by SModelS were reviewed and updated if necessary. At last a totally new public database was built out of the old internal one which followed a new structure to treat ATLAS and CMS results equally. In addition the analyses themselves were stripped off every outdated and redundant information and the labelling was changed to completely avoid CMS internal jargon. Finally every analysis which could not be fully validated (cf. subsection 5.3.2) was sorted out.

At present the entire internal database incorporates a wide range of SUSY searches. Several of these analyses consider topologies with intermediate SUSY particles in the decay chain. Since such result sets can not be used for physics studies if the respective experimentalist group provides only one mass plane, the number of result sets in the public database is considerably reduced. Furthermore it was decided that the public database should concentrate

on SUSY searches preformed at $\sqrt{s} = 8$ TeV and omit all 7 TeV results. Altogether 14 SUSY searches from the ATLAS collaboration and 13 from the CMS collaboration successfully passed the validation procedure and were included in the public database. These analyses comprise the considerable number of 24 ATLAS and 42 CMS result sets. At the end of this section Table 5.1 lists all of these analyses that are not superseded by any other publication and therefore used as default database in SModelS v1.0 .

The information and data in the database is organized in three different files for each analysis:

info.txt: a text file (cf. Listing 5.7) which holds all the so called metadata:

- the luminosity and the $\sqrt{s}$ of the respective analysis
- information about the status of the analysis:
  - the link to the respective public results page, arxiv article or journal publication, if available
  - information about analyses which are superseded by this analysis or which supersede it
  - a field which states if the data was published in digital format etc.
- the constraints that describe the topologies considered in the analysis
- the conditions and fuzzyconditions for every topology etc.

Listing 5.7: Snippet of the info.txt file to exemplify the metadata.

```
sqrts: 8.0*TeV
lumi: 19.5/fb
id: CMS-PAS-SUS-13-019
url: https://twiki.cern.ch/twiki/bin/view/CMSPublic/PhysicsResultsSUS13019
digitaldata: True
constraint: T2 -> [[['jet']],[['jet']]]
constraint: T1 -> [[['jet','jet']],[['jet','jet']]]
constraint: T2bb -> [[['b']],[['b']]]
constraint: T2tt -> [[['t']],[['t']]]
fuzzycondition: T2 -> None
fuzzycondition: T1 -> None
fuzzycondition: T2bb -> None
fuzzycondition: T2tt -> None
axes: T1: M1 M0, T2: M1 M0, T2bb: M1 M0, T2tt: M1 M0
```

sms.root: a ROOT.TFile() [59] which comprises the exclusion lines and the UL maps as ROOT.TGraph() and ROOT.TH2F() histograms, respectively

sms.py: a python file which holds the upper limit maps translated into a nested python dictionary, that can be used directly by the SModelS-program

The maintenance, the restructuring and the validation would not have been possible without a suitable work flow and accompanying software tools, as described in the next two sections.

ID	*short description*	*L*	*Ref.*	*Tx names*
ATLAS-SUSY-2013-02	0 leptons + 2–6 jets + $\not{E}_T$	20.3	[60]	T1, T2
ATLAS-SUSY-2013-04	0 leptons + $\geq$7–10 jets + $\not{E}_T$	20.3	[61]	T1tttt
ATLAS-SUSY-2013-05	0 leptons + 2 b-jets + $\not{E}_T$	20.1	[62]	T2bb
ATLAS-SUSY-2013-11	2 leptons (e, μ) + $\not{E}_T$	20.3	[63]	TChiWZ, TSlepSlep
ATLAS-SUSY-2013-12	3 leptons (e, μ, τ) + $\not{E}_T$	20.3	[64]	TChiWH, TChiWZ(off)
ATLAS-SUSY-2013-14	2 taus + $\not{E}_T$	20.3	[65]	TStauStau
ATLAS-SUSY-2013-15	1 lepton + 4(1 b-)jets + $\not{E}_T$	20.3	[66]	T2tt, T2bbWW
ATLAS-SUSY-2013-19	2 leptons + (b)jets + $\not{E}_T$	20.3	[67]	T2tt, T2bbWW, T6bbWW
ATLAS-CONF-2012-105	2 SS leptons + $\geq$4 jets + $\not{E}_T$	5.7	[68]	T1tttt
ATLAS-CONF-2013-007	2 SS leptons + 0–3 b-jets + $\not{E}_T$	20.7	[69]	T1tttt
ATLAS-CONF-2013-024	0 lepton + 6 (2 b-)jets + $\not{E}_T$	20.5	[70]	T2tt
ATLAS-CONF-2013-061	0–1 leptons + $\geq$3 b-jets + $\not{E}_T$	20.1	[71]	T1bbbb, T1tttt
ATLAS-CONF-2013-065	2 leptons + (b)jets + $\not{E}_T$	20.3	[72]	T2tt
CMS-SUS-12-024	0 leptons + $\geq$3(1 b-)jets + $\not{E}_T$	19.4	[73]	T1bbbb, T1tttt(off), T5tttt
CMS-SUS-12-028	jets + $\not{E}_T$, α_T	11.7	[27]	T1, T1bbbb, T1tttt, T2, T2bb
CMS-SUS-13-002	$\geq$3 leptons (+jets) + $\not{E}_T$	19.5	[74]	T1tttt
CMS-SUS-13-006	EW productions with decays to leptons, W, Z, and Higgs	19.5	[56]	TChiWZ(off), TSlepSlep, TChiChipmSlepL, TChiChipmSlepStau
CMS-SUS-13-007	1 lepton + $\geq$2 b-jets + $\not{E}_T$	19.3	[34]	T1tttt(off)
CMS-SUS-13-011	1 lepton + $\geq$4(1 b-)jets + $\not{E}_T$	19.5	[75]	T2tt, T6bbWW
CMS-SUS-13-012	jet multiplicity + $\not{H}_T$	19.5	[28]	T1, T1tttt(off), T2
CMS-SUS-13-013	2 SS leptons + (b-)jets + $\not{E}_T$	19.5	[76]	T1tttt(off),
CMS-PAS-SUS-13-008	3 leptons + (b)jets + $\not{E}_T$	19.5	[77]	T6ttWW, T1tttt
CMS-PAS-SUS-13-016	2 OS leptons + $\geq$4(2b-)jets + $\not{E}_T$	19.7	[78]	T1tttt(off)
CMS-PAS-SUS-13-018	1–2 b-jets + $\not{E}_T$, M_{CT}	19.4	[79]	T2bb
CMS-PAS-SUS-13-019	hadronic M_{T2}	19.5	[29]	T1, T1bbbb, T1tttt(off), T2, T2tt, T2bb
CMS-PAS-SUS-14-011	razor with b-jets	19.3	[30]	T1bbbb, T1tttt(off), T2tt

Table 5.1: List of analysis contained in the public database [36]. A detailed description of each analysis can be found in the respective publication.

5.3.1 Accessing the Database

The three files, which hold the data have to be accessed and read in a structured and convenient way. The tool developed to fit this requirement is called `databaseBrowser`. It is an object-oriented python package which is not only meant to be used within the code but is as well intended as a command line tool. Thus it facilitates to quickly browse the database, perform a pointed search of requested data and get information about the quality and quantity of its content. Listing 5.8 exemplifies these applications. The `Browser` object is built upon the result database. The path which points to the database can be given explicitly. The `Browser` class has several methods to gain statistical information about this database, e.g. how many analyses have published data in digital format. Furthermore it provides information about the number of topologies or analyses incorporated altogether in the database. It can be used to retrieve lists of these analyses and topologies, as well as individual information on a specific analysis and topology, respectively. The `Browser` can be restricted to a specified experiment (ATLAS or CMS) using python's "property" method. That way it will only take into account the part of the database associated with the corresponding collaboration. In addition the package provides several methods to make its usage as conveniently and intuitive as possible, e.g. the level of verbosity of the incorporated modules can be adapted individually.

Listing 5.8: Example for the usage of the `Browser`-object as a command line tool.

```
In [1]: browser = databaseBrowser.Browser('/path/to/smodels-database/')
In [2]: browser.databaseVersion
Out[2]: 'GrenobleNov2014 (27/11/2014)'
In [3]: browser.getTopologies()
Out[3]:
['T6ttWW',
 'T1tttt',
 'T1bbbb',
 'T1ttttoff',
 'T5tttt',
 'T2tt',
 'T2',
 'T1',
 'T6bbWW',
 '...'
 In [4]: browser.getAnalyses(topology='T6bbWW')
 Out[4]:
 ['CMS-SUS-13-011',
  'ATLAS-CONF-2013-065',
  'ATLAS-SUSY-2013-19',
  'ATLAS-SUSY-2013-05']
```

Besides this direct usage the `databaseBrowser` was designed to simplify various tasks which require database access, like the CMS summary plots (cf. subsection 4.2.3) or the validation procedure (cf. subsection 5.3.2). In the following an overview of the main modules

incorporated in the `databaseBrowser` is given. And its basic functionality is explained by means of some short example applications.

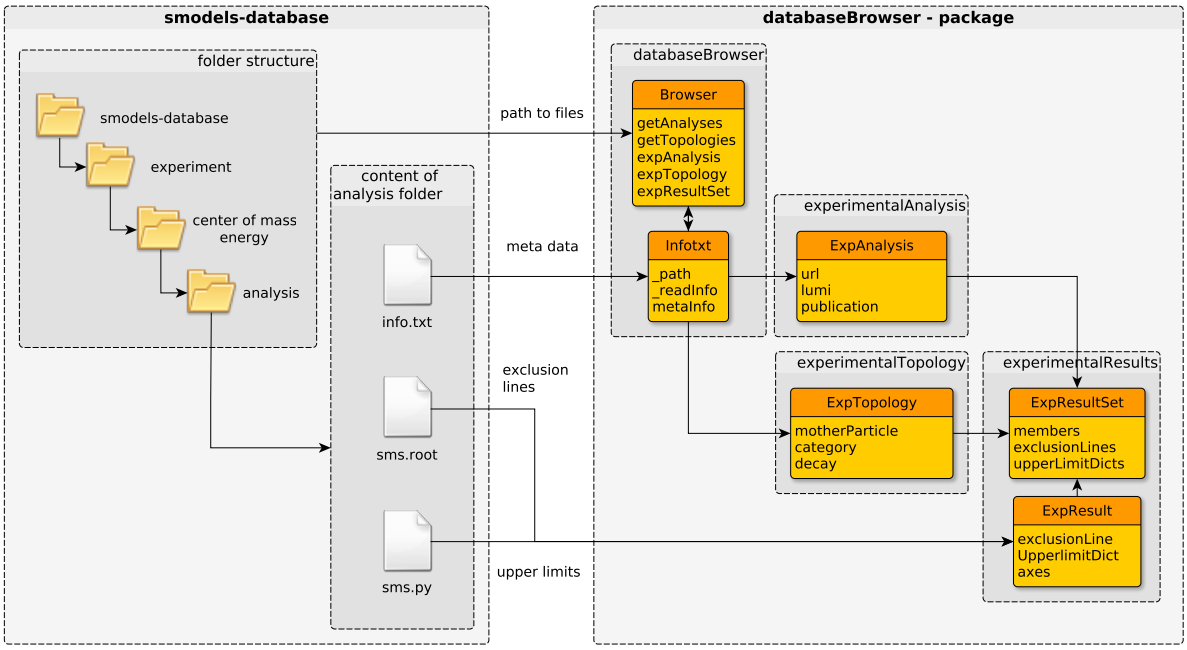

Figure 5.5: Code diagram to illustrate the main functionalities of the `databaseBrowser` package. The box on the left side shows the structure of the database. On the right side the overall structure of the package and its modules are depicted. The flow of information is indicated by the linking arrows. Each yellow box represents one object with a few exemplary methods listed.

The `databaseBrowser` is an object-oriented python package which consists of five modules. Figure 5.5 gives an overview of the code structure. The class `Browser` walks the folder structure of the database and creates a pythonic replica of this structure. It checks if all three files (*info.txt*, *sms.root*, *sms.py*) are available for a given analysis and passes the path to the *info.txt* on to the `Infotxt` class. In this module the whole metadata stored in the respective *info.txt* file is read out and processed further.

This shall be exemplified by the processing of the "axes" field. This field defines the axes of the UL maps provided by the analysis and holds additional information about intermediate masses for results involving cascade decays (cf. subsection 5.2.3). In the *info.txt* file this information is indicated by cryptic abbreviations which are added as suffix to the name of the topology to identify the corresponding upper limits (exclusion contours) in the *sms.py* (*sms.root*). To improve readability these tokens are translated into a string that describes the conjunction of the masses involved plus an attached value. Table 5.2 shows several examples of such slicing methods. The first column states the token as it is used in the axes entry. The second column shows the string (`massParametrization`) that is used to label the different

slicing methods within the `databaseBrowser` package. The attached value shown in the third column can be either a simple float or a float which carries a mass unit. A specific mass plane is clearly defined by a pair of parametrisation and related value comprised in a python tuple.

Token	*massParametrization*	*Value*	*Description*
025		0.25	"x-value"
050	massSplitting	0.50	defined by
075		0.75	$M2 = x \cdot M1 + (1-x) \cdot M0$
D010			fixed difference
sometimes also	M2-M1	1.00E+01 [GeV]	between
D(M2/M1)=10			two masses
C150	fixedM2	1.50E+02 [GeV]	one of the involved
M1300	fixedM1	3.00E+02 [GeV]	masses is set to
LSP001	fixedLSP	1.00E+00 [GeV]	a fixed value
x200	M2/M1	2.0	the ratio between two of the masses is set to a fixed value

Table 5.2: Overview of various slicing methods used to define the mass planes of the UL maps and to give additional information about the third mass. Within one topology M1 is the mass of the mother particle, M0 denotes the mass of the LSP and all intermediate states are numbered according their appearance starting with M2.

The translation of the axes tokens into the more readable python tuples is one of the main functions of the `Infotxt`. Additionally it provides analysis specific information, e.g. a list of all topologies considered by the analysis. The `Infotxt` object holds no methods that should be addressed directly. Rather the `Browser` distributes it further to the actual "experimental objects", summarised below. These objects provide access to the experimental data and the metadata preprocessed by the `Infotxt`. The `Browser` holds the factories for these experimental objects and provides the methods to address them.

`ExperimentalAnalysis`: This object refers directly to a specific analysis as it is represented by a folder in the database. It provides any information that is linked to the analysis itself like the luminosity, the identification number, which topologies were considered etc. Listing 5.9 shows an example application for this object. It is built via the factory incorporated in the `Browser` object. The first method used in this example

retrieves all available axes entries of the respective *info.txt* translated into a more readable format, a mass dictionary. Secondly, the `lumi` method gives the luminosity as a float which can be processed further. The last method (`arxiv`) shown here retrieves the URL of the arxiv web page which holds the published analysis note.

Listing 5.9: Example for the usage of the `ExperimentalAnalysis` as a command line tool.

```
In [1]: analysis=browser.expAnalysis('ATLAS-SUSY-2013-05')
In [2]: analysis.axes
Out[2]:
{'T2bb': [{'mx': 'M1', 'my': 'M0', 'mz': (None, None)}],
 'T6bbWW': [{'mx': 'M2', 'my': 'M0', 'mz': ('fixedM1', 3.00E+02 [GeV])},
            {'mx': 'M1', 'my': 'M0', 'mz': ('fixedM2', 1.50E+02 [GeV])}],
 'T6bbWWoff': [{'mx': 'M2', 'my': 'M0', 'mz': ('fixedM1', 3.00E+02 [GeV])},
               {'mx': 'M1', 'my': 'M0', 'mz': ('M2-M0', 5.00E+00 [GeV])},
               {'mx': 'M1', 'my': 'M0', 'mz': ('M2-M0', 2.00E+01 [GeV])}]}
In [3]: analysis.lumi
Out[3]: 20.1
In [4]: analysis.arxiv
Out[4]: 'http://arxiv.org/abs/1308.2631'
```

`ExperimentalTopology`: An individual experimental topology is determined by its "TNx" and corresponds to a defined decay. This decay is provided by the `ExperimentalTopology` object as string. Conveniently the user can decide if this string should be compatible with ROOT or LaTeX and the level of detailedness. In addition there are methods to get some statistical information about various characteristics of this topology throughout the whole database, e.g. the different parametrisations of the `mz` component of the mass dictionary. The usage of this object is exemplified in Listing 5.10. After it is built by addressing the `Browser`'s `expTopology` method, it is used to retrieve the associated decay string. The method `decay` returns this string in a format compatible with ROOT. Finally the `motherParticle` property is used to get the mother particle for the T6WW topology shown in Listing 5.10 and `constraints` retrieves its different constraints.

Listing 5.10: Example application of the `ExperimentalTopology` as a command line tool.

```
In [1]: topology=browser.expTopology('T6WW')
In [2]: topology.decay
Out[2]: '#tilde{q} #rightarrow q(#chi^{#pm}_{1} #rightarrow W#tilde{#chi
    }^{0}_{1})'
In [3]: topology.motherParticle
Out[3]: 'squark'
In [4]: topology.constraints
Out[4]: ["[[['jet'],['W+']],[['jet'],['W-']]]", "[[['jet'],['W']],[['jet
    '],['W']]]"]
```

ExpResultSet: This object holds all results, that are available for a given result set. Each of these results is represented by one `ExpResult` object, all of which are incorporated within the `ExpResultSet`. Both objects are comprised in the `experimentalResults` module. The `ExpResultSet` object provides access to the upper limits and the exclusion lines. One specific upper limit (exclusion line) is identified by the parameters:

1. `expected=True/False:` The database holds not only observed (`False`) upper limits and exclusion lines, but also the expected ones (`True`), if they are provided by the collaborations. If this parameter is not set explicitly, the respective observed object will be returned.
2. `sigma=-1, 0, 1:` For the exclusion lines it is likely that there are additional contours which indicate the uncertainties of one standard deviation. These additional contours can be accessed by setting sigma to `-1` or `1`. The default value `0` denotes the exclusion contour itself.
3. `massParametrization:` This variable refers to the slicing method used to obtain the result in question. Possible values for this parameter are summarised in the second column of Table 5.2.
4. `value:` Each `massParametrization` may be realized with several values. These values are exemplified in the third column of Table 5.2.

Various hidden methods define the default values for these parameters to provide maximal convenience for the user, as can be seen below.

Listing 5.11 illustrates how the `ExpResultSet` can be built using the factory provided by the `Browser`. The `members` property retrieves a dictionary which links the name of the comprised `ExpResult` objects to their respective mass plane. Thus it explains these names which can be used to address an individual `ExpResult`. This method exploits the axes entry of the *info.txt* preprocessed by the `Infotxt` object. Secondly, the `exclusionLine` method is used exemplifying the virtue of the hidden procedures of default setting. These functionalities are applied automatically, if the method `exclusionLine` or `upperLimitDict` is called without defined parameters. On the other hand, both methods can be called with defined parameters to retrieve one specified exclusion line or upper limit dictionary.

Listing 5.11: Example for the usage of the `experimentalResultSet`-module as a command line tool.

```
In [1]: resultSet=browser.expResultSet('CMS-SUS-13-006', 'TChiChipmSlepL')
In [2]: resultSet.members
Out[2]:
 {'TChiChipmSlepL005': ('massSplitting', 0.05),
  'TChiChipmSlepL050': ('massSplitting', 0.5),
  'TChiChipmSlepL095': ('massSplitting', 0.95)}
In [3]: resultSet.exclusionLine()
Out[3]: <ROOT.TGraph object ("exclusion_TChiChipmSlepL050") at 0x2476bc0>
In [4]:  resultSet.exclusionLine(expected=True, sigma=1, massParametrization
    ='massSplitting', value=0.95)
Out[4]:  <ROOT.TGraph object ("expectedexclusionp1_TChiChipmSlepL095") at 0
    x24d5ad0>
In [5]: resultSet.upperLimitDict(massParametrization='massSplitting', value
    =0.95)
Out[5]:
{100.0: {0.0: 0.4550814926624298,
  20.0: 0.9481587409973145,
  40.0: 1.678849697113037,
  ...
 120.0: {0.0: 0.1692868322134018,
  20.0: 0.2524884343147278,
  ...
```

The `databaseBrowser` package is a useful and potent tool to control every aspect of the database and survey the affluence of information accumulated in course of time. Currently it is completely overworked to be compatible with the new structure of SModelS and its attached results database which will be published as SModelS v1.1. One of the `Browser`'s many applications, the validation of the database and the code, is described in the next section.

5.3.2 Validation of the Framework

The first version of the SModelS framework used for physics studies and the corresponding database were already validated, as described in the original SModelS-paper. Since for publication the code underwent major refactoring, it was necessary to redo the process of validation.

The basic approach to perform a simple and robust test of the software and the implementation of analyses is based on applying it to a simplified model. To validate any result the input is the simplified model considered by this result. Hence, the conditions imposed by the analysis are completely satisfied and thus it should be possible to reproduce the official exclusion contour. Such an input model can be constructed by manually defining the mass table and the decay tables in the respective blocks of an SLHA file. All masses which are not involved in the simplified model are "decoupled", i.e. set to a high value and all branching ratios are set to zero, except for the decay considered by this simplified model. This can be illustrated for example by the T2tt result of the CMS-SUS-13-011 analysis (cf. Figure 5.6a).

T2tt denotes a stop ($\widetilde{t}$) decaying to top and lightest neutralino ($\widetilde{\chi}_1^0$). Consequently the exclusion line and the UL map are given in the $m_{\widetilde{t}_1} - m_{\widetilde{\chi}_1^0}$ plane. Therefore the only two BSM masses that have to be varied to generate an adequate number of model points to cover the whole mass plane, are the $m_{\widetilde{t}_1}$ and the $m_{\widetilde{\chi}_1^0}$. All the other sparticles are taken to be in the decoupling regime. In addition, the branching ratio for the decay $\widetilde{t} \to t\widetilde{\chi}_1^0$ is set to one, all others are set to zero.

The framework was applied to these models whereby the decomposition was restricted to the analysis in question. The output of the decomposition was used to sort the input points into "excluded" ($(\sigma \times BR)_{theory} > (\sigma \times BR)_{experiment}$ or r value > 1) and "allowed" (r value < 1). Furthermore from this information an exclusion line was derived. Then the points were plotted colour coded in the respective mass plane. The derived exclusion contours as well as the official exclusion lines were plotted on top. That way a multitude of validation plots accrued, two of which are depicted in Figure 5.6. A large majority of these validation plots showed a very good agreement with the official exclusion contours.

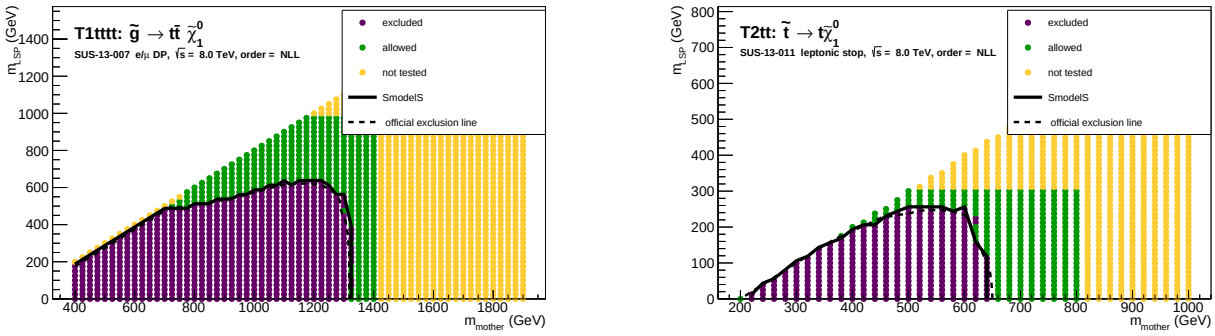

(a) Validation plot for the T1tttt result of CMS-SUS-13-007.

(b) Validation plot for the T2tt result of CMS-SUS-13-011

Figure 5.6: Example validation plots for two different CMS analyses. The excluded region and the derived exclusion contour obtained from the SModelS decomposition tool are shown in comparison with the official exclusion line published by the CMS-collaboration.

To expedite the progress of the validation procedure an automated work flow was established which incorporated various tools, e.g. a script to compare the cross sections derived with SModelS to the official CMS reference cross sections, modules to create sets of SLHA files and to compute the relevant mass ranges and binning, etc. Several of these tools were based on the `databaseBrowser` package, for example the modules which retrieved the official exclusion lines and threshold values for the mass ranges and binning. But also the module which coordinated the functional interaction of all the validation components was controlled by the `Browser`. Furthermore the script which produced the html code for the twiki page created to keep track of the validation status, used information provided by the "experimental objects" (cf. page 57). An extended description of the validation procedure as well as details on the model selection and an interpretation of the obtained results can be found in Ref. [80].

Chapter 6

Using SModelS to Investigate the LFT Parameter Space

The latest version of the framework described in the previous chapter - SModelS v1.0.3 - was applied to a set of SLHA files. This set comprises roughly 10k points of the pMSSM parameter space, all of which can be characterised as "not finely tuned", i.e. defined by parameters such that a correct SM like Higgs boson mass is predicted while avoiding severe cancellations between the individual mass terms. This characteristic of low fine tuning (LFT) will be motivated in subsection 6.1.1. Subsequently the set of model points and its main features are presented (cf. subsection 6.1.2). The implementation of the "scan" over the set of pMSSM points is described. Finally the outcome of this application to SModelS is discussed and interpreted (cf. section 6.2).

6.1 The LFT Scenario

6.1.1 The Motivation

Amongst many physicists there exists the belief that a good physical theory has to be "natural". Nevertheless there is no consensus about the question: What is natural? Throughout the development of the theoretical description of particle physics the definition of *naturalness* was subjected to mayor changes. It has to be noted, that the issue of naturalness and hence the question of low fine tuning is highly subjective. However one can get a feeling about this problem by considering a theory which involves parameters that have to cancel each other in order to predict the right value of a measurable quantity. It is quite intuitive that such a theory is not natural if these parameters have very high values in comparison to the observable quantity. In other words, theories which require finely tuned parameters seem to be unnatural.

This issue of fine tuning can be exemplified by means of the hierarchy problem, which was already introduced in subsection 3.1.2. Considering for example a Dirac fermion f which receives its mass via Yukawa coupling Y_f to the Higgs, the squared mass of the Higgs boson

at one loop level is

$$m_h^2 \approx m_{hbare}^2 - Y_f^2 \Lambda^2 \tag{6.1}$$

with $m_h \approx 125$ GeV the physical mass, m_{hbare} is the unmeasurable bare mass and Λ is the highest energy scale for which the underlying theory (here the SM) is valid. Hence, the correction to the mass squared δm_h^2 is proportional to $-Y_f^2 \Lambda^2$. A first naive approach to characterise the naturalness of this relation is to simply define

$$\mathcal{N} = \frac{\delta m_h^2}{m_h^2} \tag{6.2}$$

Assuming Λ is of the order of M_{Planck} and the fermion is a top quark with $Y_t \simeq 1$, $\mathcal{N}$ would be of the order of 10^{34}. One can justifiably call this a severe amount of fine tuning. As already mentioned before, this finely tuned cancellation is cured by SUSY leaving a logarithmic term due to symmetry breaking

$$m_h^2 \approx m_{hbare}^2 (m_{\tilde{f}}^2 - m_f^2) \ln\left(\frac{\Lambda^2}{m_{\tilde{f}}^2}\right) \tag{6.3}$$

Since the correction term ${\delta m_h}^2$ contains the mass of the sfermion $m_{\tilde{f}}$ the maximal amount of fine tuning $\mathcal{N}_{max}$ one is willing to tolerate can be used to estimate a boundary on this sfermion mass. However this is just a very rough consideration which can be replaced by a more appropriate definition of fine tuning, as explained below.

The hierarchy problem of the SM Higgs boson is not the only issue where fine tuning plays a role. The introduction of SUSY models that ought to be a natural solution to it, gives rise to further hints on fine tuning. One example that is often referred to as the "little hierarchy problem" arises in the pMSSM and shall be introduced qualitatively.

In the pMSSM as described in chapter 3 SUSY is explicitly broken at the weak scale. Hence, the Higgs potential incorporates two different types of mass terms, the SUSY preserving mass parameter $|\mu|^2$ and the soft masses for both Higgs doublets $m_{H_u}^2$ and $m_{H_d}^2$. Since H_u and H_d get non vanishing VEVs v_u and v_d, the minimisation of this potential relates the mass of the Z boson to these three parameters. At tree level this can be written as

$$m_Z^2 \approx \frac{m_{H_d}^2 - m_{H_u}^2 \tan\beta}{\tan^2\beta - 1} - |\mu|^2 \tag{6.4}$$

where $\tan\beta$ is the ratio of the VEVs. If one of the parameters on the right hand side of Equation 6.4 would be several orders of magnitude above the squared mass of the Z boson $m_Z \simeq 91$ GeV, the other ones would have to be tuned carefully to cancel this contribution. Furthermore, the Higgs doublets mix to form mass eigenstates whereby the lightest neutral scalar is denoted by h_0. In order to get the right mass m_{h_0}, i.e. in accordance with experimental constraints, its mass squared term has to get positive corrections. The dominant contributions to these corrections were found to arise from stops.

$$\delta m_{h_0}^2 \propto Y_t \ln\left(\frac{m_{\tilde{t}_1} m_{\tilde{t}_2}}{m_t^2}\right) \tag{6.5}$$

The relations (6.4) and (6.5) illustrate, that there is a tension between the masses of the stop, the lightest Higgs and the Z boson, since the leading contributions to the loop corrections of m_{H_u} and m_{H_d} also arise from Yukawa interactions of the stop. Hence, the mass of the stop is bounded above by the requirement of low fine tuning. From this it can be understood that the pMSSM comprises several parameters which potentially can be subjected to fine tuning, e.g. the soft higgs mass parameters, the mass of the stop, the mixing in the stop sector etc. The requirement of at least one light stop entails a light sbottom in case this light stop is mostly left handed. Furthermore, the gluinos, which also affect the mass of the Higgs boson via contributions to the stop mass at one loop-level, have to be moderately light in order to avoid fine tuning. Hence, the LFT parameter space is expected to have some general characteristics, like a low μ parameter, resulting in a higgsino like neutralino and chargino, a light stop and a lightish gluino.

It has to be emphasized again that the amount of fine tuning one is willing to tolerate is a very subjective quantity. Precisely because of this it is necessary to have an objective definition of fine tuning which is more appropriate than the naive approach given in Equation 6.2. Such a definition is represented by the Ellis-Barbieri-Giudice measure [81, 82]

$$\Delta = \left| \frac{p}{O(p)} \frac{\partial O(p)}{\partial p} \right| \tag{6.6}$$

which describes the effect of variation of a parameter p on an observable $O(p)$. If Δ is large a small change in p results in a severe change in O, hence p has to be tuned very carefully to get the correct observed value O. Even with such a definition it is still a "personal choice" which value is regarded as low.
In fact, the consensus about the amount of fine tuning that can be tolerated while still believing that SUSY is a natural solution to the hierarchy problem changes to higher and higher values with the increasing constraints on SUSY particles. Hence, the regions of parameter space of the pMSSM that could provide low fine tuned model points are particularly interesting. First of all, it has to be trialled if such LFT model points have already been targeted by current interpretations of SUSY searches at LHC. The question arises how experimental results could be reinterpreted in order to improve their applicability on such LFT model points. Finally one can ask, which additional interpretations may be beneficial in order to probe this region of parameter space in the next run of the LHC with $\sqrt{s} = 13$ TeV. The investigation of such a scenario using SModelS v1.0.3 helps answering these questions (cf. section 6.2).

6.1.2 The Parameter Space

In order to understand the findings gained from the "LFT-scan" initially it is necessary to get an impression on the scenario considered. Each point, which will henceforth also be called a model, corresponds to a specific set of values for every degree of freedom in the underlying parameter space and is given in SLHA file format. The set of SLHA files originally was created to perform a survey of SUSY signatures at the LHC presented in *"pMSSM Studies at the 7, 8 and 14 TeV LHC"* [83]. Thus a detailed description of the creation and the model selection

process can be found there and in an accompanying publication [84]. Nevertheless, this section gives an overview on the main features of the LFT parameter space and the selected models.

First of all the ranges of the 19 parameters in the RPC pMSSM with a neutralino LSP were chosen such that the models tend to fulfil the requirements stated below. Within this preset ranges, roughly 3×10^8 model points were generated randomly. This set was then subjected to several theoretical and experimental constraints gained from e.g. flavour precision measurements, DM and collider physics. In particular:

- The models should provide a neutralino LSP that saturates the combined relic density ($\Omega h^2 = 0.1153 \pm 0.095$) given by WMAP and Planck (cf. subsection 3.1.3).
- The "correct" SM like Higgs mass ($m_h = 126 \pm 3\ GeV$) should be predicted.
- The amount of fine tuning produced by the models should be better than 1% measured by the Ellis-Barbieri-Giudice parameter (cf. Equation 6.6).
- An additional correlation between the higgsino mass parameter μ and the bino mass parameter $M1$ is required $\left|\frac{M1}{\mu}\right| < 1.2$.
- The mixing of the stops quantified by $|A_t - \mu \cot \beta|$ should exceed the geometric mean of the tree level stop masses.

Out of the large model set generated, only 10.2×10^3 models survived this selection procedure. In the following some of the common features of the LFT model set shall be examined.

neutralino LSP: As explained in subsection 3.2.1 the lightest neutralino $\widetilde{\chi}_1^0$ comprises contributions from all four neutral gauge eigenstates of the electroweak gauge sector in the pMSSM (cf. Equation 3.32). These fractions of gauge eigenstates (cf. Equation 3.33) are depicted in Figure 6.1 as function of the mass of the $\widetilde{\chi}_1^0$. In order to enlarge the interesting regions, a lower (upper) cut was applied to the axis which shows the bino (wino, higgsino) content. From Figure 6.1a it can be seen, that the contributions of the wino to the $\widetilde{\chi}_1^0$ can be neglected in this scenario. Secondly the comparison of Figure 6.1b and Figure 6.1c conveys that generally the neutralino is a heavily mixed state. In each of these plots a small gap for $m_{\widetilde{\chi}_1^0} \simeq 70$ GeV is perceptible. Roughly 60% of all models have LSP masses below this gap. These models provide a bino LSP around $m_{\widetilde{\chi}_1^0} \simeq 50$ GeV. The remaining 40% have a $\widetilde{\chi}_1^0$, which shows a bino higgsino mixture with a tendency to higher fractions of bino content. This characteristics of the nature of the LSP origin in the mechanisms to achieve the correct relic density, as is explained in detail in Ref. [83, 84].

lightest chargino: The lower bound on the mass of the lightest chargino $\widetilde{\chi}_1^\pm$ is given by the LEP constraint $m_{\widetilde{\chi}_1^\pm} > 103.5$ GeV [85]. Figure 6.1d shows that a vast majority of the models provide a higgsino like $\widetilde{\chi}_1^\pm$. Roughly 60% of all the models do have a $\widetilde{\chi}_1^\pm$ which is

a higgsino to more than 90% ($f(\widetilde{\mathrm{H}}^{\pm}) > 0.9$). The major part of the rest of the models have a $\widetilde{\chi}_1^{\pm}$ which is mostly higgsino like and infrequently models provide a wino like $\widetilde{\chi}_1^{\pm}$.

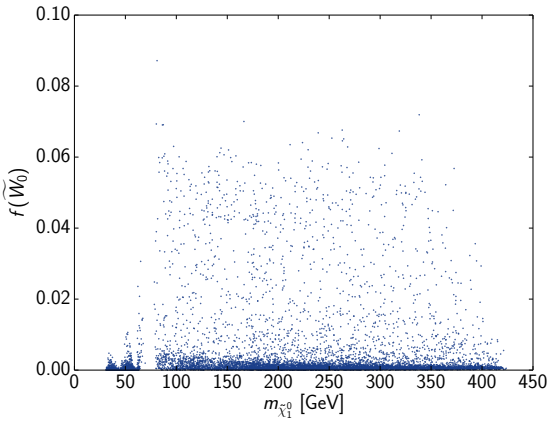

(a) content of wino $f(\widetilde{\mathrm{W}})$ of the lightest neutralino

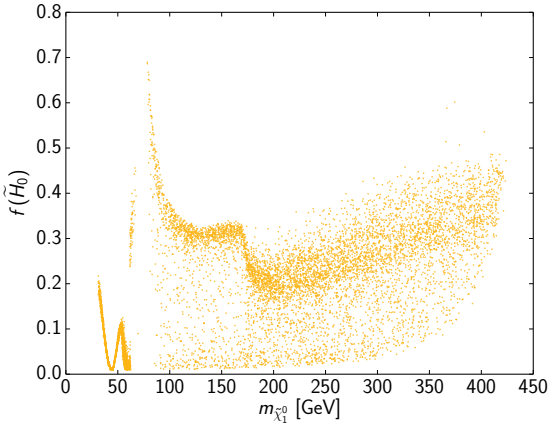

(b) content of higgsino $f(\widetilde{\mathrm{H}})$ of the lightest neutralino

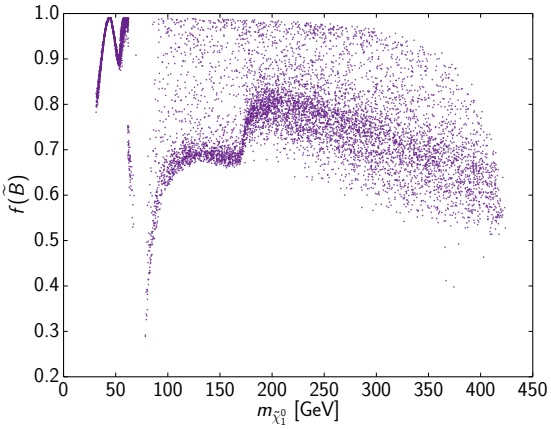

(c) content of bino $f(\widetilde{\mathrm{B}})$ of the lightest neutralino

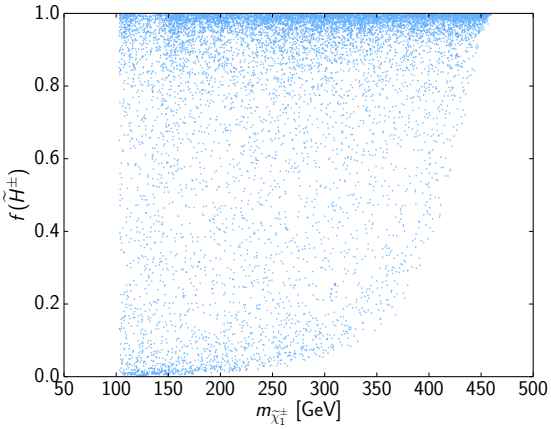

(d) content of higgsino $f(\widetilde{\mathrm{H}}^{\pm})$ of the lightest chargino

Figure 6.1: Fraction of the wino (a), higgsino (b) and bino (c) content of the lightest neutralino as well as the higgsino content of the lightest chargino (d) as function of the respective sparticle mass.

stops and sbottoms: Another characteristic feature within the LFT scenario are relatively light stops. Figure 6.2a shows the nature of the lightest stop $\widetilde{t}_1$, which is mostly left handed for the bigger part of the models. Since the LH stops and sbottoms are enclosed in an $SU(2)$ doublet, the $\widetilde{b}_1$ is expected to be very close in mass to the $\widetilde{t}_1$ in case it is also mostly left handed. This is indeed true for a majority of the $\widetilde{b}_1$, as can be seen from Figure 6.2b. The temperature depicts the fraction $f(\widetilde{b}_R)$ of the $\widetilde{b}_1$ as a function

of $m_{\widetilde{b}_1}$ and $m_{\widetilde{t}_1}$. The figure elucidates the small mass splitting between the $\widetilde{t}_1$ and the $\widetilde{b}_1$ for a major part of the model points. It also shows that the $\widetilde{b}_1$ is generally in a pure gauge eigenstate and that it is clearly right handed for $m_{\widetilde{b}_1} < m_{\widetilde{t}_1}$. Concretely, 80% of all models have a light sbottom that is left handed to more than 90%.

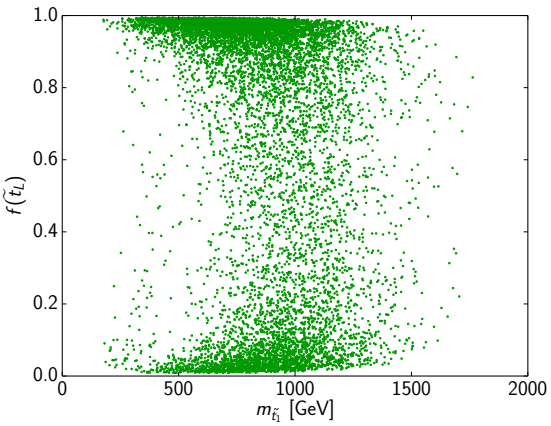

(a) content of left handed stop of the $\widetilde{t}_1$ as function of the $m_{\widetilde{t}_1}$

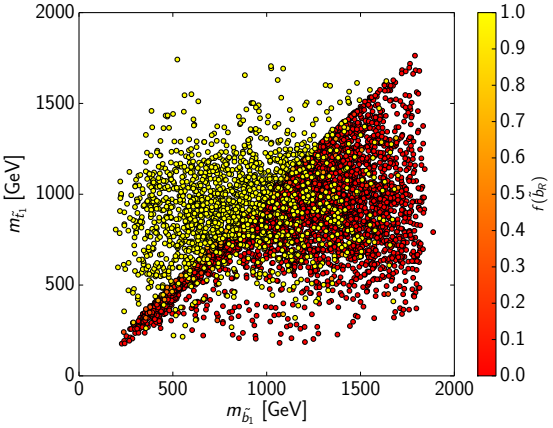

(b) content of sbottom right of the $\widetilde{b}_1$ indicated by the temperature as function of $m_{\widetilde{b}_1}$ and $m_{\widetilde{t}_1}$

Figure 6.2: Fraction of the left handed stop of the $\widetilde{t}_1$ as function of $m_{\widetilde{t}_1}$ (a). The temperature plot shows the fraction of the right handed sbottom of the $\widetilde{b}_1$ in the $m_{\widetilde{b}_1} - m_{\widetilde{t}_1}$ plane (b).

light flavoured squarks and gluinos: Since gluinos $\widetilde{g}$ contribute to the stop mass at one loop-level and therefore also feed into the mass of the Higgs boson at two loop-level, they are in general assumed to be moderately light. Unlike the gluinos and the third generation squarks, the first and second generation squarks (simply denoted squarks or $\widetilde{q}$ in the following) are not bound by fine tuning constraints. Hence, there are no affiliations between $\widetilde{q}$ and $\widetilde{g}$. This is in contrast to the general assumptions in the SUSY searches at LHC, where squarks and gluinos are usually taken to be decoupled ($m_{\widetilde{g}} \gg m_{\widetilde{q}}$ or $m_{\widetilde{g}} \ll m_{\widetilde{q}}$). Figure 6.3 shows a projection of all model points into the $\widetilde{g} - \widetilde{q}_{min}$ mass plane. Hereby the lightest of the squarks is taken as $\widetilde{q}_{min}$ for each model.

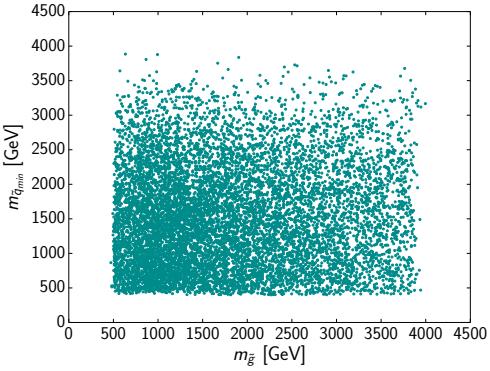

Figure 6.3: All model points are projected onto the $\widetilde{g} - \widetilde{q}_{min}$ mass plane. $\widetilde{q}$ denotes all eight light flavoured squarks and $\widetilde{q}_{min}$ is the lightest of these in each point.

The common features of the LFT model points foster a typical mass spectrum, as illustrated

in Figure 6.4. The majority of the models has a set of very light eweakinos at the bottom of this spectrum and rather light $\widetilde{t}_1$ and $\widetilde{b}_1$ which are nearly mass degenerate. Gluinos are typically located in the middle of the spectrum, whereas squarks can be at the top of the spectrum. Sleptons are not affected by LFT constraints and can therefore populate the whole mass range.

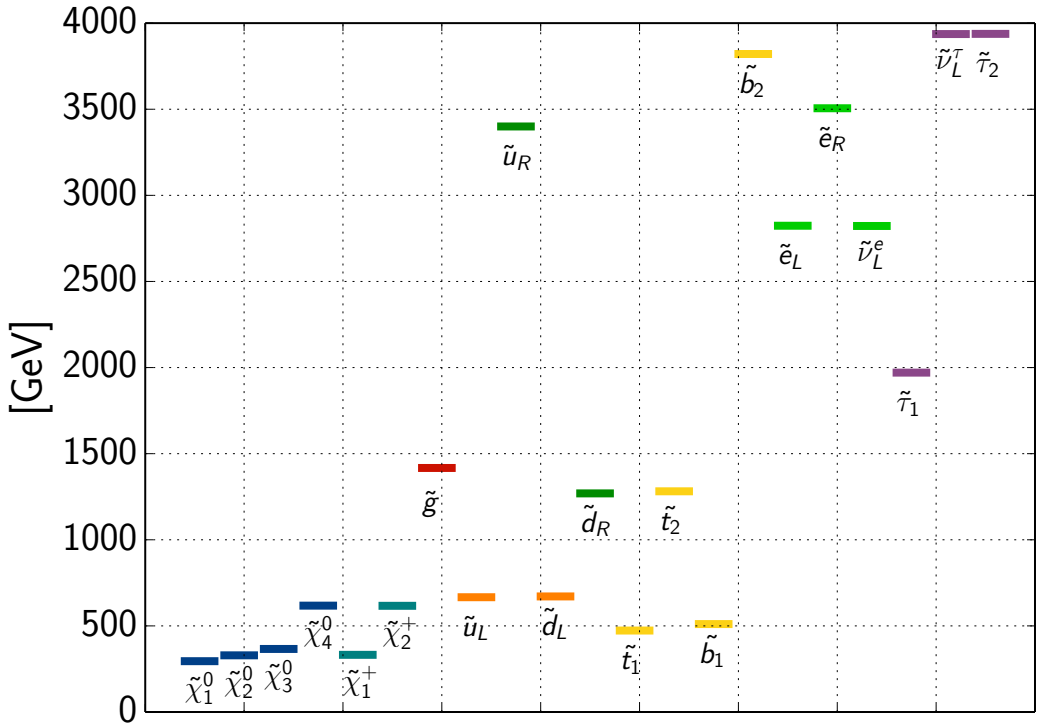

Figure 6.4: A typical mass spectrum in the LFT scenario.

These kinematic configurations lead to rather complex decay patterns particularly for $\widetilde{b}_1$, $\widetilde{t}_1$ and $\widetilde{g}$. Figure 6.5 shows such a typical decay pattern, generated using the SModelS-walkding [58]. This plot shows that the light stops and sbottoms in principle decay to all lighter eweakinos with comparable branching fractions producing mostly tops and bottoms, respectively. The gluinos behave similarly, depending on the kinematics. Finally the higher indexed eweakinos decay directly or via cascades into the $\widetilde{\chi}_1^0$, producing on- and off-shell W, Z and Higgs bosons.

This complex decay scheme is a very characteristic feature of the LFT models, which severely effects the applicability of most of the experimental results incorporated in the SModelS database, as will be described below (cf. page 69).

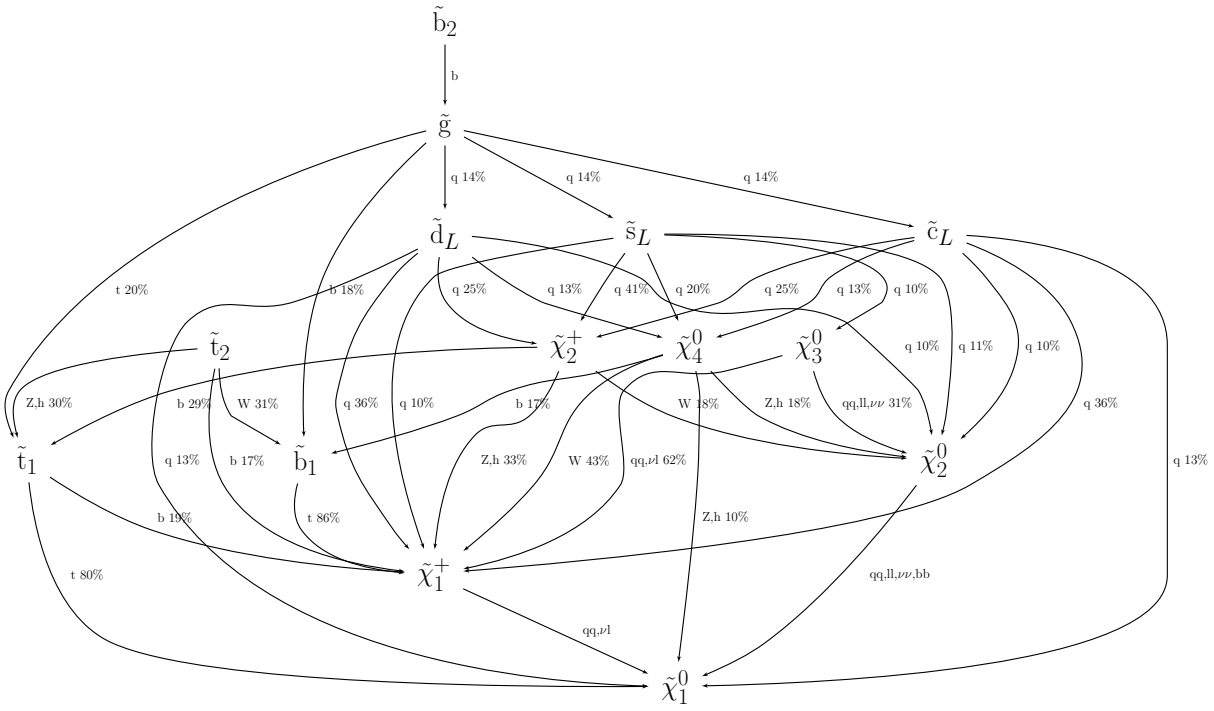

Figure 6.5: Typical decay pattern in the LFT scenario, generated by the SModelS-walkding.

6.2 Results and Interpretation

As explained above, the LFT model set comprises roughly 10k SLHA files, each of which represents a specific set of parameters. To confront these models with the experimental constraints collected in the result database, first of all the production cross sections had to be calculated for $\sqrt{s} = 8$ TeV. To this end SModelS' internal cross section computer was used, which is based on Pythia and NLLfast (cf. subsection 5.2.1). Hereby the number of simulated events was set to 5×10^4 as a compromise between the need of reasonably large statistics and moderate computing time. The parameter settings as described in chapter 5 were chosen to be $minmassgap = 5$ GeV, $maxcondition = 0.2$ and $\sigma_{cut} = 0.01fb$ [1]. Subsequently the model set was subjected to the decomposition and confronted with the full result database incorporated in SModelS v1.0.3 . For every point of the LFT set SModelS v1.0.3 provided a summary file, which contained a result table and a table for missing topologies (cf. subsection 5.2.4 and subsection 5.2.5). The analysis and interpretations of the outcome is mainly based on these summary files.

In this section an overview on the findings of the LFT scan is followed by a more detailed discussion of these results.

[1] the SModelS parameter card can be found in Appendix A

6.2.1 Summary of Results

As set out in subsection 6.1.2, the relevant features of the LFT scenario are dominated by the masses of the sparticles which mainly are affected by LFT constraints. In particular these are the third generation squarks $\widetilde{\mathrm{t}}$ and $\widetilde{\mathrm{b}}$, the gluinos $\widetilde{\mathrm{g}}$ and their decay products, namely the charged and neutral eweakinos $\widetilde{\chi}^{\pm}$ and $\widetilde{\chi}^{0}$. Hence, it is illuminating to give an overview on the models which could be excluded by SModelS and which remain valid, in the mass planes given by these relevant sparticles. Figure 6.7 summarises these result plots, which show all model points excluded by at least one experimental result plotted on top of the points remaining valid. These have to be compared with Figure 6.8 which shows the very same plots but with the valid points on top of the excluded ones. At first glance it is clear that the majority of the model points ($\approx 77\%$) remains valid whereas only roughly 22% could be excluded by SModelS . 108 points could not be tested, because the database contains no experimental results applicable for the signal topologies of these models. These points are not shown in the plots in Figure 6.7 and Figure 6.8. In addition the plots illustrate the full mass range for the respective sparticles. In the following the individual mass planes in Figure 6.7 and Figure 6.8 are discussed.

gluino neutralino plane: Using the SMS approach, current SUSY searches at LHC exclude gluinos up to roughly 1.5 TeV. However, this conclusion is only applicable under certain assumptions (100% branching ratio for a specific decay channel, squarks in the decoupling regime etc.). Since these assumptions are not fulfilled by the LFT models it is understandable that the result plot Figure 6.7 shows no clear correlation of the excluded points with $m_{\widetilde{g}}$. Moreover the plot in Figure 6.8 reveals that the LFT model set contains valid points for almost every gluino mass. The typical mass spectrum provided by a given LFT point, indicates that the dominant decay modes for the gluinos involve the relatively light third generation squarks and the whole set of eweakinos. There are no applicable interpretations of experimental results available for such decays. Hence, it is particularly interesting to study the behaviour of the gluinos in the LFT scenario in greater detail, as will be elucidated below.

stop neutralino and sbottom neutralino plane: The right panels in Figure 6.7 and Figure 6.8 depict the exclusion of models as a function of the sbottom mass (top) and the stop mass (middle) against the mass of the LSP. These first two result plots do not show any correlation between the exclusion of points and the masses of the third generation squarks. In fact, only very few points with $m_{\widetilde{b}_1}$ ($m_{\widetilde{t}_1}$) < 500 GeV and an LSP around 50 GeV are found to be excluded. The same considerations as for the gluinos are applicable. In addition the $m_{\widetilde{t}_1} - m_{\widetilde{b}_1}$ mass plane is shown in the bottom panel. Whereby the high density of excluded points along the diagonal is due to the fact, that the mass degeneration of $\widetilde{b}_1$ and $\widetilde{t}_1$ results in an artificial enhancement of $(\sigma \times BR)_{theory}$ for $\widetilde{\mathrm{b}}(\widetilde{\mathrm{t}}) \to \mathrm{b}(\mathrm{t})\widetilde{\chi}^{0}_{1}$. This incrementation will happen if the chargino decay in the cascade $\widetilde{\mathrm{b}}(\widetilde{\mathrm{t}}) \to \mathrm{t}(\widetilde{\mathrm{b}})\widetilde{\chi}^{\pm} \to W^{*}\widetilde{\chi}^{0}_{1}$ is invisible. For such configurations it can not be distinguished if the respective final state stems from a sbottom or a stop decay, thus the weights for

both topologies will be added up and potentially lead to the exclusion of such points.

chargino neutralino plane: Looking at the middle left panel of Figure 6.7 and Figure 6.8, the first salient fact is the distribution of model points throughout this mass plane. The gap on the $m_{\widetilde{\chi}_1^0}$-axis at $m_{\widetilde{\chi}_1^0} \simeq 70$ GeV, which separates the region of the bino like $\widetilde{\chi}_1^0$ from the region where it is a bino higgsino mixture, is clearly discernible.

Each model point can be assigned to one of the two clearly separated regions in this mass plane. In general a light higgsino parameter μ determines the masses of the chargino and the two lightest neutralinos leading to degeneration among them. Hence, the eweakinos in the diagonal region are controlled vigorously by the μ parameter. On the contrary, in the off diagonal region around $m_{\widetilde{\chi}_1^0} \simeq 50$ GeV the neutralino is basically 100% bino. Figure 6.6 shows the difference between the higgsino fractions of $\widetilde{\chi}_1^0$ and $\widetilde{\chi}_1^\pm$, which is minimised at the diagonal. This confirms the fact, that both eweakinos are indeed mostly controlled by the higgsino mass parameter in this specific region of parameter space.

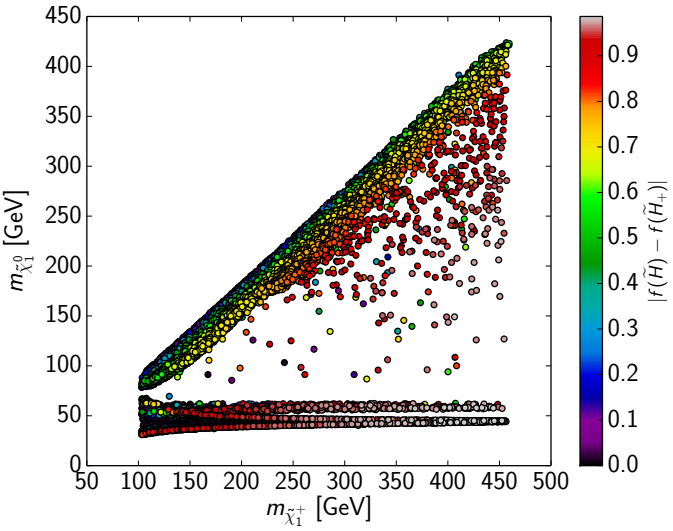

Figure 6.6: The temperature represents the splitting between the fraction of higgsino content of the lightest neutralino and the lightest chargino, depicted in the $m_{\widetilde{\chi}_1^+} - m_{\widetilde{\chi}_1^0}$ mass plane.

Another fact that is depicted in the result plot in Figure 6.7 is that the fraction of excluded models drops with increasing $m_{\widetilde{\chi}_1^0}$. This matches the expectations given the fact that the SUSY mass spectra get heavier with increased $m_{\widetilde{\chi}_1^0}$, since the LSP is always the end product of a decay chain. Therefore SUSY searches become less sensitive due to the reduction of the production cross sections of heavier sparticles.

The comparison with Figure 6.8 reveals a vanishingly small region with a bino neutralino of roughly 50 GeV and a chargino just above the LEP limit which is actually excluded.

squark neutralino plane: The bottommost result plot on the left shows the mass of the lightest of the first and second generation squarks plotted against $m_{\widetilde{\chi}_1^0}$. Hereby the excluded region for the mixed neutralino mainly origins from $\widetilde{q} \to q\widetilde{\chi}_1^0$ (T2) results, as will be shown later. However, it has to be taken into account, that all experimental results for squark searches assume mass degenerate light flavoured squarks, which is not the case in the LFT scenario. Hence, the correlation discernible in Figure 6.7 is lost if one concentrates on a specific quark flavour. This conclusion is strengthened by comparison

of Figure 6.7 and Figure 6.8 which reveals that actually no region can be excluded completely.

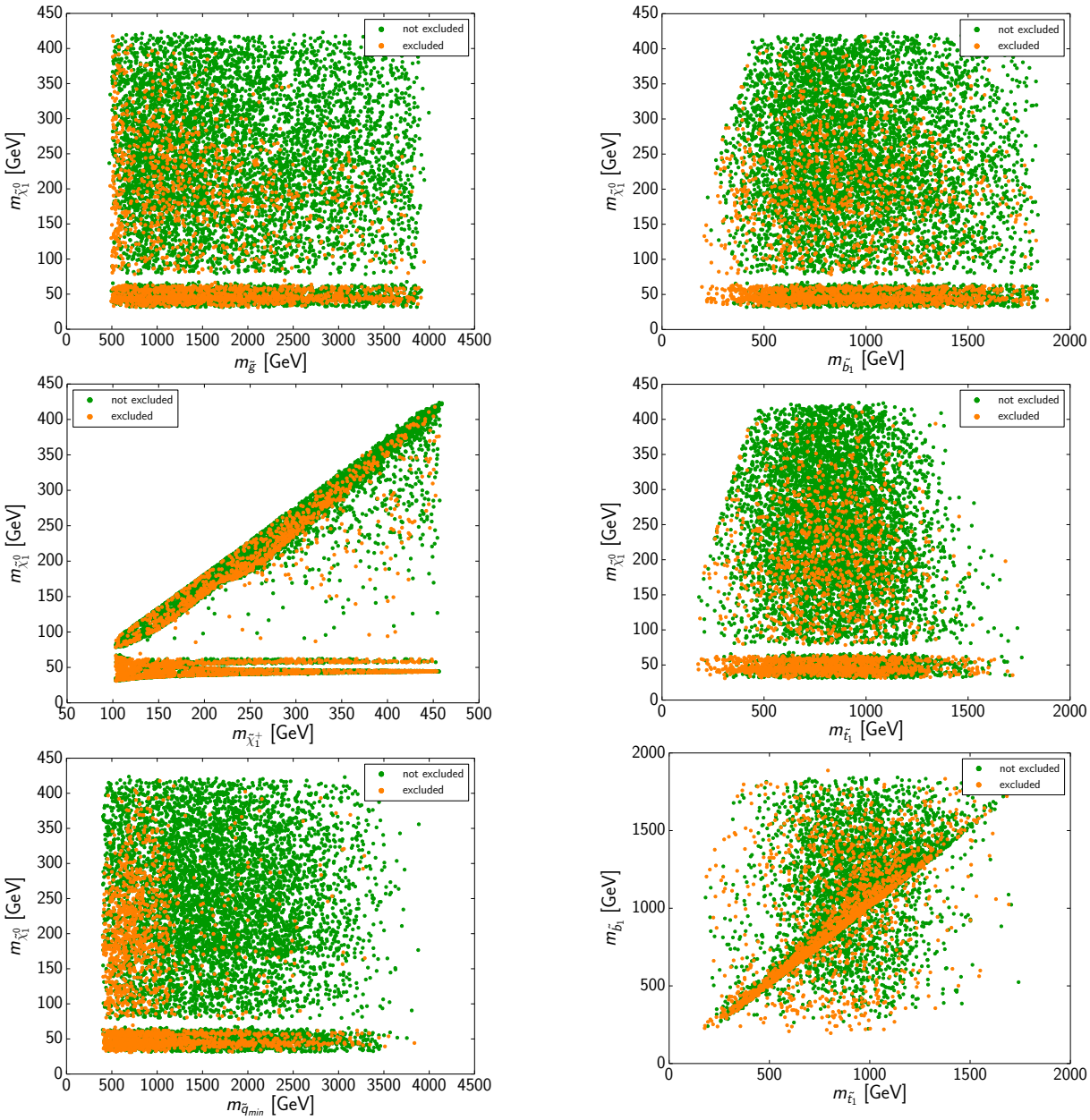

Figure 6.7: Summary of results of the LFT scan. Each plot shows all excluded points plotted on top of the not excluded points. Mass planes on the left from top to bottom are $m_{\tilde{g}} - m_{\tilde{\chi}_1^0}$, $m_{\tilde{\chi}_1^\pm} - m_{\tilde{\chi}_1^0}$ and $m_{\tilde{q}_{min}} - m_{\tilde{\chi}_1^0}$ (where $\tilde{q}_{min}$ is the lightest of the light flavoured squarks) and on the right $m_{\tilde{b}_1} - m_{\tilde{\chi}_1^0}$, $m_{\tilde{t}_1} - m_{\tilde{\chi}_1^0}$ and $m_{\tilde{t}_1} - m_{\tilde{b}_1}$.

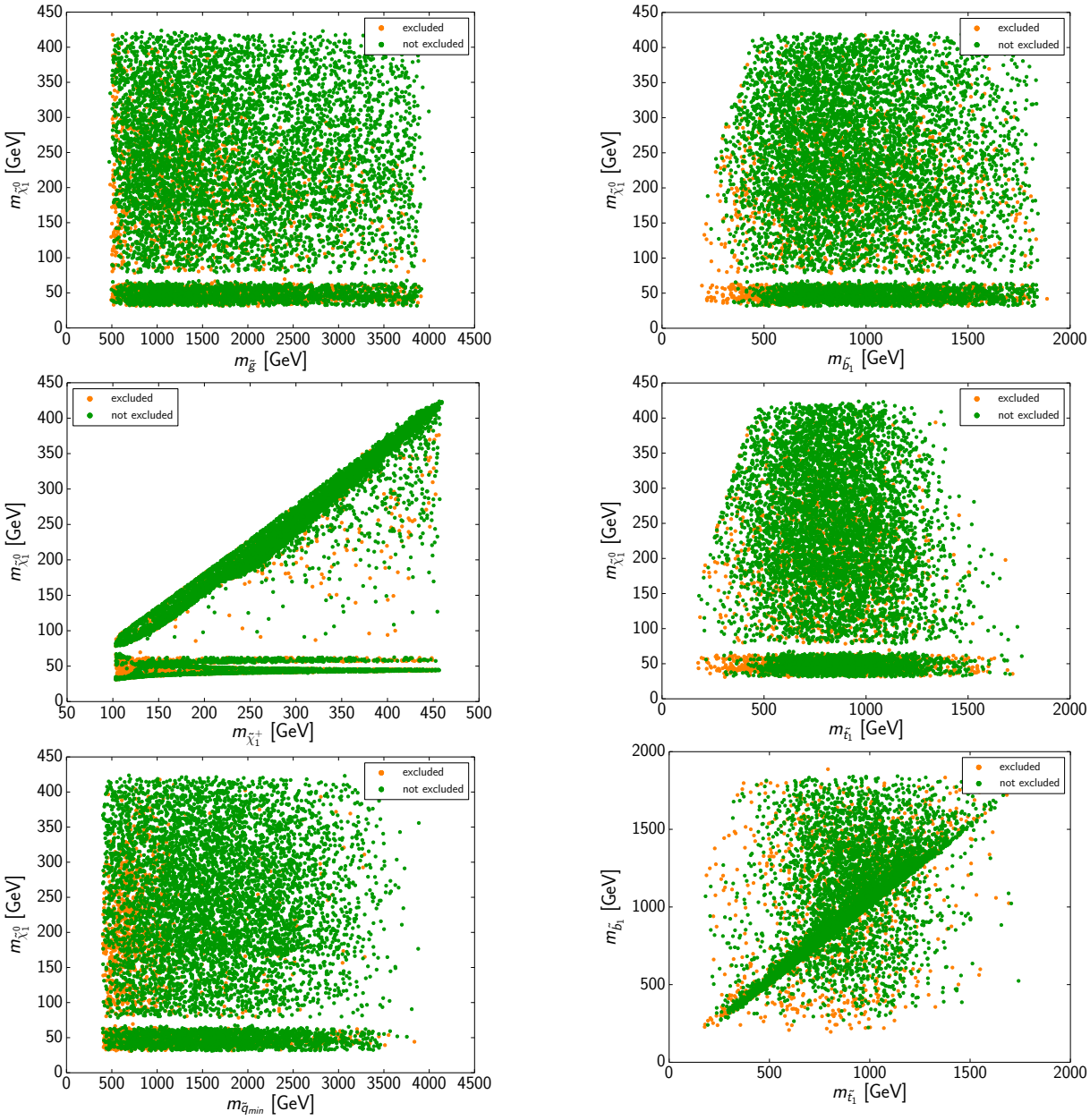

Figure 6.8: Same as Figure 6.7 but with the not excluded points plotted on top of the excluded points.

The comparison of these summarising result plots allow for a first glance on the outcome of the investigation of the LFT model set. The fact that there are no clearly excluded regions, in particular for the third generation squarks and the gluinos, gives rise to the question which experimental results are most constraining for these sparticles. Secondly it has to be clarified why the majority of model points could not be excluded.

6.2.2 Survey of Excluded Model Points

In order to analyse which experimental results have the highest significance in the LFT scenario, this section exclusively concentrates on the excluded points. All plots presented below follow the same approach.

First of all, every excluded model point is projected onto the respective mass plane and thus shown as background. Secondly the analysis leading to the highest ratio of $(\sigma \times BR)_{theory}$ to $(\sigma \times BR)_{experiment}$ is chosen as the most constraining one. Then the model points are sorted on the basis of these most constraining analyses. Subsequently they are depicted in several mass planes. Topologies irrelevant to a given mass plane are ignored, e.g. constraints which stem from eweakino decays are not shown in the $m_{\tilde{g}} - m_{\tilde{\chi}_1^0}$ plane. The axes are cut in order to enlarge the interesting mass region and results that exclude fewer than ten points are omitted. Finally these plots are overlaid with the official exclusion lines for the most relevant results, if available.

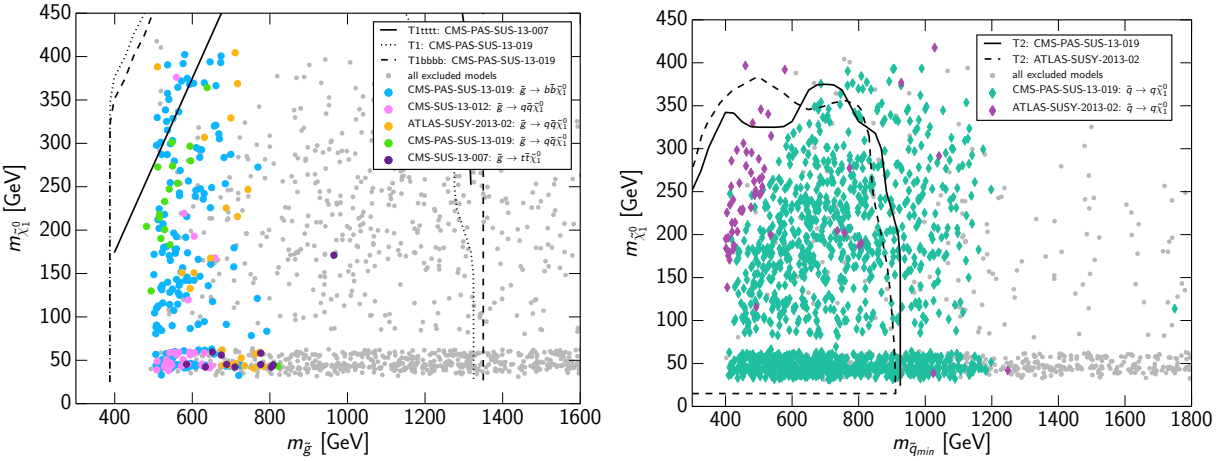

(a) Most constraining results for gluino topologies. The official exclusion lines shown are T1 (dotted) and T1bbbb (dashed) from CMS-PAS-SUS-13-019 and T1tttt from CMS-PAS-SUS-13-007 (solid).

(b) As before $m_{\tilde{q}_{min}}$ denotes the lightest of the first and second generation squarks. The exclusion lines shown in the plot correspond to the T2 results from CMS-PAS-SUS-13-019 (solid) and ATLAS-SUSY-2013-02 (dashed).

Figure 6.9: The relevant excluded model points in the $m_{\tilde{g}} - m_{\tilde{\chi}_1^0}$ (a) and $m_{\tilde{q}_{min}} - m_{\tilde{\chi}_1^0}$ (b) mass plane.

Following this approach Figure 6.9a shows the most excluding results in the $m_{\tilde{g}} - m_{\tilde{\chi}_1^0}$ mass plane, which are relevant for constraining the sparticle in question, namely the gluino. In particular these are the results for gluino three body decays to two quarks, tops or bottoms plus LSP (T1, T1tttt and T1bbbb) from the hadronic analyses CMS-PAS-SUS-13-019 and ATLAS-SUSY-2013-02 as well as T1tttt from the CMS single lepton search CMS-SUS-13-007. A first noteworthy conclusion can be drawn from this result plot. The T1tttt topology basically plays no role in the LFT scenario. This can be understood from the typical mass configuration

and the branching fractions for gluinos, stops and sbottoms dominating in this scenario, which among others favour gluino decays via on-shell stops and sbottoms. To the contrary, the experimental results for gluino decays always assume off-shell stops and sbottoms, respectively. The interplay between these three sparticles will be examined in detail in subsection 6.2.3.

The right panel in Figure 6.9 shows the distribution of excluded model points as a function of the minimal squark mass and the LSP mass. As already stated above, the most constraining experimental results for the light flavoured squarks stem from hadronic analyses considering direct squark decays to quark and LSP, like the T2 results from CMS-PAS-SUS-13-019 and ATLAS-SUSY-2013-02 (cf. Figure 6.9b). The exclusion lines for both results are shown, whereby the solid (dashed) line represents the region excluded by the CMS (ATLAS) result. It has to be taken into account that both analyses assume squarks to be mass degenerate, which is not the case in the LFT scenario. Secondly, in this scenario gluinos are not necessarily decoupled, thus increasing the production cross section of squarks. Due to this facts the region excluded by SModelS exceeds the officially excluded region for heavier squarks.

Figure 6.10 depicts the $m_{\tilde{\chi}_1^\pm} - m_{\tilde{\chi}_1^0}$ mass plane. The result summary in the previous section already indicated a small excluded region, which is again clearly identifiable. Moreover, it can be assigned to the off-shell part of the CMS-SUS-13-006-TChiWZ result. The exclusion line shown in this plot likewise belongs to this experimental result. The kinematic edge where the W (Z) boson enters the off-shell regime is indicated by the dashed (dotted) line. In the on-shell region the strongest constraints are provided by the ATLAS-SUSY-2013-12 result for this topology. In addition the most constraining results with intermediate charginos are shown. These are the T6ttWW and T6bbWW CMS results, where a sbottom (stop) cascade decays via top (bottom) and chargino into a W boson and the LSP.

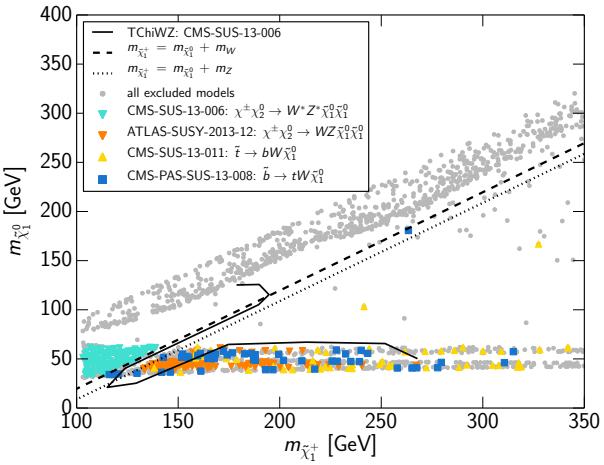

Figure 6.10: Models excluded by the relevant results in the $m_{\tilde{\chi}_1^\pm} - m_{\tilde{\chi}_1^0}$ mass plane. Again all excluded model points are shown as background.

These two topologies can be used to constrain the sbottom and stop mass, respectively. Figure 6.11 shows the corresponding results in the respective mass planes with the additional most relevant T2bb and T2tt CMS results. The stop and sbottom topologies are depicted conjointly due to the mass degeneration of the lightest stops and sbottoms for a large number of LFT model points.

The $m_{\tilde{t}_1} - m_{\tilde{\chi}_1^0}$ mass plane is shown in Figure 6.11a. One can see, that the region excluded by stop topologies T2tt and T6bbWW is well below the exclusions for these two CMS-SUS-13-011 results, as indicated by the official lines. The main reasons for this are again the typical mass configuration and branching ratios in this scenario, as explained below.

Finally, in Figure 6.11b the constraints on the sbottom mass can be seen. This plot shows nicely that models with light sbottoms are excluded by the T2bb result of CMS-PAS-SUS-13-019. With increasing sbottom mass the T2bb result of CMS-PAS-SUS-13-018 becomes the most constraining one. In addition the apparent correlation of the points excluded by stop topologies, once again elucidates the fact, that the bigger part of the sbottoms is almost in a left handed gauge eigenstate.

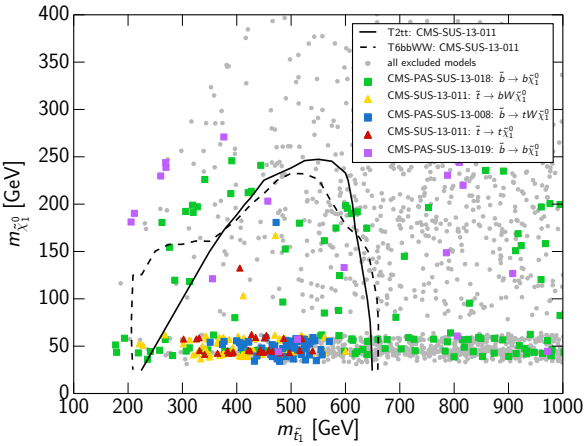

(a) The most relevant results in the plane of stop and neutralino masses. The official exclusion lines belong to the T2tt (solid) and T6bbWW (dashed) result of CMS-SUS-13-011.

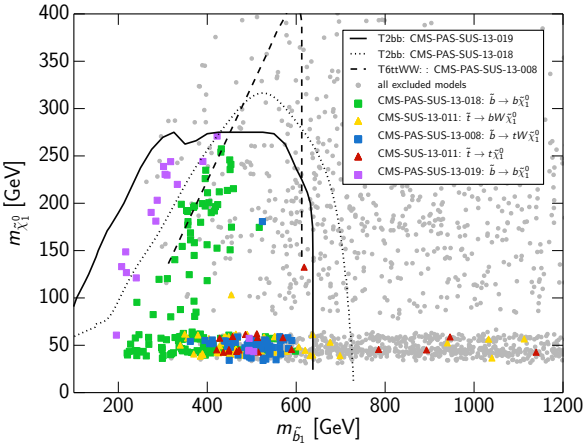

(b) The most relevant results as function of $m_{\tilde{b}_1}$ and $m_{\tilde{\chi}_1^0}$ overlaid by the official exclusion contours for the T2bb result from CMS-PAS-SUS-13-019/18 (solid/dotted) and for the T6ttWW result of CMS-PAS-SUS-13-008 (dashed).

Figure 6.11: Same as Figure 6.9 but here the $m_{\tilde{t}_1} - m_{\tilde{\chi}_1^0}$ (a) and $m_{\tilde{b}_1} - m_{\tilde{\chi}_1^0}$ (b) planes are shown.

Both plots in Figure 6.11 show that basically all points excluded by the T6ttWW and T6bbWW results are located in the region where the $\tilde{\chi}_1^0$ is almost a pure bino. Since the models with a mixed LSP populate the diagonal in the $m_{\tilde{\chi}_1^\pm} - m_{\tilde{\chi}_1^0}$ mass plane (cf. Figure 6.10), it is understandable that for these models only results considering the W boson off-shell are applicable. Unfortunately such off-shell T6ttWW and T6bbWW caused severe technical problems during the validation procedure and are therefore not yet included in the public database of SModelS.

Summarising the results presented in this section, it is clear that for a wide range of SUSY searches at LHC the interpretation of experimental results currently available, can not be used to constrain the investigated LFT scenario. Even if one considers the fact, that excluded regions in the parameter space of full models usually fall below the exclusions in a reduced SMS parameter space, mainly due to branching ratios below 100%, the number of model points which could be excluded is unexpectedly low. Hence, it has to be clarified why so many

results could not be applied on the LFT models. In particular it is interesting to understand which interpretations could target such a scenario.

6.2.3 Suggestions for Future SMS Topologies

The big discrepancy between the exclusions on sparticle masses provided by the ATLAS- and CMS-collaboration and the ones gained by applying SModelS v1.0.3 to the LFT model set has several reasons which shall be explained in this section. These considerations lead directly to the question of future SMS interpretations of LHC results with $\sqrt{s} = 13$ TeV.

The sparticles that are most affected by LFT constraints are the stops and due to loop corrections to the stop mass, the gluinos (cf. subsection 6.1.1). Hence it is important to understand why the common results of stop and gluino searches failed to constrain the LFT model set. A possible explanation can be found from interpreting the missing topology table provided by SModelS (cf. subsection 5.2.5). Therefore all deliberations in this section concentrate on the model points that could not be excluded. These points will be examined in detail particularly with regard to stops and gluinos. In addition several SMS topologies will be proposed which can be used to constrain the LFT parameter space.

Stop Topologies

The result plots in the mass plane relevant for the investigation of stops (the $m_{\tilde{t}_1} - m_{\tilde{\chi}_1^0}$ plane) presented in the previous section, reveals that roughly 1% of the LFT models can be excluded by applying stop results (T2tt and T6bbWW). In order to understand this meagre percentage it is illuminating to consider the main decay modes of the stops in this scenario.

The left panel in Figure 6.12 shows the production cross sections for stop pair production in the relevant mass plane, which are comparable to the CMS reference cross sections [86] (cf. Figure A.1). The right panel depicts the main decay modes of the stops. From this it can be understood that for the major part of models the stop decays either to $\widetilde{\chi}^{\pm}$ or to the third and second lightest $\widetilde{\chi}^0$. The decay mode $\widetilde{t} \to b\widetilde{\chi}^{\pm}$ in particular, seems to point towards a cascade decay which in principle matches the T6bbWW topology, $\widetilde{t} \to b\widetilde{\chi}^{\pm} \to W^*\widetilde{\chi}_1^0$. From Figure 6.11a it can be seen that the T6bbWW result is not as constraining as expected. Indeed, less than 1% of all models can be excluded by any of the available T6bbWW results (cf. Table 5.1). As indicated by the typical mass configuration shown in Figure 6.4, the mass splitting between the $\widetilde{\chi}_1^{\pm}$ and the $\widetilde{\chi}_1^0$ may not be sufficient to provide an on-shell W boson. Hence one might think, that the big number of valid points is related to the fact that the database does not yet contain the off-shell regime for this topology. However this is not quite the case, as shall be shown in the following via the usage of SModelS' missing topologies option.

As explained in subsection 5.2.5, the interpretation of the missing topologies is not straight forward. This shall be exemplified by the process which eventually leads to useful assertions about possible stop topologies.

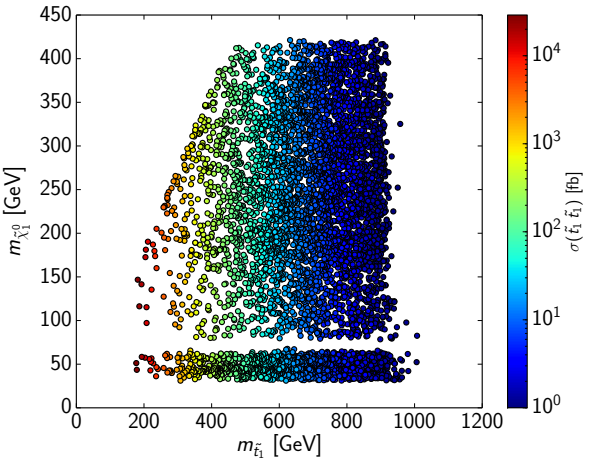

(a) Production cross section for stop pair production indicated by the temperature as function of $m_{\tilde{t}_1}$ and $m_{\tilde{\chi}_1^0}$. Models with $\sigma_{production} < 1$ fb are rejected.

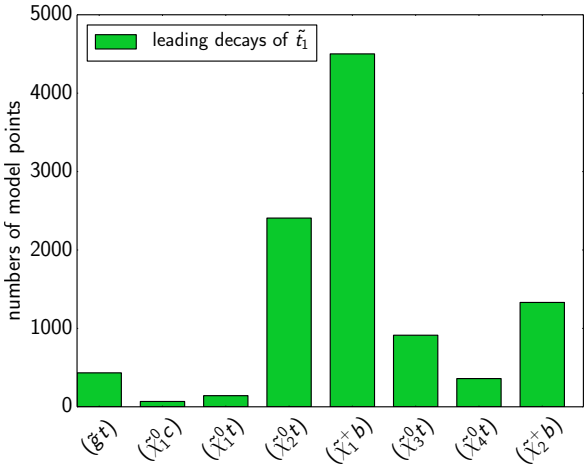

(b) For each model point the stop decay channel with the highest branching ratio is taken. The plot shows the number of models for the most relevant decay channels.

Figure 6.12: Production cross sections (a) and main decay modes (b) for $\widetilde{t}_1$in the LFT scenario.

In a first approach the missing topology with the highest weight, i.e. $(\sigma \times BR)$, for each not excluded point is depicted in the $m_{\tilde{t}_1} - m_{\tilde{\chi}_1^0}$ mass plane. The resultant plot is shown in Figure 6.13, whereby the topologies depicted have weights exceeding 1 fb. The legend shows the respective nested bracket notation introduced in subsection 5.2.2 and the interpretation of this notation in terms of decays. Hereby it has to be considered, that for the missing topologies the information about the BSM masses gets lost. Hence, an arbitrary missing topology may comprise several decays, all of which yield the same signature, or final states. This can be illustrated by the example of the di-jet plus $\not{E}_T$ final state $([[], [[jet, jet]]])$ which clearly dominates the plot in Figure 6.13. One branch contains no SM states at all, the other one has one vertex with 2 hadronic jets, i.e. first and second generation squarks. Since there are several possible sparticles which may decay into two squarks, additional information is needed to find the actual decays contributing to this missing topology. The first branch without SM particles is simply a directly produced $\widetilde{\chi}_1^0$. Since the associated production of eweakinos and hadronic sparticles is suppressed it seems unlikely that the second branch represents for example a gluino decay. Another option is to consider these jets as decay products of SM vector bosons W and Z. Hence, the di-jet plus MET topology can be interpreted as associated $\widetilde{\chi}_1^0$ - $\widetilde{\chi}_1^\pm/\widetilde{\chi}_2^0$ -production. To probe this assumption all points, for which this topology is dominant, are projected into the $m_{\widetilde{\chi}_1^\pm} - m_{\widetilde{\chi}_1^0}$ and the $m_{\widetilde{\chi}_2^0} - m_{\widetilde{\chi}_1^0}$ mass plane. In these projections all the points are located in the diagonal, hence the mass splitting between the involved sparticles is sufficiently small for off-shell SM vector bosons. In addition, all three eweakinos in this region of parameter space are mostly higgsino like, or at least a higgsino bino mixture. These facts

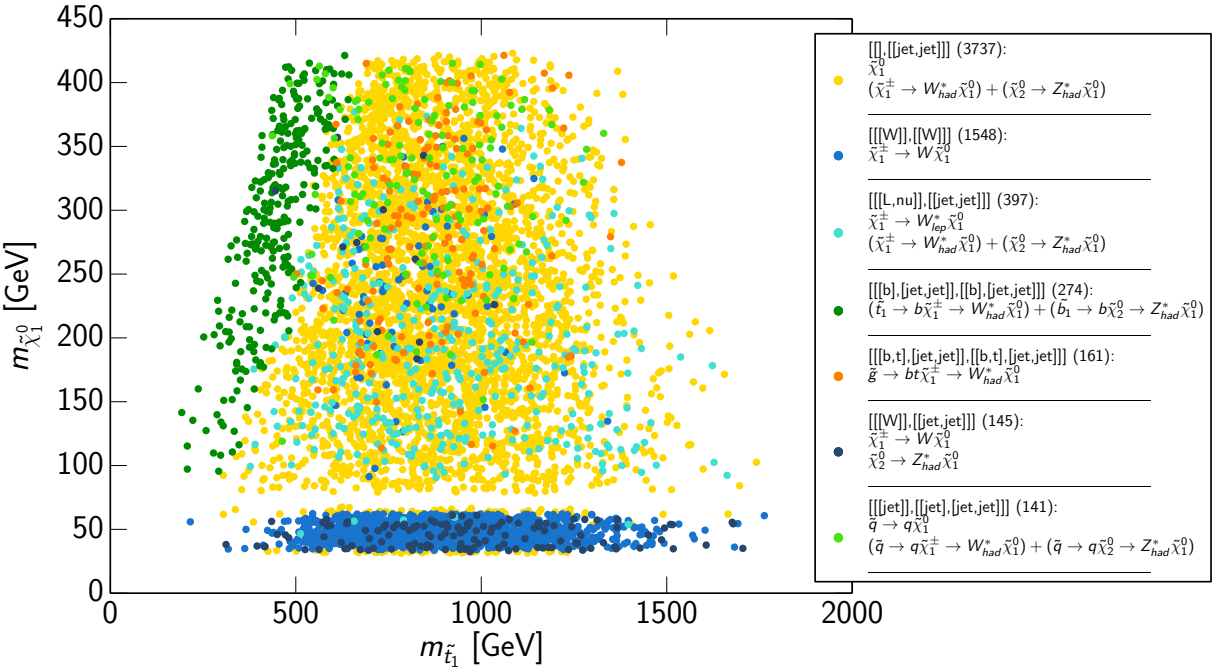

Figure 6.13: First plot of missing topologies with weight $(\sigma \times BR) > 1$ fb in the $m_{\tilde{t}_1} - m_{\tilde{\chi}_1^0}$ mass plane. The legend states the nested bracket notation as well as the decays contributing. The number of points for each topology is given in parenthesis.

foster the associate production of $\widetilde{\chi}_1^0$ - $\widetilde{\chi}_1^\pm$ and $\widetilde{\chi}_1^0$ - $\widetilde{\chi}_2^0$. Following this and similar procedures [2] a sum of contributing decays can be found for each of the missing topologies. This example shows plainly that SModelS' missing topologies functionality do not yield a precise analysis of the underlying BSM scenario. Nevertheless it can be used to get a sense of the respective parameter space and an impression of strategies to explore it.

Various tests have shown, that the di-jet plus MET topology comprises only eweakino decays. Moreover, there is a wide range of missing topologies which stem from similar eweakino decays via on- and off-shell SM vector bosons. Whereby it becomes apparent that most of the off-shell W and Z decay hadronically. Since current interpretations of SUSY searches consider only leptonic channels for such decays, it is understandable that even the implementation of the off-shell results, such as T6bbWW would not significantly increase the number of excluded points in this scenario.

However, it is understandable that pure eweakino signal topologies can not be used to constrain the stops, thus can justifiably be ignored. The only interesting topology shown in Figure 6.13 is denoted $[[[b],[jet,jet]],[[b],[jet,jet]]]$. It comprises contributions from stop and sbottom decays and the distribution of its assigned model points is clearly correlated with $m_{\tilde{t}_1}$. This gives rise to the question if there are additional stop signatures covered by the vast

[2] These procedures include detailed examination of the SModelS decomposition for samples of model points, searches for correlations with respect to the nature of the involved sparticles etc.

amount of eweakino topologies, dominating the mass plane in Figure 6.13. Consequently in a next step the di-jet plus MET topology is discarded and instead the second most contributing missing topology is taken in these points (cf. Figure 6.14). Indeed, this plot reveals another interesting signature ($[[[t],[jet,jet]],[[t],[jet,jet]]]$) which shows an unambiguous correlation with the mass of the stop.

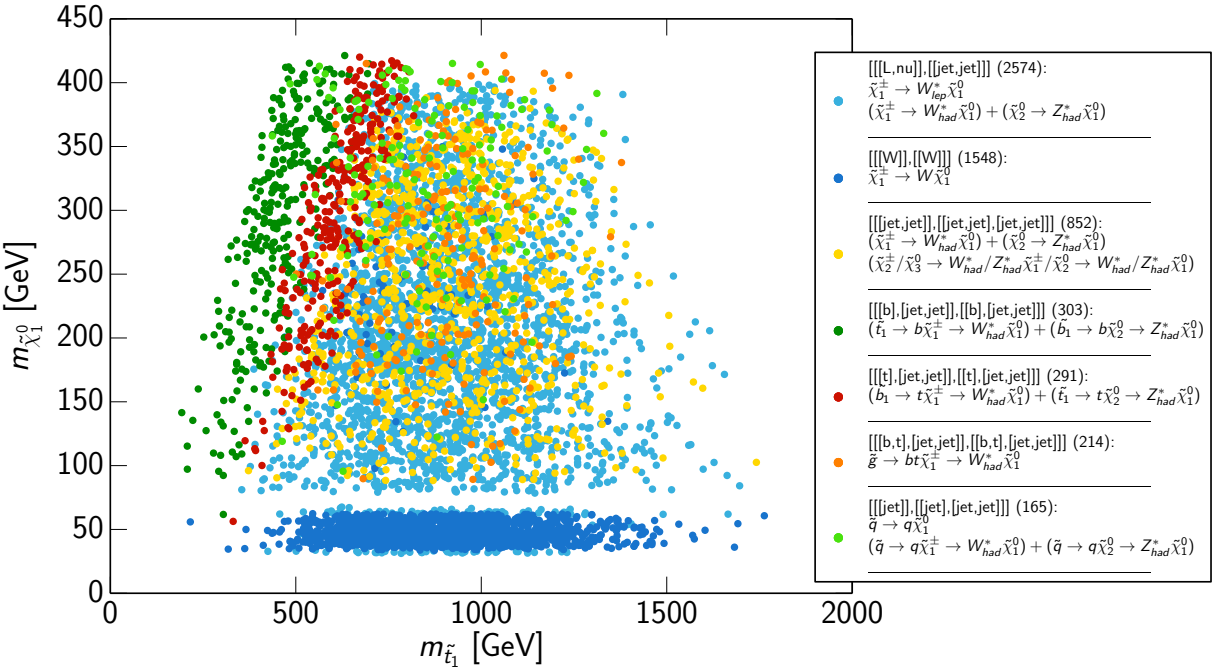

Figure 6.14: Similar to Figure 6.13 but for every point originally assigned to di-jet plus MET signature, here the second most contributing topology is taken.

Following up on this approach it is advantageous to take into account the entire missing topology table provided by SModelS. Therefore all missing topologies are sorted according their frequency of appearance. Subsequently every signature which is not relevant in a given mass plane is rejected.

The resultant plot (cf. Figure 6.15) depicts only hadronic decay channels, whereby only the seven most frequent topologies are shown to improve clearness. In each point all most frequent topologies are plotted on top of each other, which allows for several conclusions:

- With increasing $m_{\tilde{t}_1}$ the stop production cross section drops rapidly (cf. Figure 6.12a) for $\sqrt{s} = 8$ TeV. Therefore no signal topologies containing stop decays can be found for $m_{\tilde{t}_1} > 800$ Gev.
- The most powerful topology for constraining the stop mass in the LFT scenario considers pair produced stops which cascade decay via an intermediate neutralino into a hadronically decaying off-shell Z and the LSP. Whereby the contribution from sbottom pair production is accounted for by the nature of the sbottoms which are mostly left handed.

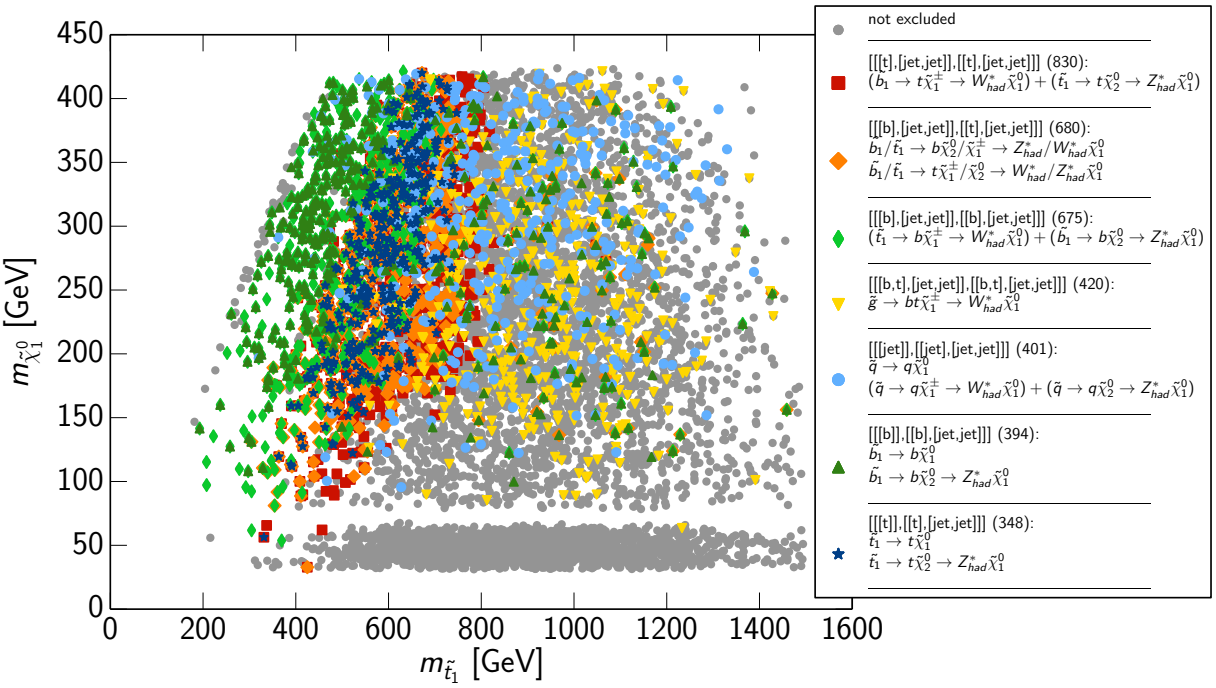

Figure 6.15: Most frequent missing topologies with $(\sigma \times BR) > 1$ fb and relevant decays only, as function of $m_{\tilde{t}_1}$ and $m_{\tilde{\chi}_1^0}$.

- Considerably large contributions come from $\widetilde{\mathrm{t}}$ and $\widetilde{\mathrm{b}}$ pair production, respectively. Such production modes result in an asymmetric topology comprising cascade decays via intermediate chargino (neutralino) to off-shell W (Z) and the LSP (cf. Figure 6.16a). Whereby very few points are located in the region with $m_{\tilde{t}_1} > 800$ GeV. These points most likely originate from right handed sbottoms.

- Roughly 10% of the not excluded models could be probed by results interpreted in terms of T6bbWW in the hadronic off-shell regime.

- Last but not least contributions are found from an asymmetric stop (sbottom) topology. One branch shows a cascade decay via an intermediate neutralino to a hadronic off-shell Z and the LSP, whereas the other is a direct stop (sbottom) decay to top (bottom) and LSP (cf. Figure 6.16b).

These assertions can be summarised as follows. In order to constrain pMSSM model points providing low amounts of fine tuning with respect to the stop mass, it is beneficial to consider interpretations of experimental search results in terms of stop cascade decays via hadronically decaying SM vector bosons. In addition topologies with asymmetric branches should be taken into account. These conclusions are even more noteworthy since the production cross sections for stops will increase in the $\sqrt{s} = 13$ TeV run of LHC which is about to start in the next couple of weeks.

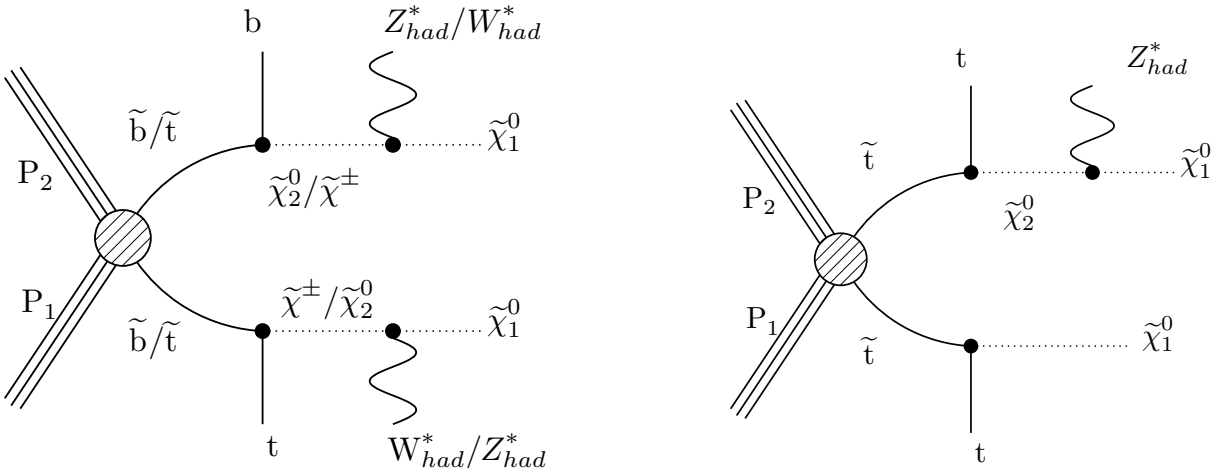

(a) $[[[b],[jet,jet]],[[t],[jet,jet]]]$ (b) $[[[t]],[[t],[jet,jet]]]$

Figure 6.16: Feynman diagrams for the asymmetric stop topologies.

Gluino Topologies

Gluinos are also subjected to fine tuning, hence they shall be examined in greater detail. In the previous section it was shown, that the gluino masses of models which could be excluded fall way below the exclusions found by ATLAS and CMS using simplified models. There are several conceivable explanations for this under-exclusion.

First of all, common interpretations of the experimental results in terms of SMS assume squarks to be completely decoupled, which certainly is not the case in the LFT scenario. On the one hand, this non-decoupling of the squarks may affect the production cross section, since additional production channels are opened (cf. Figure 4.1a). Figure 6.17a shows the production cross sections exceeding 1 fb as a function of $m_{\tilde{g}}$ and $m_{\tilde{\chi}^0_1}$. The comparison with the relevant CMS reference cross sections [87] (cf. Figure A.1) reveals a slight preponderance of the LFT cross sections, but it is small enough to be neglected. On the other hand, the non-decoupling increases the number of possible decay channels, since the decays of gluinos via on-shell squarks of all three generations are always favoured when kinematically allowed (cf. subsection 4.1.2). Another significant fact is the assumption of 100% branching ratio in the SMS interpretation of experimental results. Considering for example the T1tttt topology, the gluino decays exclusively into two tops and the LSP, i.e. there is only one open channel. On the contrary, from Figure 6.17b one can see, that for a vast majority of the gluinos in this scenario a large number of channels is open. The plot shows the total number of possible decay modes in the $m_{\tilde{g}}-m_{\tilde{t}_1}$ plane. Whereby this number is maximised in a narrow region right at the kinematic edge, where the decays via on-shell stops become available. Right below this region the number of open channels drops dramatically and then slowly increases again for higher gluino masses. Hence, the assumption of 100% BR is gravely violated in the LFT scenario, thus counteracting the exclusion of model points by applying SMS results.

In addition, the comparison with Figure 6.17a exhibits, that processes occurring for $m_{\tilde{g}} >$

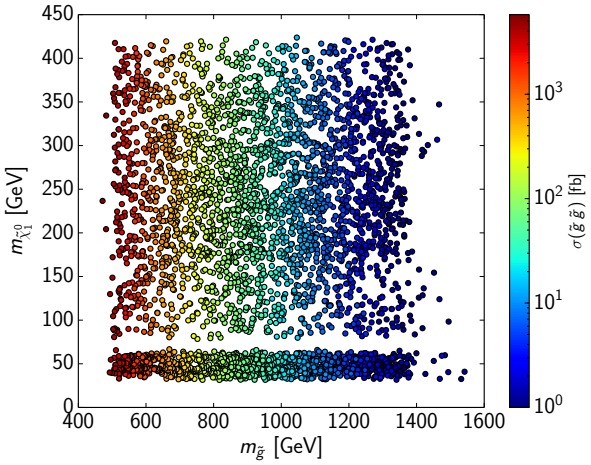

(a) Production cross section for gluino pair production indicated by the temperature as function of $m_{\tilde{t}_1}$ and $m_{\tilde{\chi}_1^0}$. Models with $\sigma_{production} < 1$ fb are rejected.

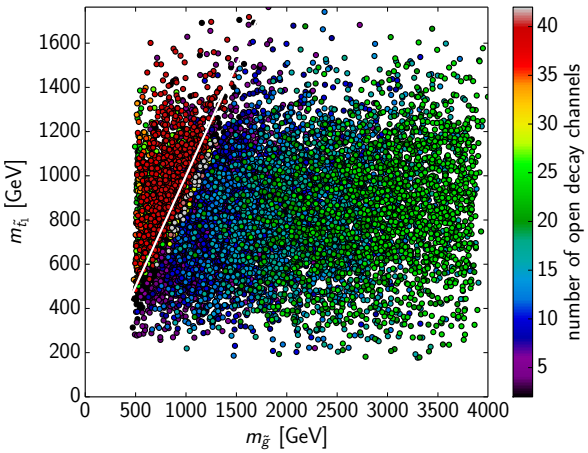

(b) The temperature indicates the total number of gluino decay modes available, shown in the $m_{\tilde{g}}-m_{\tilde{t}_1}$ plane. The white line marks the kinematic edge $m_{\tilde{g}} = m_{\tilde{t}_1}$.

Figure 6.17: Production cross sections (a) and number of decay modes (b) for $\tilde{g}$ in the LFT scenario.

1400 GeV are severely suppressed, since the statistics for calculating the production cross sections was too low to get reasonable gluino cross sections in this region.

Taking into account the complex decay patterns, it is understandable, that the weights for individual signal topologies originating from gluinos are rather low and often restricted to particular small regions in the parameter space. Nevertheless, a very interesting decay channel can be found, which could be exploited to constrain the gluino mass. This decay mode $\tilde{g} \to bt\tilde{\chi}^{\pm}$ is dominant for at least roughly 800 models, as will be examined in detail below.

Following the same approach as described previously for the stops, assertions can be made about the missing topologies relevant in the $\tilde{g}$ -$\tilde{\chi}_1^0$ mass plane. Figure 6.18 depicts the seven most frequent missing topologies with weights above 1 fb for every model point plotted on top of each other, whereby non-hadronic topologies are vetoed.

At a first glance one can see that basically all decays involve the above mentioned process of gluinos decaying to top, bottom and chargino, with the chargino decaying via on- and off-shell W bosons. According to the CMS naming convention, this topology would be referred to as T5btbtWW or as T7btbtWW in case the third generation squark in the first vertex is on-shell. Figure 6.19 shows the Feynman graphs of these decay channels.

The frequency plot of missing topologies in the $m_{\tilde{g}}-m_{\tilde{\chi}_1^0}$ plane (cf. Figure 6.18) can be interpreted as follows:

- A total number of 867 different missing topologies relevant for gluino decays are available, most of which are very rare. Thus the frequency of the individual topologies may

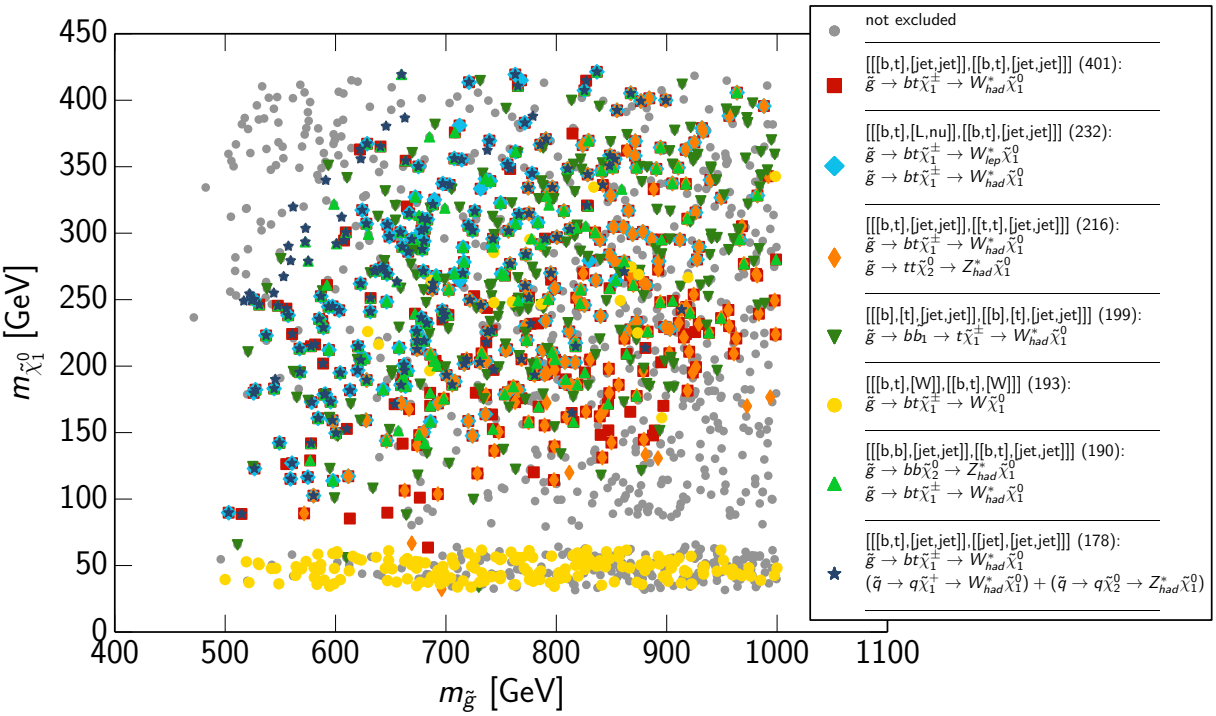

Figure 6.18: Most frequent missing topologies with $(\sigma \times BR) > 1$ fb and hadronic decays only in $\tilde{g}$ -$\tilde{\chi}_1^0$ plane.

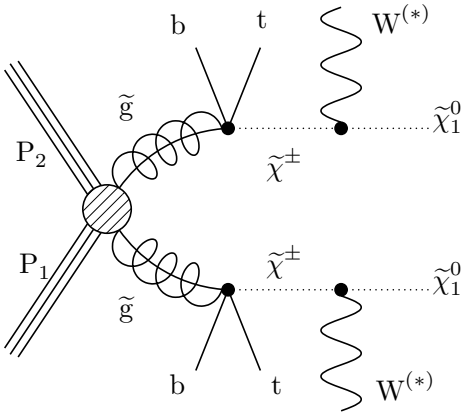

(a) $\tilde{g} \to bt\tilde{\chi}^\pm \to W^{(*)}_{(had/lep)}\tilde{\chi}_1^0$

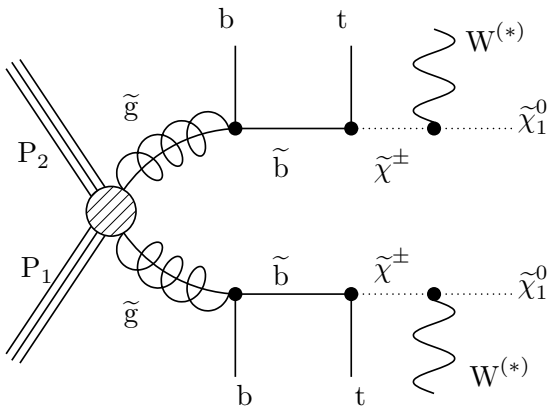

(b) $\tilde{g} \to b\tilde{b} \to t\tilde{\chi}^\pm \to W^{(*)}_{(had/lep)}\tilde{\chi}_1^0$

Figure 6.19: Feynman diagrams for the T5btbtWW (a) and T7btbtWW (b) topology.

be arbitrarily small. In fact plenty of them show up only once. This is expected from the rather complex gluino decay patterns, which greatly vary throughout the parameter space. In addition the great number of decay channels open for the gluino in a given model point (cf. Figure 6.17b) strikingly decreases the branching ratio for the single decays. Hence most of the gluino topologies are suppressed by small $(\sigma \times BR)$.

- The highest contributions come from the T5btbtWW topology with off-shell W bosons. It occurs in two different manifestations. One with the W* decaying hadronically in both branches ($[[[b,t],[jet,jet]],[[b,t],[jet,jet]]]$). The second signature ($[[[b,t],[L,nu]],[[b,t],[jet,jet]]]$) exhibits one W* decaying into two jets and the other one leptonically whereby the capital L comprises all three lepton generations.
- Additional final states ($[[[b,t],[jet,jet]],[[t,t],[jet,jet]]]$ and $[[[b,b],[jet,jet]],[[b,t],[jet,jet]]]$) origin from very similar decay modes. Whereby one branch contains a gluino decaying into the second lightest neutralino plus two tops and bottoms, respectively. The $\widetilde{\chi}_2^0$ decays further to a hadronically decaying off-shell Z.
- The region of parameter space, where the LSP is bino like with $m_{\widetilde{\chi}_1^0} \simeq 50$ GeV, is clearly dominated by the T5btbtWW topology with the W boson on-shell, since the mass splitting between the chargino and the LSP is sufficient ($m_{\widetilde{\chi}_1^\pm} > m_{\widetilde{\chi}_1^0} + m_{\mathrm{W}}$).
- The most infrequent topology shown in Figure 6.18 is an associated production of gluino and light flavoured squarks. The gluino once more decays according to T5btbtWW, whereas the squark cascade decays via chargino or neutralino into a final state with two hadronic jets and MET. These jets stem from SM vector bosons, which are produced in the decay of the respective eweakinos.

Given the presence of the T5btbtWW topology and the absence of models excluded by T1tttt results, the weights for these two are compared in Figure 6.20. The left panel depicts the combined weight for the T5btbtWW for on-shell W as well as hadronic and leptonic final states in the off-shell regime. Hereby a lower cut of 1 fb on the topology weight is applied. The right panel shows the weight for T1tttt, whereby it was refrained from applying a lower cut. The comparison of these two plots reveals a preponderance of the weight of T5btbtWW of about one to two orders of magnitude for comparable gluino and LSP masses. Regarding the negligible weights of the T1tttt topology it is completely understandable why the corresponding results could not be used to constrain the gluino mass. On the other hand, Figure 6.20a shows that T5btbtWW has a reasonably high weight which is limited only by the gluino production cross section. Hence, this topology is expected to become even more present with increased centre of mass energy and therefore increased gluino production cross sections.

The conclusions that can be drawn from the deliberations above shall be summarised again. The applicability of current interpretations of experimental results considering gluino decays is very limited in the LFT scenario. Instead a reinterpretation of events yielding final states with top, bottom and W boson, as gluino decays may be more fruitful. Secondly, due to the heterogeneous structure of the gluino sector, it is expected that inclusive searches will perform best in constraining the LFT parameter space. It has to be emphasized, that it may be useful to allow for non-decoupled third generation squarks, to target this specific region of the pMSSM parameter space. In addition it becomes apparent once more, that the hadronic decay channels of the SM vector bosons should be taken into account. Finally, asymmetric topologies have been found, which not only involve gluino pair production, but also associated production of gluinos and light flavoured squarks.

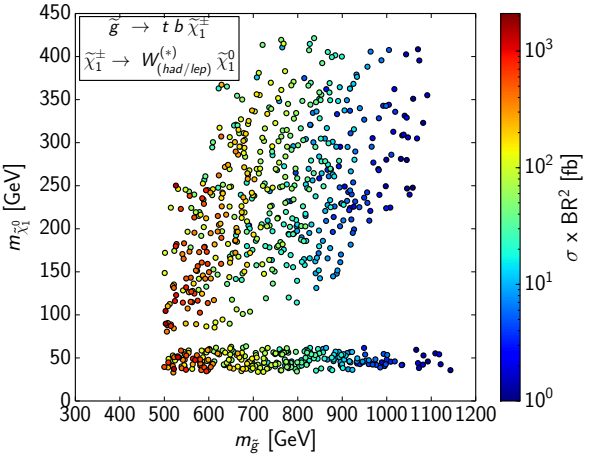

(a) The pair produced gluinos decay via a three body decay into top, bottom and chargino. The chargino decays further to on- or off-shell W and the LSP. Points with weights below 1 fb are rejected.

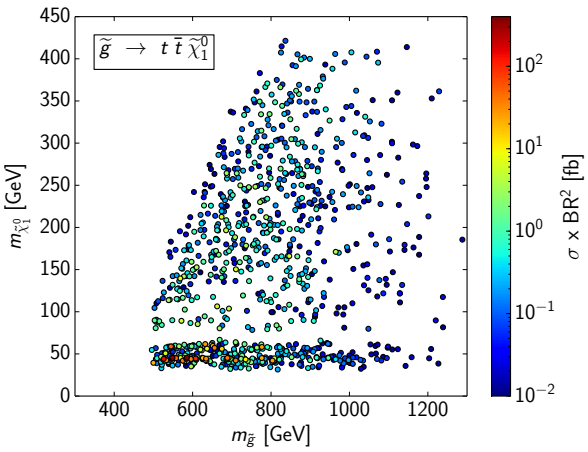

(b) Weight for the gluino three body decay into two tops plus the LSP (T1tttt).

Figure 6.20: $(\sigma_{production} \times BR^2)$ for gluino topologies indicated by the temperature as function of $m_{\tilde{g}}$ and $m_{\tilde{\chi}_1^0}$.

Monojet Signature

The occurrence of the associated gluino squark production in the previous considerations of the missing topology results, already indicates that sparticles in the LFT scenario are not necessarily pair produced. Amongst a wide range of various signatures origin from eweakino production modes, missing topologies have been found, which contain associated productions of SUSY particles.

One of these very interesting signatures shall be introduced in this section. This missing topology is characterised by a single hadronic jet and MET in the final state and will therefore be referred to as "monojet" in the following. This monojet topology was found to be a co-production of a light flavoured squark and a neutralino. Given the fact that such associated productions of strongly and weakly coupling sparticles are suppressed, it is quite surprising that this specific mode occurs in roughly 60% of all LFT model points and also in 60% of the models which could not be excluded. Therefore this monojet signature shall be examined in greater detail.

Figure 6.21a shows the topology weight for the monojet signal topology as a temperature plot in the mass plane of the lightest of the first and second generation RH squarks and the fraction of bino content of the LSP. Only points are taken into account which provide a monojet weight above 0.1 fb. These are at least 27% of all model points. In principle such points can be found up to very high squark masses, nevertheless the $m_{\tilde{q}^R_{1min}}$ - axis was cut at 2 TeV in order to improve clearness. The plot reveals a nice correlation of the weight with the

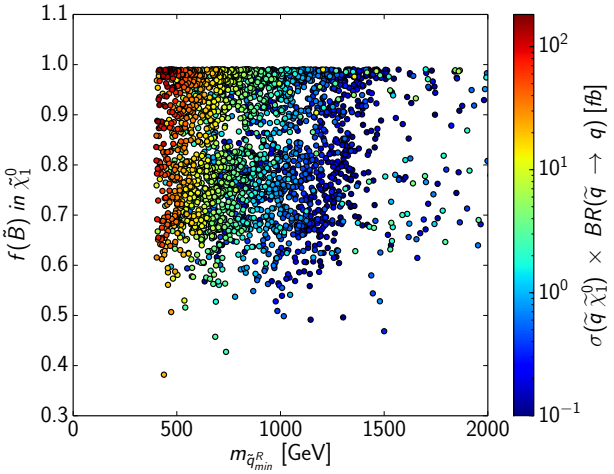

(a) Weight for squark neutralino co-production with the squark decaying into quark plus neutralino. Points with weights below 0.1 fb are rejected.

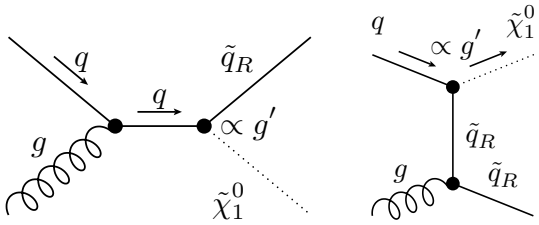

(b) Tree-level s- and t-channel Feynman diagrams for the associated production of squark and neutralino.

Figure 6.21: $(\sigma_{production} \times BR)$ indicated by the temperature as a function of the minimal RH squark mass and the bino content of the LSP $f(\widetilde{\mathrm{B}})$ (a) and the production modes (b) for the monojet topology.

mass of the lightest RH squarks. From this it can be understood, that the squarks causing the jet plus MET signature are right handed. Also the bino fraction slightly effects the cross section for this topology, hence one can assume that the eminent frequency of this signature originates from the associated production of a RH squark and a bino neutralino.

The two tree-level Feynman diagrams depicted in Figure 6.21b are accountable for such an associated production. These production processes are controlled by a weak and a strong gauge coupling and thus are suppressed in comparison to pure strong processes such as e.g. gluino pair production. Nevertheless, the nature of the neutralino in the LFT scenario fosters such a production mode. Since this signal was found to originate from RH squarks and the bino LSP, the respective vertices in Figure 6.21b are controlled by a coupling proportional to g' the coupling constant of the $U(1)_Y$ gauge group.

As a side note it should be mentioned that this vertex could also dominate annihilation processes of DM. Assuming the lightest neutralino is the particle source of DM, in the early universe there may have been a squark mediated annihilation mode, where two neutralinos produced two quarks. Hence this vertex is particularly interesting if such a monojet signature would be found at LHC. Measuring the coupling strength of this vertex could provide information about the nature of the LSP and about the value of its thermal relic. A detailed description of supersymmetric monojets, possible analytical strategies for background suppression and predictions on the reachable accuracy of measuring of the coupling strength of the monojet vertex can be found in Ref. [88].

Chapter 7

Conclusion and Outlook

SModelS - an automated tool to decompose any $\mathbb{Z}_2$-symmetric BSM model into its SMS topologies and systematically confront it with the relevant experimental constraints - and its results database were improved and the code was published.

To this end an object-oriented python package, the `databaseBrowser`, was developed which facilitates the access to every information stored in the results database. By means of this software tool the database was maintained and restructured. The `databaseBrowser` was also deployed in the work flow of the validation procedure of the SModelS framework and the database. Furthermore it was an indispensable part of the scripts which were used to produce the official CMS summary plots. These summary plots allow for an overview of the current status of SUSY searches at LHC and give an idea of the range of masses of sparticles explored at $\sqrt{s} = 8$ TeV. Given the sheer number of results published over the last years the necessity of such comparative plots becomes obvious. However, one has to keep in mind that the summary plots only reflect the most optimistic reaches for the SUSY searches and the results they represent are based on severe model assumptions.

The latest updated version of the SModelS framework, SModelS v1.0.3 , was applied to a specialised subset of the 19-parameter RPC pMSSM with a neutralino LSP characterised by a low fine tuning scenario. This scenario favours a typical mass spectrum with very light eweakinos. The lighter stops and the majority of the lighter sbottoms are also located at the bottom of the spectrum very frequently. Gluinos and squarks are not decoupled, thus allowing for complex decay patterns, in particular of third generation squarks and gluinos. Wide ranges of the LFT parameter space are determined by a bino like or a mixed bino higgsino LSP, which saturates the thermal relic density and a mostly higgsino like lightest chargino.

The application of SModelS to this set of pMSSM model points shows that the majority of current SMS interpretations of experimental SUSY search results are of limited suitability in this specialised scenario. In fact, merely about 22% of all the points could be excluded by applying the relevant experimental constraints. The bigger part of the model set was found to be dominated by various eweakino decays producing hadronically (and more infrequently leptonically) decaying W, Z and Higgs bosons. Additionally, gluino decays, which result in a

final state with tops, bottoms and on- or off-shell W bosons, were found to have reasonably large ($\sigma \times BR$) in wide regions of the LFT parameter space. Topologies arising from stop or sbottom pair production could be exploited in order to constrain the LFT scenario with regard to these sparticle masses.

In the light of the $\sqrt{s} = 13$ TeV run of LHC, general assertions can be made from the investigation of the LFT model set using SModelS. First of all, for future interpretations of search results it may be beneficial to consider gluino decays with non-decoupled third generation squarks and vice versa. Secondly, the hadronic off-shell regime for SM vector bosons, which could be explored potentially by search strategies concentrating on events with multiple jets, zero-leptons and MET final states, may be useful to constrain this sub set of the pMSSM parameter space. Another interesting consequence arising from the nature of the LSP has been encountered. The mostly bino like LSP and the non-degenerated RH light flavoured squarks enable an associated production of these two sparticles resulting in a single hadronic jet. This monojet topology was found to have reasonably large ($\sigma \times BR$) in particular regions of the parameter space.

The investigation of the LFT scenario elucidates the problems of phenomenological studies exploiting SMS interpretations and the virtue of SModelS for these studies. The SModelS-group aims at constant improvements of the framework itself and regular updates of the accompanying results database. To this end the experimental side of the SModelS framework is completely overworked at the moment. The database is restructured in order to deal with future analyses based on data of the second LHC run. In addition it is prepared to include not only upper limit maps but also efficiency maps, which correspond to a set of simulated values of acceptance times efficiency ($\mathcal{A} \times \epsilon$) for specific signal regions. The usage of efficiency maps (EM) is a more fundamental concept than the application of upper limit maps. For a given analysis every EM corresponds to one signal topology. Hence, EM can be used to compute UL maps for topologies differing from those considered by the analysis. Moreover, the usage of EM enables the combination of several topologies to a single upper limit. Among others, these alterations will be included in SModelS v1.1, which is expected to be released this winter.

Appendix A

Auxiliary Figures

Listing A.1: Parameter card used in SModelS v1.0.3 to perform the LFT scan.

```
[path]
databasePath = ./smodels-database/
[options]
inputType = SLHA
checkInput = True
doInvisible = True
doCompress = True
findMissingTopos = True
[parameters]
sigmacut = 0.01
minmassgap = 5.
maxcond = 0.2
[database]
analyses = all
txnames = all
[stdout]
printDecomp = True
addElmentInfo = True
printAnalyses = True
addAnaInfo = True
printResults = True
[file]
expandedSummary = True
addConstraintInfo = True
```

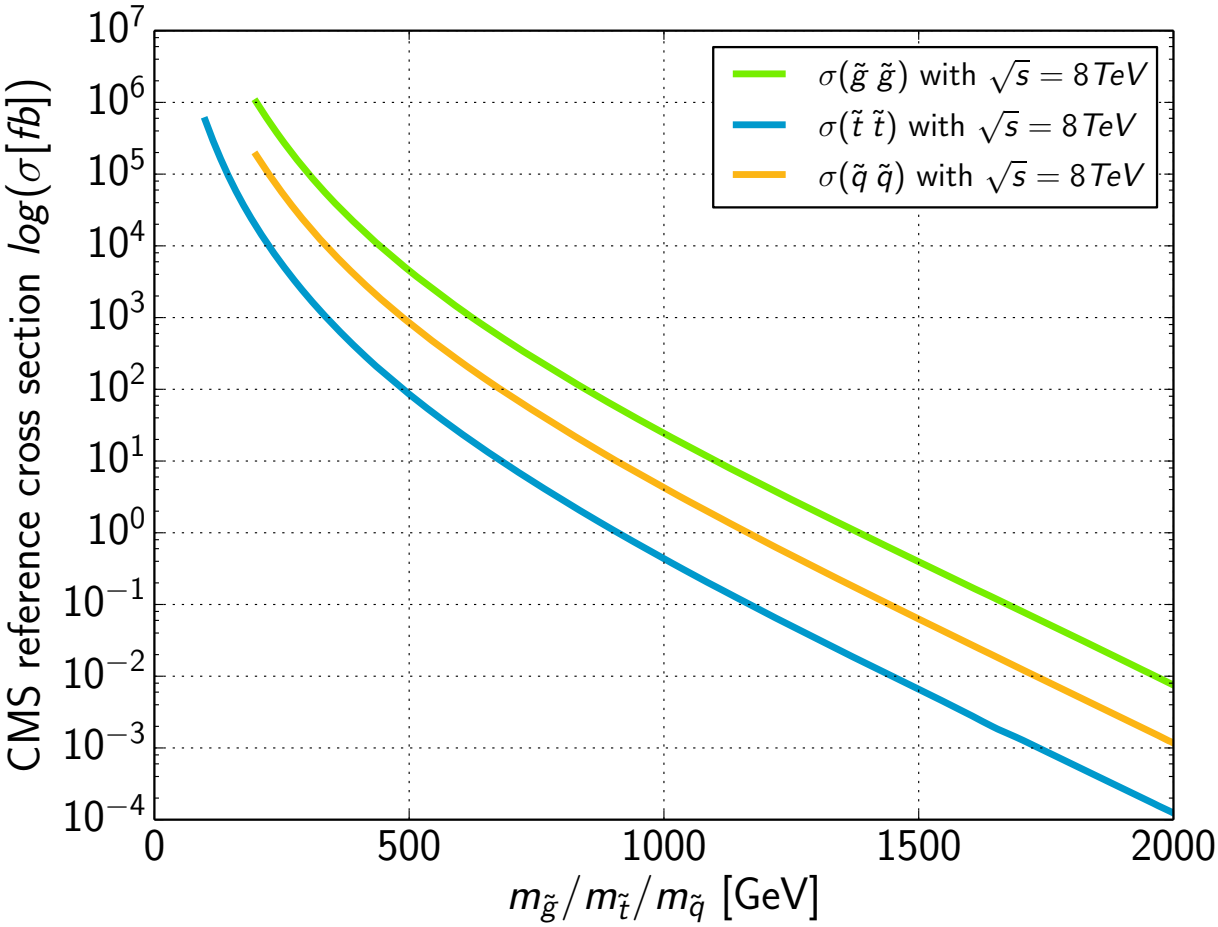

Figure A.1: CMS reference cross sections for pair production of gluinos [87], stops [86] and squarks [89].

List of Figures

List of Tables

Listings

Bibliography

[1] G. Aad *et al.* Observation of a new particle in the search for the Standard Model Higgs boson with the ATLAS detector at the LHC. *Physics Letters B*, 716(1):1 – 29, 2012.

[2] S. Chatrchyan *et al.* Observation of a new boson at a mass of 125 GeV with the CMS experiment at the LHC. *Physics Letters B*, 716(1):30 – 61, 2012.

[3] ATLAS. Supersymmetry Public Results. https://twiki.cern.ch/twiki/bin/view/AtlasPublic/SupersymmetryPublicResults. Accessed 24 May 2015.

[4] CMS. CMS physics results. https://twiki.cern.ch/twiki/bin/view/CMSPublic/PhysicsResults. Accessed 25 May 2015.

[5] Christiane Lefèvre. The CERN accelerator complex. Complexe des accélérateurs du CERN. Dec 2008.

[6] CERN AC. Layout of ATLAS. Dessin representant le detecteur ATLAS. Mar 1998.

[7] G. Aad *et al.* The ATLAS Experiment at the CERN Large Hadron Collider. *JINST*, 3:S08003, 2008.

[8] ATLAS. Public Results. https://twiki.cern.ch/twiki/bin/view/AtlasPublic. Accessed 25 May 2015.

[9] CMS Collaboration. Detector Drawings. CMS Collection, Mar 2012.

[10] S. Chatrchyan *et al.* The CMS experiment at the CERN LHC. *JINST*, 3:S08004, 2008.

[11] CMS. CMS physics paper timeline. http://cms.web.cern.ch/org/physics-papers-timeline. Accessed 25 May 2015.

[12] NIST. The NIST Reference on Constants, Units, and Uncertainty; fine-structure constant. http://physics.nist.gov/cgi-bin/cuu/Value?alph. Accessed 26 May 2015.

[13] Sheldon L. Glashow. Partial-symmetries of weak interactions. *Nuclear Physics*, 22(4):579 – 588, 1961.

[14] Abdus Salam. Weak and electromagnetic interactions. Originally printed in *Svartholm: Elementary Particle Theory, Proceedings Of The Nobel Symposium Held 1968 At Lerum, Sweden*, Stockholm 1968, 367-377.

[15] Steven Weinberg. A model of leptons. *Phys. Rev. Lett.*, 19:1264–1266, Nov 1967.

[16] F. Englert and R. Brout. Broken symmetry and the mass of gauge vector mesons. *Phys. Rev. Lett.*, 13:321–323, Aug 1964.

[17] Peter W. Higgs. Broken symmetries and the masses of gauge bosons. *Phys. Rev. Lett.*, 13:508–509, Oct 1964.

[18] Mark Levinson. Particle Fever. http://particlefever.com/. Accessed 25 May 2015.

[19] N. Cabibbo. Unitary symmetry and leptonic decays. *Phys. Rev. Lett.*, 10:531–532, 1963.

[20] Joseph Lykken and Maria Spiropulu. The future of the Higgs boson. *Physics Today*, 66:28, December 2013.

[21] NASA. What is the Universe Made Of? http://map.gsfc.nasa.gov/universe/uni_matter.html. Accessed 26 May 2015.

[22] Wikipedia. Dunkle Materie. http://de.wikipedia.org/wiki/Dunkle_Materie. Accessed 26 May 2015.

[23] NASA. Wilkinson Microwave Anisotropy Probe. http://map.gsfc.nasa.gov/. Accessed 26 May 2015.

[24] ESA. PLANCK Space Opervatory. http://www.esa.int/Our_Activities/Space_Science/Planck/. Accessed 26 May 2015.

[25] Stephen P. Martin. A Supersymmetry primer. 1997.

[26] Chatrchyan, S. *et al.* Interpretation of searches for supersymmetry with simplified models. *Phys. Rev. D*, 88:052017, Sep 2013.

[27] Serguei Chatrchyan et al. Search for supersymmetry in hadronic final states with missing transverse energy using the variables α_T and b-quark multiplicity in pp collisions at $\sqrt{s} = 8$ TeV. *Eur.Phys.J.*, C73(9):2568, 2013.

[28] Serguei Chatrchyan et al. Search for new physics in the multijet and missing transverse momentum final state in proton-proton collisions at $\sqrt{s}$= 8 TeV. *JHEP*, 1406:055, 2014.

[29] Search for supersymmetry in hadronic final states using MT2 with the CMS detector at $\sqrt{s} = 8$ TeV. Technical Report CMS-PAS-SUS-13-019, CERN, Geneva, 2014.

[30] Exclusion limits on gluino and top-squark pair production in natural SUSY scenarios with inclusive razor and exclusive single-lepton searches at 8 TeV. Technical Report CMS-PAS-SUS-14-011, CERN, Geneva, 2014.

[31] A L Read. Presentation of search results: the cl s technique. *Journal of Physics G: Nuclear and Particle Physics*, 28(10):2693, 2002.

[32] CMS. CMS summary of comparison plots in simplified models spectra for the 8TeV dataset. https://twiki.cern.ch/twiki/bin/view/CMSPublic/SUSYSMSSummaryPlots8TeV. Accessed 24 May 2015.

[33] ICHEP. 37th International Conference on High Energy Physics. http://ichep2014.es/. Accessed 26 May 2015.

[34] Serguei Chatrchyan et al. Search for supersymmetry in pp collisions at $\sqrt{s}$=8 TeV in events with a single lepton, large jet multiplicity, and multiple b jets. *Phys.Lett.*, B733:328–353, 2014.

[35] Sabine Kraml, Suchita Kulkarni, Ursula Laa, Andre Lessa, Wolfgang Magerl, Doris Proschofsky, and Wolfgang Waltenberger. SModelS: a tool for interpreting simplified-model results from the LHC and its application to supersymmetry. *Eur.Phys.J.*, C74:2868, 2014.

[36] Sabine Kraml, Suchita Kulkarni, Ursula Laa, Andre Lessa, Veronika Magerl, Wolfgang Magerl, Doris Proschofsky, Michael Traub, and Wolfgang Waltenberger. SModelS v1.0: a short user guide. 2014.

[37] Sabine Kraml, Suchita Kulkarni, Ursula Laa, Andre Lessa, Veronika Magerl, Wolfgang Magerl, Doris Proschofsky, Michael Traub, and Wolfgang Waltenberger. SModelS: A tool for interpreting simplified-model results from the LHC. http://smodels.hephy.at. Accessed 26 May 2015.

[38] Peter Z. Skands, B.C. Allanach, H. Baer, C. Balazs, G. Belanger, et al. SUSY Les Houches accord: Interfacing SUSY spectrum calculators, decay packages, and event generators. *JHEP*, 0407:036, 2004.

[39] Johan Alwall, A. Ballestrero, P. Bartalini, S. Belov, E. Boos, et al. A Standard format for Les Houches event files. *Comput.Phys.Commun.*, 176:300–304, 2007.

[40] B.C. Allanach. SOFTSUSY: a program for calculating supersymmetric spectra. *Comput.Phys.Commun.*, 143:305–331, 2002.

[41] A. Djouadi, M.M. Mühlleitner, and M. Spira. Decays of supersymmetric particles: The Program SUSY-HIT (SUspect-SdecaY-Hdecay-InTerface). *Acta Phys.Polon.*, B38:635–644, 2007.

[42] Werner Porod. SPheno, a program for calculating supersymmetric spectra, SUSY particle decays and SUSY particle production at e+ e- colliders. *Comput.Phys.Commun.*, 153:275–315, 2003.

[43] Torbjörn Sjöstrand, Jesper Christiansen, Nishita Desai, Philip Ilten, Stephen Mrenna,Stefan Prestel, Christine Rasmussen, Peter Skands. PYTHIA. http://home.thep.lu.se/~torbjorn/Pythia.html. Accessed 26 May 2015.

[44] W. Beenakker, R. Hopker, and M. Spira. PROSPINO: A Program for the production of supersymmetric particles in next-to-leading order QCD. 1996.

[45] Christoph Borschensky *et al.* NLL-fast. http://pauli.uni-muenster.de/~akule_01/nllwiki/index.php/NLL-fast. Accessed 26 May 2015.

[46] Torbjörn Sjöstrand, Stephen Mrenna, and Peter Z. Skands. PYTHIA 6.4 Physics and Manual. *JHEP*, 0605:026, 2006.

[47] W. Beenakker, R. Hopker, M. Spira, and P.M. Zerwas. Squark and gluino production at hadron colliders. *Nucl.Phys.*, B492:51–103, 1997.

[48] W. Beenakker, M. Krämer, T. Plehn, M. Spira, and P.M. Zerwas. Stop production at hadron colliders. *Nucl.Phys.*, B515:3–14, 1998.

[49] A. Kulesza and L. Motyka. Threshold resummation for squark-antisquark and gluino-pair production at the LHC. *Phys.Rev.Lett.*, 102:111802, 2009.

[50] A. Kulesza and L. Motyka. Soft gluon resummation for the production of gluino-gluino and squark-antisquark pairs at the LHC. *Phys.Rev.*, D80:095004, 2009.

[51] Wim Beenakker, Silja Brensing, Michael Krämer, Anna Kulesza, Eric Laenen, et al. Soft-gluon resummation for squark and gluino hadroproduction. *JHEP*, 0912:041, 2009.

[52] Wim Beenakker, Silja Brensing, Michael Krämer, Anna Kulesza, Eric Laenen, et al. Supersymmetric top and bottom squark production at hadron colliders. *JHEP*, 1008:098, 2010.

[53] W. Beenakker, S. Brensing, M. Krämer, A. Kulesza, E. Laenen, et al. Squark and Gluino Hadroproduction. *Int.J.Mod.Phys.*, A26:2637–2664, 2011.

[54] Andy Buckley. PySLHA: a Pythonic interface to SUSY Les Houches Accord data. 2013.

[55] Les Houches. Extending the SLHA: cross section information. http://phystev.cnrs.fr/wiki/2013:groups:tools:slha. Accessed 26 May 2015.

[56] Vardan Khachatryan et al. Searches for electroweak production of charginos, neutralinos, and sleptons decaying to leptons and W, Z, and Higgs bosons in pp collisions at 8 TeV. *Eur.Phys.J.*, C74(9):3036, 2014.

[57] Search for direct top squark pair production in final states with one isolated lepton, jets, and missing transverse momentum in $\sqrt{s} = 8$ TeV pp collisions using 13.0 fb^{-1} of ATLAS data. Technical Report ATLAS-CONF-2012-166, CERN, Geneva, Dec 2012.

[58] Sabine Kraml, Suchita Kulkarni, Ursula Laa, Andre Lessa, Wolfgang Magerl, Doris Proschofsky, and Wolfgang Waltenberger. The SModelS walkding for the pMSSM model. http://smodels.hephy.at/online/pmssm.py. Accessed 26 May 2015.

[59] CERN. ROOT - Data Analysis Framework. https://root.cern.ch/drupal/. Accessed 26 May 2015.

[60] Georges Aad et al. Search for squarks and gluinos with the ATLAS detector in final states with jets and missing transverse momentum using $\sqrt{s} = 8$ TeV proton–proton collision data. *JHEP*, 1409:176, 2014.

[61] Georges Aad et al. Search for new phenomena in final states with large jet multiplicities and missing transverse momentum at $\sqrt{s}$=8 TeV proton-proton collisions using the ATLAS experiment. *JHEP*, 1310:130, 2013.

[62] Georges Aad et al. Search for direct third-generation squark pair production in final states with missing transverse momentum and two b-jets in $\sqrt{s} = 8$ TeV pp collisions with the ATLAS detector. *JHEP*, 1310:189, 2013.

[63] Georges Aad et al. Search for direct production of charginos, neutralinos and sleptons in final states with two leptons and missing transverse momentum in pp collisions at $\sqrt{s} =$ 8 TeV with the ATLAS detector. *JHEP*, 1405:071, 2014.

[64] Georges Aad et al. Search for direct production of charginos and neutralinos in events with three leptons and missing transverse momentum in $\sqrt{s} = 8$TeV pp collisions with the ATLAS detector. *JHEP*, 1404:169, 2014.

[65] Georges Aad et al. Search for the direct production of charginos, neutralinos and staus in final states with at least two hadronically decaying taus and missing transverse momentum in pp collisions at $\sqrt{s} = 8$ TeV with the ATLAS detector. *JHEP*, 1410:96, 2014.

[66] Georges Aad et al. Search for top squark pair production in final states with one isolated lepton, jets, and missing transverse momentum in $\sqrt{s} = 8$ TeV pp collisions with the ATLAS detector. 2014.

[67] Georges Aad et al. Search for direct top-squark pair production in final states with two leptons in pp collisions at $\sqrt{s} = 8$TeV with the ATLAS detector. *JHEP*, 1406:124, 2014.

[68] Search for Supersymmetry in final states with two same-sign leptons, jets and missing transverse momentum with the ATLAS detector in pp collisions at $sqrts = 8$ TeV. Technical Report ATLAS-CONF-2012-105, CERN, Geneva, Aug 2012.

[69] Search for strongly produced superpartners in final states with two same sign leptons with the ATLAS detector using 21 fb^{-1} of proton-proton collisions at $\sqrt{s} = 8$ TeV. Technical Report ATLAS-CONF-2013-007, CERN, Geneva, Mar 2013.

[70] Search for direct production of the top squark in the all-hadronic ttbar + etmiss final state in 21 fb^{-1} of p-pcollisions at $\sqrt{s} = 8$ TeV with the ATLAS detector. Technical Report ATLAS-CONF-2013-024, CERN, Geneva, Mar 2013.

[71] Search for strong production of supersymmetric particles in final states with missing transverse momentum and at least three b-jets using 20.1 fb^{-1} of pp collisions at $\sqrt{s} = 8$ TeV with the ATLAS Detector. Technical Report ATLAS-CONF-2013-061, CERN, Geneva, Jun 2013.

[72] Searches for direct scalar top pair production in final states with two leptons using the stransverse mass variable and a multivariate analysis technique in $\sqrt{s} = 8$ TeV pp collisions using 20.3 fb^{-1} of ATLAS data. Technical Report ATLAS-CONF-2013-065, CERN, Geneva, Jul 2013.

[73] Serguei Chatrchyan et al. Search for gluino mediated bottom- and top-squark production in multijet final states in pp collisions at 8 TeV. *Phys.Lett.*, B725:243–270, 2013.

[74] Serguei Chatrchyan et al. Search for anomalous production of events with three or more leptons in pp collisions at $\sqrt{s} = 8$ TeV. *Phys.Rev.*, D90:032006, 2014.

[75] Serguei Chatrchyan et al. Search for top-squark pair production in the single-lepton final state in pp collisions at $\sqrt{s} = 8$ TeV. *Eur.Phys.J.*, C73(12):2677, 2013.

[76] Serguei Chatrchyan et al. Search for new physics in events with same-sign dileptons and jets in pp collisions at $\sqrt{s} = 8$ TeV. *JHEP*, 1401:163, 2014.

[77] Search for supersymmetry in pp collisions at $\sqrt{s} = 8$ TeV in events with three leptons and at least one b-tagged jet. Technical Report CMS-PAS-SUS-13-008, CERN, Geneva, 2013.

[78] Search for supersymmetry in pp collisions at $\sqrt{s} = 8$ TeV in events with two opposite sign leptons, large number of jets, b-tagged jets, and large missing transverse energy. Technical Report CMS-PAS-SUS-13-016, CERN, Geneva, 2013.

[79] Search for direct production of bottom squark pairs. Technical Report CMS-PAS-SUS-13-018, CERN, Geneva, 2014.

[80] Michael Traub. New data standard for SModelS database containing LHC results for supersymmetry searches. Master's thesis, Technische Universität Wien, 2015. in progress.

[81] John R. Ellis, K. Enqvist, Dimitri V. Nanopoulos, and F. Zwirner. Observables in Low-Energy Superstring Models. *Mod.Phys.Lett.*, A1:57, 1986.

[82] R. Barbieri and G.F. Giudice. Upper bounds on supersymmetric particle masses. *Nuclear Physics B*, 306(1):63 – 76, 1988.

[83] M. Cahill-Rowley, J.L. Hewett, A. Ismail, and T.G. Rizzo. pMSSM Studies at the 7, 8 and 14 TeV LHC. 2013.

[84] M. Cahill-Rowley, J.L. Hewett, A. Ismail, and T.G. Rizzo. Lessons and prospects from the pMSSM after LHC Run I. *Phys.Rev.*, D91(5):055002, 2015.

[85] LEP SUSY Working Group. http://lepsusy.web.cern.ch/lepsusy, dec 2013.

[86] CMS. CMS stop/sbottom cross section with squarks and gluinos decoupled using 8TeV pp collisions. https://twiki.cern.ch/twiki/bin/view/LHCPhysics/SUSYCrossSections8TeVstopsbottom. Accessed 25 May 2015.

[87] CMS. CMS gluino gluino cross section with squarks decoupled using 8TeV pp collisions. https://twiki.cern.ch/twiki/bin/view/LHCPhysics/SUSYCrossSections8TeVgluglu. Accessed 25 May 2015.

[88] Benjamin C. Allanach, Sebastian Grab, and Howard E. Haber. Supersymmetric monojets at the large hadron collider. *Journal of High Energy Physics*, 2011(1), 2011.

[89] CMS. CMS squark anti-squark cross section with gluinos (and stops) decoupled using 8TeV pp collisions. https://twiki.cern.ch/twiki/bin/view/LHCPhysics/SUSYCrossSections8TeVsquarkantisquark. Accessed 25 May 2015.